The influence of initially unsaturated clay on the macro-stability of river dikes

Niels Walrave

TU Delft ARCADIS INPIJN BLOKPOEL INGENIEURS

The influence of initially unsaturated clay on the macro-stability of river dikes

by

N.S. Walrave

to obtain the degree of Master of Science
at the Delft University of Technology,
Faculty of Civil Engineering and Geosciences

Student number:	4348567	
Project duration:	November 22, 2020 – October 15, 2021	
Thesis committee:	Dr. ir. A.A.M. (Anne-Catherine) Dieudonné,	TU Delft (Chair)
	Dr. ir. C. (Cor) Zwanenburg,	TU Delft & Deltares
	Dr. ir. R.C. (Robert) Lanzafame,	TU Delft
	Dr. ir. R. (Rodriaan) Spruit,	TU Delft
	Ir. M.G. (Mark) van der Krogt,	TU Delft
	Ing. R. (Rimmer) Koopmans,	Arcadis
	Dr. I.E. (Inge) van Gelder,	Inpijn Blokpoel ingenieurs

An electronic version of this thesis is available at http://repository.tudelft.nl/.

Cover Image: Picture of the Maasdijk in the dike trajectory Ravenstein-Lith.

List of Tables

List of Figures

List of Symbols

Greek symbols

α	Empirical fitting parameter: inverse of the air entry suction
β	Reliability index
χ	Bishop's factor
ϵ	Axial strain
γ	Shear strain
$\hat{\mu}$; $\hat{\sigma}^2$	Maximum likelihood estimates
κ	Material constant
κ; b	Slope in unloading-reloading in a compression test
λ; a	Slope of the virgin compression line
μ	Mean value of a normal distribution
ϕ'	(Effective) friction angle
ϕ'_{cs}	Critical state friction angle
ϕ^b	Fredlund and Morgenstern (1977) friction angle
ρ_d	Bulk density
ρ_w	Saturated density
ρ_{dry}	Dry density
σ	Standard deviation of a normal distribution
σ	Total stress
σ'	Effective stress
σ'_2	Intermediate principal stress
σ'_n	Normal stress acting on the diagonal failure plane
σ'_v	Vertical effective stress
σ'_{xx}	Horizontal effective stress
σ'_{yy}	Vertical effective stress
σ'_{zz}	Effective out of plane horizontal stress
σ^s	Suction stress
σ_1	Major principal stress
σ_3	Minor principal stress
σ_r	Residual water content
τ	Shear stress
τ_c	Triaxial compression shear strength
τ_d	Direct Simple Shear shear strength

τ_e	Triaxial extension shear strength
τ_f	Undrained shear strength at failure
τ_{fail}	Shear stress along the diagonal failure plane
τ_{max}	Maximum shear strength of a sample
$\tau_{residual}$	Residual shear strength of a sample
θ_{sat}	Saturated volumetric water content
$\phi'_{mob,ps}$	Plane strain mobilized friction angle
$\sigma - u_a$	Net normal stress
τ_{Bishop}	Bishop undrained shear strength
q	Deviator stress
$u_a - u_w$	Matric suction
$\tau_{Fredlund}$	Fredlund and Morgenstern (1977) undrained shear strength
τ_{SSCC}	SSCC undrained shear strength
ψ	Matric suction
θ	Volumetric water content

Latin symbols

u_a	Pore air pressure
V_s	Volume of solids
V_v	Volume of voids
V_w	Volume of water
R^2	Coefficient of determination
s'	Mean effective stress
t	Undrained shear strength
D_{sample}	Diameter of the sample
u_w	Pore water pressure
w	Gravimetric water content
$\frac{s_u}{\sigma'_{vc}}$	Normalised shear strength
S_r	Degree of saturation
A_c	Corrected area of the specimen
A_i	Initial area of the specimen
A_t	Activity of a sample
A_{fail}	Cross-sectional area of the failure plane
c'	Effective cohesion
D	Diameter of the shear box
e	Void ratio
e_o	Initial void ratio

e_w	Water ratio
F_h	Horizontal load on the failure plane
F_s	Horizontal load applied to a sample
F_v	Vertical load on the failure plane
G_s	Specific gravity of the solids
H_{eff}	Effective height of a specimen
I_c	Consistency index
K0	Ratio between the horizontal and vertical effective stress
LL	Liquid limit
M	Critical state parameter
m	SHANSEP parameter
n	Empirical fitting parameter: measure of the pore-size distribution
N_{kt}	Empirical cone factor
p'	Mean stress
P_{fa}	Probability of failure
pF	Logarithm of the absolute value of soil matric potential
PI	Plasticity index
PL	Plastic limit
S	Undrained shear strength ratio
S_e	Degree of effective saturation
s_u	Undrained shear strength
u	Pore pressure
w_n	In-situ water content of a sample
w_{final}	Water content of a sample at the end of a test
$w_{initial}$	Water content of a sample at the start of a test
x_i	Observations
Y	Normally distributed random variables

Preface

This MSc thesis marks the culmination of my studies at Delft University of Technology. This research has been conducted in cooperation with Arcadis & Inpijn Blokpoel Ingenieurs. I would like to thank Rimmer Koopmans and Inge van Gelder for providing me with a graduation internship in which I could conduct extensive laboratory research, and which aims to improve the understanding on how to deal with partially saturated Dutch river dikes in both the geotechnical laboratory as well as how to deal with it as an engineer determining the strength of existing dikes. Especially in these unprecedented times where most students would graduate at home, I am thankful I received the opportunity to spend a great amount of time in the laboratory doing hands-on work.

I especially would like to thank the laboratory technicians at the geotechnical laboratory of Inpijn-Blokpoel ingenieurs in Son who assisted me and taught me how to set up and conduct laboratory tests, and were eager to help come up with solutions whenever a deviation from a norm was thought to be necessary. I would like to express my gratitude for their help and to make the long days in the laboratory memorable to Sjoerd 't Hart, Marco Janssen, Stanley Sterken, Arjen Box, Rohullah Safi & Elvira Imamova and I would also like to extend my appreciation to the colleagues at Arcadis for making it a pleasant experience.

Furthermore, I would like to express my gratitude to my daily supervisor from TU Delft, Cor Zwanenburg for our great deal of meetings and emails where we discussed both fundamental concepts and possible hypothesis based on the laboratory results. Moreover, I would like to thank him for the opportunity to perform Direct Shear tests in the laboratory facilities of Deltares and Mark de Hart for assisting and teaching me how to perform these tests. I would like to thank Alexander van Duinen for explaining his research and sharing his findings with me of an ongoing research project into the initially unsaturated zone. Additionally, I would like to thank the water board Aa & Maas for providing me with their latest interpretation of the geotechnical parameters and D-Stability analysis such that I could compare my laboratory results to the latest results and effectively determine the influence of taking the unsaturated strength into account. Moreover, I would like to express my gratitude to the other members of my thesis committee for their feedback and critical comments: Rodriaan Spruit, Robert Lanzafame, Mark van der Krogt and Anne-Catherine Dieudonné.

I have made many memories over the years during my time in Delft over a TJCburger, a specialty beer or whisky night. I'm grateful that I got the opportunity to study in Norway where I experienced the Northern lights and learned to play Rumpeldunk. With fond memories I'm looking back at my BSc thesis in Costa Rica which I completed in the USA with a trip to my aunt and uncle in the USA. Thank you to everyone who made my time in Delft so enjoyable, and who supported me during my thesis over a coffee break, a drink, through a message or a video call. Thank you for your unconditional support, proofreading and always believing in me. I could not have done it without you: friends, family and my girlfriend. I sincerely hope you enjoy reading this thesis as much as I enjoyed writing it.

Summary

In recent years the Netherlands has experienced drier than average summers, which lowered the groundwater levels, and usually took until the following spring before returning to their initial levels once again. In the Netherlands the design condition for a dike is surmised to occur during the winter season, where it is assumed that the dike is fully saturated. However, this may not necessarily be the case in practice. Preliminary results from a measurement campaign in the Eastern part of the Netherlands by Van Duinen (2020) and interpreted by Buiten (2020) indicate that suction remains present, albeit ever decreasing, during the winter season. This means that it would be possible for a dike to dry out during the summer period such that it becomes unsaturated and any effects associated with this could still be present to some degree as the dike may not have become fully saturated yet during a normative event (a high water level).

This problem is two-fold, as (i) it is known from the literature that the strength of an unsaturated soil is higher than that of a saturated soil, and (ii) it is unknown how the strength associated with the initially unsaturated zone can be modelled in a macro-stability calculation as it varies temporally. This report investigates the strength of the initially unsaturated zone in clay river dikes in the Eastern part of the Netherlands and it explores the opportunities which the better understanding of the strength may present for the factor of safety in a macro-stability calculation. Simultaneously, this research is aimed at establishing a clear framework for future comparable studies into dikes at other locations and with different compositions.

In the first phase of this research the feasibility and applicability of the Suction Stress Characteristic Curve (SSCC) as formulated by Lu and Likos (2006) was investigated. With this concept, it is possible to use conventional geotechnical laboratory tests to determine unsaturated strength parameters. The main advantages of this concept are that few modifications must be made to the current testing procedures used for dike design in the Netherlands. However, to date in the literature, this concept has not been applied to two commonly used conventional geotechnical laboratory tests in the Netherlands for dike design: the K0-Consolidated Anisotropic Undrained (K0-CAU) triaxial test and the Direct Simple Shear (DSS) test. In addition to this, a literature review was performed to bundle international knowledge on unsaturated soil behavior which is relevant in the context of dike design. Moreover, special attention was paid to the two aforementioned laboratory tests to fully understand their applicability and limitations such that these can be interpreted correctly using the SSCC concept.

In the second phase of this research, geotechnical laboratory testing was performed on relatively silty clay samples from the dike trajectory of Ravenstein-Lith in the North-Eastern part of the province Noord-Brabant in the Netherlands. The Soil Water Characteristic Curve (SWCC) was determined to establish the relationship between volumetric water content and matric suction of the soil. In general, testing procedures using the SSCC concept were scarcely published, and hence a testing procedure had to be developed and verified for each type of test. It was found that this concept, when determining strength parameters using strain-compatibility, can be successfully applied to K0-CAU triaxial tests and yields good results. Strain compatibility showed that geotechnical strength parameters can be determined at 10% axial strain compared to 25% as prescribed by the guidelines on dike stability assessment (Ministerie van Infrastructuur en Waterstaat, 2019) for this type of clay. Compared to a conventional K0-CAU triaxial test, the saturation stage has to be skipped in order to test samples which have been air-dried under laboratory conditions to a prescribed volumetric water content which can then be linked to an amount of suction using the SWCC. To further substantiate this claim that the SSCC concept can be successfully applied to K0-CAU triaxial tests, the Van Genuchten based closed-form expression of the SSCC as formulated by Lu et al. (2010) was determined and the results agreed well with the experimentally determined values. As a result, this means that unsaturated geotechnical strength parameters can be determined using the conventional K0-CAU laboratory equipment and the SSCC concept.

For DSS tests, the SSCC concept proved to be unsuccessful in determining geotechnical strength parameters. The interpretation of a DSS test is subject to a number of boundary conditions and especially for DSS tests performed at lower than in-situ water content, the sample was prone to shrinkage. In that case both the membrane and the stack of rings provided insufficient restraint during the test. Moreover, the pins located on the porous stones were unable to sufficiently grip the sample as they failed to pen-

etrate air-dried samples. For sufficiently saturated tests, the slip phenomenon was observed in addition to the formation of a diagonal failure plane within the sample. This research was able to pinpoint at which shear strain slip would occur, and hence when tests can be considered to be valid. Results from direct shear tests indicated that critical state conditions approximately have been achieved when the slip phenomenon is expected to engage in DSS tests (around 15% shear strain). This means that DSS tests on clay samples can indeed be valid and used for engineering designs based on the critical state framework.

Finally, a case study was performed on a representative cross-section located at DP 604 in the dike trajectory of Ravenstein-Lith. This cross-section was produced for the currently ongoing dike reinforcement program in accordance with the current design guidelines. If the additional strength due to the initially unsaturated zone is considered, this could have a positive effect on the factor of safety. Following the field measurements of Van Duinen (2020) and Calabresi et al. (2013) a conservative estimate of the additional strength based on the K0-CAU triaxial tests was modelled which also accounted for reduction in strength due to desiccation cracking of up to 50% in the top meter of the dike based on research by Molenaar (2020). This led to an increase in the factor of safety of at least 1.7% in the most conservative case and at least 5.0% in a scenario supported by field measurements. Although it is likely that the increase is more than 1.7%, this cannot be substantiated with the current limited number of field measurements, and hence it is advised to perform more of these such that the initially unsaturated zone in a clay river dike can be modelled effectively and reliably with a high degree of certainty.

To conclude, with the application of the SSCC concept, the additional strength produced by considering the initially unsaturated zone in clay river dikes in the Netherlands leads to an opportunity where the dike can be designed more efficiently by reducing conservatism. Thus, taking the initially unsaturated zone in a dike into account can be considered as a valuable contribution to the toolbox of Dutch geotechnical engineers.

Contents

1. Introduction

1.1 Background

In the Netherlands flood protection measures are of vital importance to ensure that low-lying areas remain dry and habitable. To make sure that these structures are in fact capable of doing that, safety standards are continuously updated. In the safety analysis of dikes, the macro-stability is of critical importance. With the introduction of the most recent safety standard, WBI2017, the assessment is performed under undrained conditions which represents short-term soil deformation and strength development behaviour in the Western part of the Netherlands more accurately. For this analysis, the strength parameters are derived from the critical state of the soil and hence Critical State Soil Mechanics (CSSM) theory is applied. Additionally, the undrained shear strength profile of a dike is to be assessed using the SHANSEP (Stress History and Normalized Soil Engineering Properties) concept (Ladd & Foott, 1974). This concept relates the Over Consolidation Ratio (OCR) and the normalised shear strength (s_u/σ'_{vc}) of the soil. Using this, the current and future stress state a soil experiences in-situ can be replicated.

In the so-called 'upper river' area, the Eastern part of the Netherlands, so-called "heavy" clay (18-19 kN/m^3) is often found in dikes. Heavy clay is characterised by larger amounts of either silt or sand than typically is expected to be found in a clay. This means that a heavy clay generally has a higher hydraulic conductivity compared to a typical clay and thus is more sensitive to desiccation. In recent years substantially warmer and drier summers have occurred in the Netherlands and therefore it is of interest to investigate the behaviour of these type of soils. As a result, a part of the dyke body may be (partially) unsaturated. During dry periods (which usually occur during the summer season), the extent of this part will increase. In the Eastern part of the Netherlands these dikes, but also the cover layer behind the dike, may become partially unsaturated. Generally, the degree of saturation increases with decreasing distance to the ground water level. The hydromechanical response of a dike under these conditions is therefore especially of interest.

In man-made earth dams and embankments made of compacted fine-grained material such as clayey silt, partial saturation is often found to be prevailing (e.g. Schmertmann (2006) and Calabresi et al. (2013)). According to the current design guideline, the dike is assumed to be subjected virtual steady-state flow during a high-water event. However, in practice, this is only true if the dike consists of a coarse-grained material. This assumption is unlikely to be realistic when a dike consists of a fine-grained material as the duration of a high-water event is smaller than the time required to reach a virtual steady-state condition (Calabresi et al., 2013) and suction can remain present. The preliminary results of ongoing research by Deltares (Van Duinen, 2020) shows that in these types of dikes capillary rise is of importance and varies throughout the year. In addition, it appears that suction, which is produced as an effect of capillary rise, is present to some extent for most of the year. This effect is strongest when the subsoil is at its driest and least present when the subsoil is at its wettest (and therefore the continuous potential precipitation surplus as measured by KNMI is maximum). The current guidelines suggest that in the assessment of slope stability a steady-state pore pressure distribution should be assumed following the design high-water event which thus may be over-conservative as realistically suction may positively contribute to the strength of a dike. Jommi and Della Vecchia (2013) showed that the steady-state assumption may lead to an overestimation of the dimensions of the embankment meaning that the cross-section of a dike, in theory, could be smaller to guarantee a similar factor of safety if suction is taken into account. In addition to this, the structure of the subsoil affects the permeability and this is governed by the cyclic dehydration and hydration which influences the hydromechanical response. In short, the degree of saturation during the year is varying and thus also the effect of capillary rise. Depending on the local situation, this can influence the sliding surfaces and can therefore be important for the macro-stability of the dike.

Recent research by Buiten (2020) concluded that measured suction stresses could be taken into account and that this has a favourable outcome on the determination of the factor of safety for macro-stability. Buiten (2020) also concluded that during a normative WBN-event, the top 1.5 m of the dike will be influenced by the weather and that suction stresses may not be assumed to be present. Currently for dikes, geotechnical site investigation and laboratory research is most often performed in the summer

season (March-October) and hence these samples may therefore be partially unsaturated. This means that when geotechnical strength parameters are determined, the soil may not be fully saturated and suction may be present. However, design calculations which assume saturated conditions, do no take any suction stress and any positive contribution to the strength parameters into account. In addition to this effect, recent research by Gori (2020) on Gorinchem clay showed that conventional laboratory tests may be unreliable when strength parameters are determined at the specified strains in WBI2017 (Ministerie van Infrastructuur en Waterstaat, 2019) due to excessive softening. Triaxial compression and extension tests were found to be unreliable beyond 10% axial strain and beyond 15% shear strain in direct simple shear tests (whereas they are normally determined at 25% axial strain and 40% shear strain respectively) .

This therefore poses the question whether representative geotechnical strength parameters can be quantified using conventional laboratory tests for initially unsaturated clay and how this may influence the macro-stability of river dikes. It is interesting to investigate to what extent this soil behavior deviates in conventional laboratory tests used in the Netherlands to describe soil behavior and to investigate its influence on the existing method of calculating macro stability in order to adequately quantify any possible effect.

As the shear strength is a function of, among other things, the degree of saturation, it is important to understand this properly. Laboratory research can serve to determine the strength parameters of clay under different degrees of saturation. The results of this laboratory work could be simulated in using the soil test facility in Plaxis, such that the laboratory test can be fitted to a constitutive model of interest. In D-Stability, users can define their own shear strength parameters such that the step to a stability calculation can be made based on normative situations. For a more realistic D-stability calculation, the assessment of the shear strength should consider changes in pore water pressure which implies that a model should preferably incorporate coupled time-dependent unsaturated flow.

1.2 Motivation and problem statement

Opportunities for the understanding and use of unsaturated soil behaviour of clay river dikes occur in two areas. First of all, in the Netherlands, there is little experience available in how to deal with unsaturated soils. This thesis therefore aims to bundle the available knowledge which is relevant for dike design of clay river dikes in the Netherlands and which leads to greater understanding. As an engineer one tries to model physical behaviour. However, these models are simplifications to deal with the complexity imposed by nature. In order to make sure that the model remains an accurate description of nature, the underlying assumptions should be critically checked and validated. Although the WBI2017 is an improvement over the previous norm, it does not state much about how to deal with initially unsaturated behaviour and is therefore potentially over-conservative. This thesis may help give engineers more certainty in deriving strength parameters in the initially unsaturated zone such that the factor of safety of a dike can be calculated more accurately, and also contributes to the optimisation of dike reinforcement designs. Although, due to the importance of the dikes in the Netherlands, it is important to show the potential of promising new techniques first on a small scale before widely adopting any changes.

Moreover, there is a social-economic and environmental relevance to this research. If the soil behaviour is better understood, the strength of the dike can be more accurately predicted. If this can be done, the potential dike reinforcement may not have to occur or could be less. Dike reinforcement projects are often expensive, in the order of tens of millions of euros, and so small improvements in the understanding of soil behaviour may easily pay for themselves. Besides costs, a dike reinforcement may lead to a higher crest height. In order to obtain a higher crest level at the same slope angle, the dike body needs to increase in width. Although this may not be much of a problem in uninhabited area's where there is grassland on the inner side of the dike, it could prove to be problematic if the dike is in close proximity to buildings. A recent example is the vocal opposition from local residents near the Markermeerdijken whom had strong feelings about their potentially diminished view. It is therefore of importance to quantify the strength of the dike such that any potential dike reinforcement can be optimised by reducing possible conservatism leading to a more efficient design. Moreover, a dike reinforcement program generally has an impact on the environment as the cross-section of the dike has to be altered resulting in transport of a considerable amount of soil from outside the immediate project area.

1.3 Research questions

In this section the research objective will be introduced. From this research objective a main research question will be defined. This will be complemented by sub-questions which aim to aid in answering the main research question.

1.3.1 Research objective

The main objective of this research is to provide a comprehensive overview of international knowledge on how to deal with initially unsaturated soil behaviour in river dikes, but also to explore and investigate the opportunities of applying this knowledge in the Dutch context. It aims to investigate the possibilities and challenges of the determination of the unsaturated strength of clay river dikes in the laboratory and its application. This master thesis therefore aims to provide both hydraulic and geotechnical engineers with knowledge on the execution unsaturated geotechnical laboratory tests and their application in macro-stability calculations.

1.3.2 Main research question

From the problem statement the following main research question can be derived:

"What is the influence of initially unsaturated clay on the macro-stability of river dikes in the Netherlands and is it possible to quantify this soil behaviour using conventional laboratory experiments?"

1.3.3 Sub-questions

To help answer the main research question several sub-questions should be answered first. Each sub-question is designed in such a way that it helps to answer a small part of the overall research question, but is still highly specific.

Part I: Theory
This part presents the relevant theory required for both unsaturated soil behaviour and delves into laboratory testing. It investigates the following sub-questions:

1. Which of the methods to determine undrained shear strength is most suitable for initially unsaturated soil in the Netherlands?

2. How can the strength parameters of clay under variable degrees of saturation be determined using conventional laboratory tests?

Part II: Geotechnical laboratory testing of unsaturated clay
This part describes the geotechnical laboratory tests and investigates the following sub-question:

1. Do geotechnical laboratory test which are performed in line with the SSCC concept, allow the determination of an optimal parametric probability distribution that represents the laboratory data?

Part III: The application of unsaturated soil parameters for macro-stability assessment
The third is focused on the application of the laboratory results such that macro-stability can be assessed. For this purpose the following sub-questions have been formulated:

1. How does the degree of saturation change within a dike subjected to changing ground- and river water level and can this be simplified to several zones for each relevant design condition using site specific laboratory tests?

2. What is the influence of unsaturated clay on the macro-stability in relevant design conditions and can this be quantified?

1.4 Scope limitations

It is important to define the scope of the research, as it helps to give the researcher focus by providing limitations to the research topic. The scope of the project is defined as:

- This thesis focuses on dike section Ravenstein-Lith, but in principle, the knowledge may be applied elsewhere.
- The focus of this thesis is to try to quantify geotechnical strength parameters using conventional laboratory equipment as available in Dutch geotechnical laboratories with minimal changes to the equipment and in principal with adherence to the prevailing norms and guidelines used in the Netherlands.
- In this thesis only the prevailing geotechnical tests for dike design in the Netherlands will be thoroughly investigated. Although concepts may be applicable to other, more advanced geotechnical tests too, these will be not be investigated.
- The determination of an empirical correlation factor N_{kt} for unsaturated undrained shear strength is outside the scope of this research. Therefore, this means that this thesis will not investigate any unsaturated effects which could be found in Cone Penetration Testing (CPT) or Field-Vane Testing (FVT).
- The hydraulic conductivity in clay layers is, among others, dependent on cracks in layers, but also by vegetation. Cracks may form due to suction pressure and may close again when suction forces disappear. Furthermore, the hydraulic conductivity in cracks is typically much greater than that of the pore space in the same soil. The effect of temporally varying hydraulic conductivity during a normative event will be outside the scope of this research.
- The stability of the dike is time-dependent as a result of a temporally varying degree of saturation. To sufficiently quantify the time-dependent behaviour of a dike, a range of safety factors should be considered. In order to accomplish this, an extensive numerical analysis would be required. As such, assumptions will be made to limit the extent of this study.

1.5 Methodology

In this thesis, for each part the research method varied, and as such a short description is offered hereof based on the structure of the report.

Part I: Theory
In this first part of the research the theoretical sub-questions are investigated after a comprehensive literature study using scientific papers, books as well as several master theses. The objective of chapter 2 is to familiarize the reader with the most relevant methods to determine the undrained shear strength and to the principles of how to deal with and understand unsaturated soils. Next, the determination of the geotechnical strength parameters and the most relevant laboratory tests are introduced in chapter 3.

Part II: Geotechnical laboratory testing of unsaturated clay
The second part of this thesis elaborates on the challenges encountered during the testing of unsaturated soils. In chapter 4, a laboratory plan is designed and an extra iterative step is introduced. Results and lessons learned from preliminary tests can then be used to update the test plan, such that successive tests can benefit from this. Moreover, in this chapter an analysis is performed on the tests to determine geotechnical strength parameters.

Part III: The application of unsaturated soil parameters for macro-stability assessment
The third part, in chapter 5, macro-stability calculations will be performed such that the influence of unsaturated clay on the factor of safety can be quantified.

1.6 Structure

The thesis will be executed in a logical sequence such that all research questions can be answered in an efficient manner. The workflow is schematised in Figure 1.1 where the different phases and steps in each phase are visualised. Four distinct phases have been identified of which three have previously been discussed. The final part, part IV, answers the main research question. This part contains a discussion, a conclusion, but also suggest recommendations for further research in chapter 6 and 7 respectively.

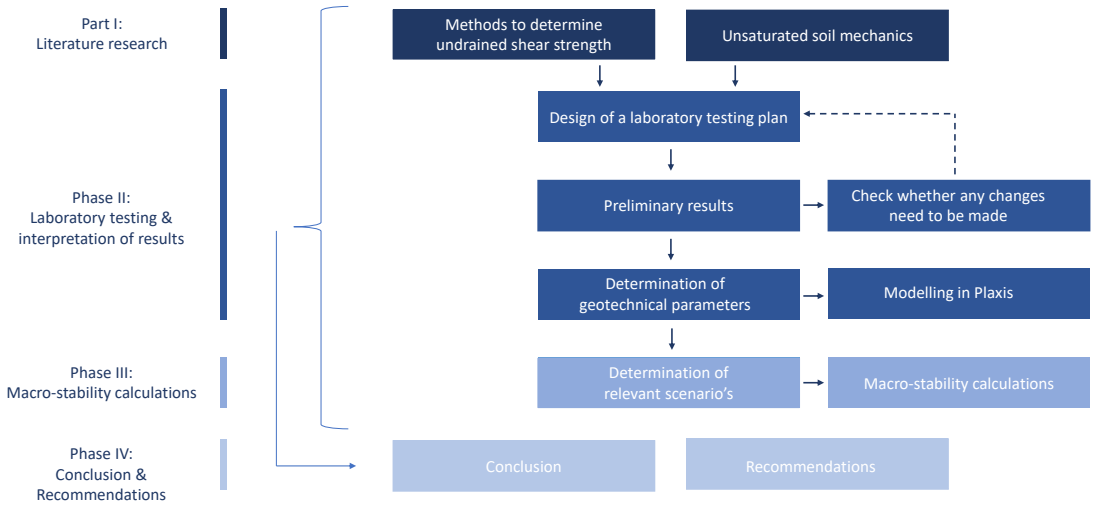

Figure 1.1: Schematized thesis workflow

Part I: Theory

2. A framework for stress in unsaturated soil

In this chapter a literature review will be presented which aims to provide a comprehensive overview of the most prominent processes involved when dealing with unsaturated soils. First the soil water characteristic curve will be introduced in section 2.1. Afterwards section 2.2 explains the different approaches to characterizing the stresses in an unsaturated soil. A concept which allows conventional laboratory tests to be conducted on partially saturated soils is then discussed in section 2.3.

2.1 The Soil Water Characteristic Curve

The Soil Water Characteristic Curve (SWCC) is the relationship between the matric suction (ψ) and one of the following: (i) the volumetric water content (θ), (ii) the gravimetric water content (w) or (iii) the degree of saturation (S_r). These soil characteristics are defined using Equations 3.1 through 3.4.

$$\psi = u_a - u_w \tag{2.1}$$

where u_a represent the pore air pressure and u_w the pore water pressure.

$$\theta = \frac{V_w}{V_v + V_s} = \frac{e_w}{1+e} \tag{2.2}$$

where V_w, V_v and V_s are the volume of water, voids, and solids respectively. The water and void ratio are represented by e_w and e.

$$w = \frac{M_w}{M_s} \tag{2.3}$$

where M_w is the mass of water and M_s is the mass of solids.

$$S_r = \frac{V_w}{V_v} = \frac{e_w}{e} = \frac{\theta}{\theta_{sat}} = \frac{w * G_s}{e} \tag{2.4}$$

where θ_{sat} is the saturated volumetric water content and G_s is the specific gravity of the solids.

The current Dutch framework (WBI2017) assumes that the soil above the phreatic level does not contain any positive or negative (suction) pore water pressures. This could be viewed as if the soil was completely dry and thus it does not contain any pore water. This is a conservative estimate as in practice the soil will never be completely dry. In the vadose zone (see Figure 2.1) which is the zone situated above the phreatic level, matric suction occurs, as in practice a soil will never be completely dry. Directly above the phreatic surface a so-called capillary fringe is located, where the pores are filled with water. The height of this zone is determined by the air-entry head. Above this zone, the vadose zone is located where the degree of saturation decreases with height. It must be noted that this is not a linear process and thus it can cause strong gradients in suction too. The characteristics of theses zones are highly soil dependent. TAW (2001) provides an indication of the capillary height for Dutch conditions of 0.02-0.05 m for coarse sand, 0.70-1.50 m for silt and 2.00-4.00 m or more can be expected for clay.

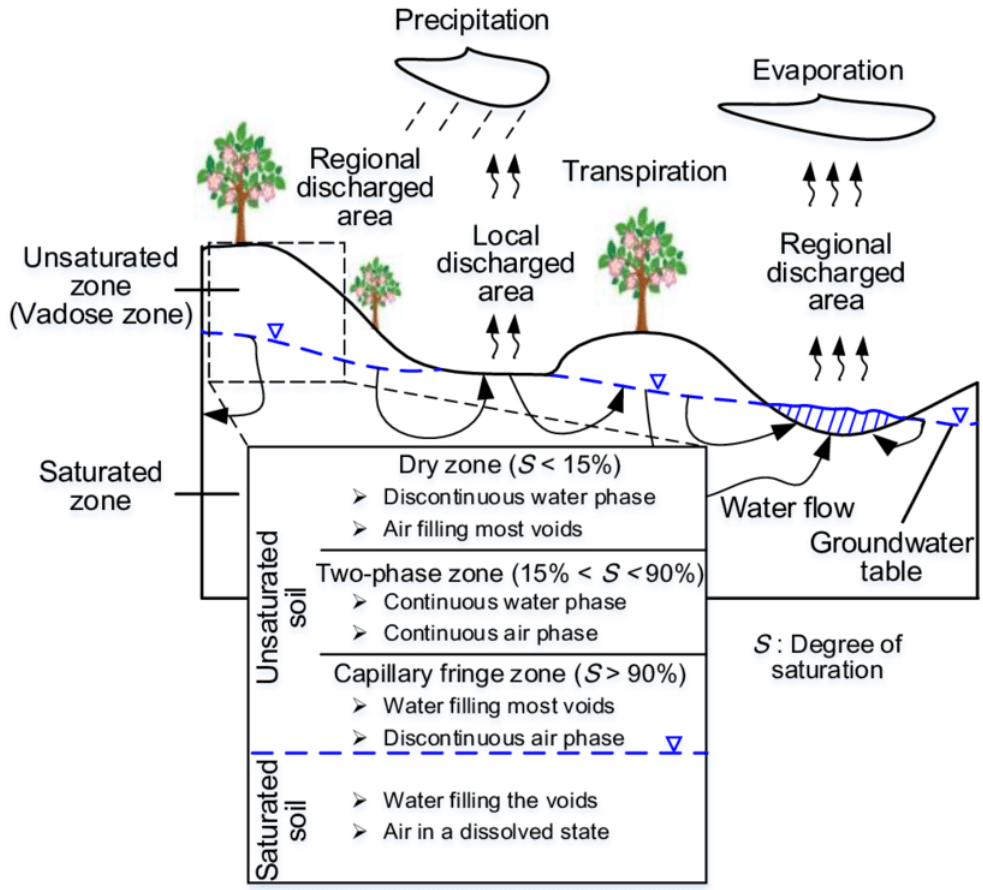

Figure 2.1: Schematic overview of the saturated and unsaturated zone. Adopted from Ren (2019) who modified the picture after Fredlund et al. (2012)

2.1.1 The effect of hysteresis

The SWCC uses elementary capillary theory to explain both water retention and water transmissivity characteristics of a soil. It can approximately be divided into three different zones: (i) the boundary effect zone where the matric suction is lower than the Air Entry Value (AEV), (ii) the transition zone where the water content decreases with increasing height and matric suction is between the AEV and residual matric suction where a sample has reached its residual water content and (iii) the residual zone in which the micropores in the soil starts to dehydrate and where matric suction is beyond the residual matric suction. A typical overview of this is displayed in Figure 2.2. It must be noted that this Figure only displays the initial drying curve of the soil as a hysteresis effect is expected to occur. This allows a soil to have two different states at the same saturation level depending on the drying or wetting situation. It will be further discussed later in this chapter, but this implies that two possible effective stresses can be experienced by the soil at a given saturation level.

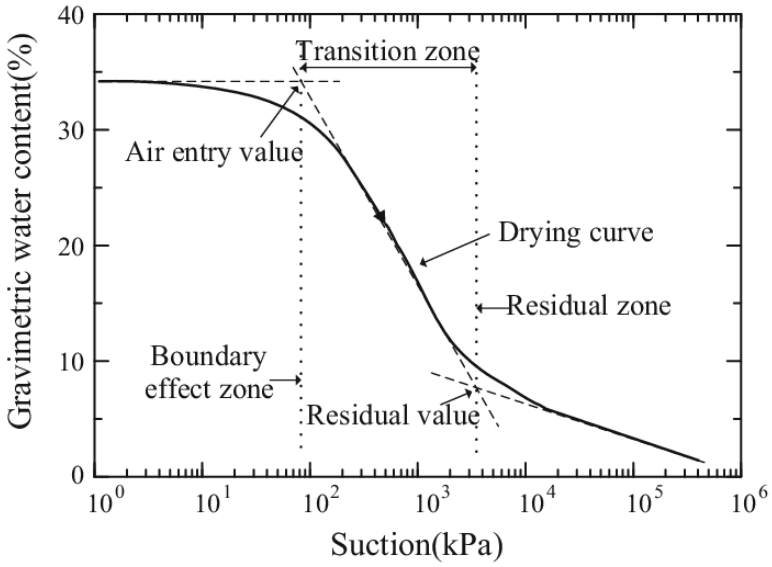

Figure 2.2: Typical SWCC with different regions of desaturation. Adopted from Sun et al. (2016)

The shape of the SWCC is governed by five factors: (i) initial dry density, (ii) initial water content, (iii) pore size distribution, (iv) stress history and (v) plasticity index. Vanapalli et al. (1999) showed that as the plasticity of the soil increases, the AEV increases too. Thus, this implies that a clay has a high AEV value and sand has a relatively low value. Generally, if the dry density of a soil increases, the soil becomes denser and as the result the pore size decreases. In turn, this requires a higher magnitude of matric suction to reach the AEV (i.e. Croney and Coleman, 1954; Gallage and Uchimura, 2010; Yang et al., 2004). The AEV was found to increase with increasing confining stress as this generally reduces the void ratio and thus subsequently to initiate desaturated a higher matric suction is required (i.e. Ng and Pang, 2000; Thu et al., 2007).

In literature (i.e. Fredlund et al., 2012) four mechanisms have been identified as the cause of hysteresis in a SWCC:

1. "Capillary theory (Taylor, 1948; Fredlund and Rahardjo, 1993)"
2. "The swelling and shrinking of 'aged' soil (Hillel and Mottes, 1966)"
3. "The contact-angle (between air-water and soil solids) effect (Hillel, 1971; Bear, 1979)"
4. "The presence of entrapped air in a soil" (Hillel, 1971; Fredlund and Rahardjo, 1993)"

A soil only follows the primary drying curve if aggregates have not been formed yet (i.e. a completely remoulded sample). As soon as these are formed, the initial (often loose) state collapses, and as a result there will be an irreversible decrease of both water content and soil volume. This decrease can be seen when the primary wetting curve is followed to zero suction. In Figure 2.3 it can be observed that if a soil has deviated from the initial drying curve, the initial volumetric water content can never be reached again. If the soil, is then dried again, a new primary drying curve will be followed. If the soil is subsequently partly wetted before partly drying, so-called scanning curves will develop. An infinite amount of scanning curves exists, but they will always be situated between the primary wetting and drying curve.

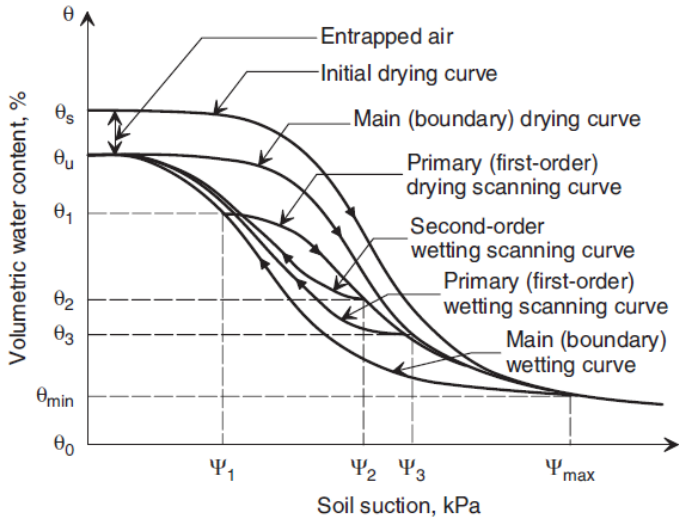

Figure 2.3: Schematic overview of drying, wetting and scanning curves of a unsaturated soil. Adopted from Pham and Fredlund (2003)

2.1.2 Characteristics during Shearing on Cycle of Drying and Wetting

The shear strength of a sample is depending on the drying or the wetting path (i.e. Goh et al., 2014). Their laboratory work showed that a specimen on the first-cycle drying path has a higher shear strength than a comparative sample on the first-cycle wetting path at a given matric suction which can be attributed to hysteresis. According to Goh et al. (2010) and Goh et al. (2014) the hysteresis effect results in the specimen on the first-cycle drying path to obtain a higher peak shear strength, lower stiffness and a higher axial strain at failure and for a comparative sample on the first-cycle wetting path, more ductile behaviour and less dilation during shearing could be observed for a given matric suction. This behaviour is displayed in Figure 2.4.

Goh et al. (2010) observed that the shearing behaviour of a specimen on the first-cycle drying path was reminiscent to the shearing behaviour of a normally consolidated (NC) specimen and similarly a sample on the first-cycle wetting path was reminiscent to that of an overconsolidated soil. Additionally, a specimen on the first-cycle drying path was observed to experience larger dilatancy at increasing matric suction. This agrees with the statement in the previous section where for a specimen with high matric suction a low void ratio is to be expected and that more dilation is to be expected for a specimen at a lower matric suction as it is expected to have a higher void ratio. Goh et al. (2014) found that the dilatancy of the specimen during shearing was governed by the amount of matric suction as this can be regarded as having an important role in keeping the structure of the soil particles intact and hence can affect the strength and deformation of a soil.

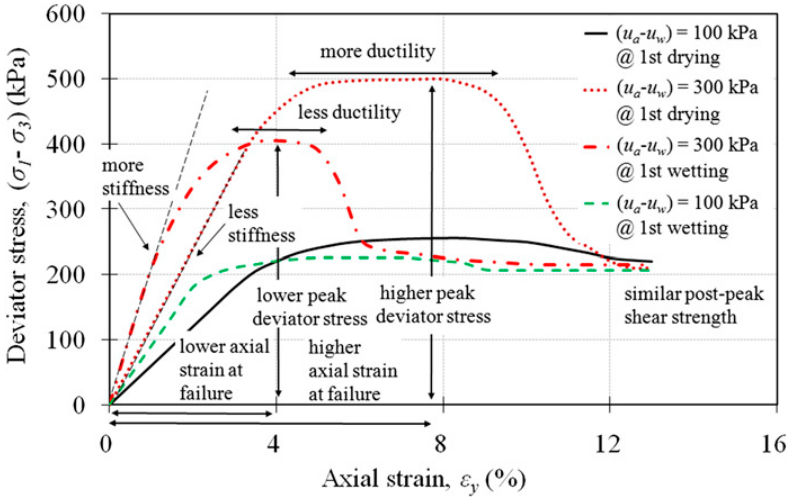

Figure 2.4: Schematic overview of the strength of a specimen in the first cycle of drying and wetting under different matric suctions. Adopted from Goh et al. (2014)

Goh et al. (2014) investigated how the strength characteristics due to hysteresis would be affected by subsequent cycles of drying and wetting during shearing too. Generally, they observed that only a slightly higher shear strength and axial strain at failure could be found for a specimen on a drying path compared to one on the wetting path. Research by Rahardjo et al. (2004) and Goh (2012) showed that this can be attributed to hysteretic effects on the specimen.

Goh et al. (2014) found that in subsequent cycles the difference between the shear strength on the drying and wetting path was relatively small compared to the difference that was observed during the first cycle. This difference was found to be closely related to the volumetric water content of a specimen. The increase in shear strength is directly proportional to the wetted area of soil when subjected to matric suction. Their experimental results showed that on subsequent cycles of drying and wetting, specimens generally exhibit similar stiffness, ductility and volume change characteristics reminiscent of an overconsolidated soil. This can be explained as the soil can be imagined to have undergone an effect similar to a preconsolidation pressure, when the magnitude of matric suction on subsequent levels does not exceed the highest level recorded on the first cycle of the drying and wetting process (Rahardjo and Fredlund, 2003; Goh et al., 2010). After the second complete cycle any effect on the shear strength induced by hysteresis is largely gone (Goh et al., 2014; Tse and Ng, 2008; Sayem and Kong, 2016).

In practice, a dike is during its engineering lifetime exposed to numerous drying and wetting cycles, before it may be partially altered by i.e. a renovation. If one were to view that during each year only one complete drying and wetting cycle per year is assumed, this would mean that if a dike has been unaltered for at least three complete cycles (thus three years), there would be little contribution to the shear strength induced by hysteresis. To verify the validity of this hypothesis when designing for a normative event, an analysis should be carried out to investigate whether the dike has completed three full cycles such that any effects due to hysteresis can be neglected.

2.1.3 Determination of a SWCC

A SWCC can be determined experimentally using several methods, such as a tensiometer, a pressure plate, a Tempe cell, through the dew point chilled mirror technique, the filter paper technique or by means of the axis translation technique. Not all of these methods can cover the entire spectrum of matric suction and therefore a combination of techniques may be required if the entire SWCC must be determined. Nam et al. (2010) performed a comparison on these techniques and concluded that the expected scatter from soil heterogeneity is larger than the difference in results from the different test methods. The determination of a SWCC is time-consuming process and as such often few datapoints are available for a project. Houston et al. (2006) succeeded in determining a SWCC based on a single measurement per curve which they found was an acceptable reliable approximation of the SWCC. If only, the index properties are known, the SWCC can be predicted using the model of i.e. Zapata et al.

(2000); Perera et al. (2005). Fredlund et al. (2012) reviewed the determination of the SWCC based on grain-size distribution curves which could be categorized as follows: "(i) statistical estimates of water contents at various soil suctions, (ii) estimation of soil parameters for an algebraic function for the SWCC and (iii) physico-empriral models where a grain distribution curve is used in the prediction of the SWCC". According to their work, this type of determination could help estimate the SWCC for groups of soils where the SWCC is particularly difficult to estimate such as "(i) soils containing a large amount of clay-size particles, (ii) soils that contain large amounts of coarse-size particles mixed with fines, (iii) soils that exhibit bimodal behaviour such as sand-bentonite mixtures and (iv) man-made soils such as mine tailings".

Fissel and Breitmeyer (2016) showed that if only a single SWCC is determined that the variability in parameters may be greater than 14% of median estimates even when the specimen is carefully prepared, and high precision instrumentation is used. This variability can likely be attributed a combination of both the random positioning and distribution of pore geometry in a packed soil specimen. Using prior knowledge on a limited number of test data, Wang et al. (2018) developed a Bayesian approach to using a Markov Chain Monte Carlo Simulation determine a site-specific SWCC and reduce uncertainty. If several SWCC are available from a site a Bayesian approach based on copula theory can be adopted to obtain SWCC parameters Prakash et al. (2021).

Zhang and Yan (2015) used random finite element modelling to investigate the effect on the stability analysis using spatial variability in the SWCC and found that apparent cohesion could be described well using the lognormal distribution and that the correlation length is of importance in the convergence to a stable probability of failure.

The measurements can be fitted to an empirical so-called pedotransfer function. In literature a large number of these empirical functions can be found which are based on laboratory experiments. Fredlund et al. (2012) provides a comprehensive overview of the different equations. This overview states that generally, these equations have "(i) a variable that bears a relationship to the air-entry value of the soil, (ii) a variable that is related to the rate at which a soil desaturates and (iii) some use a third variable which allows the low-suction range near the air entry value to have a shape that is independent of the SWCC in the high-suction range near residual conditions". Some of these equations are better suited to low magnitudes of suction, whereas others attempt to capture the entire curve or attempt to capture bimodal behaviour. Sillers (1997) compared the use of the different empirical SWCC equations and assesses the fit using the average Akaike information criteria on eight different United States Department of Agriculture (USDA) soil classification groups. This showed that the D. G. Fredlund and Xing (1994) equation performs the best followed by the Van Genuchten-Mualem (1980) equation. In this research the Van Genuchten-Mualem equation will be used as this can then be compared with the Dutch Staring series (Heinen et al., 2020).

$$\theta(\psi) = \theta_r + \frac{\theta_s - \theta_r}{[1 + (\alpha|\psi|)^n]^{1-\frac{1}{n}}} \tag{2.5}$$

In this equation θ_r is the residual volumetric water content [m3/m3], θ_s is the saturated volumetric water content [m3/m3], α is the inverse of the air entry suction (empirical fitting parameter) [kPa-1], n is a measure of the pore-size distribution (empirical fitting parameter) [-] and ψ is the matric suction [kPa]. In this formula, the volumetric water contents are to be used. As one typically measures the gravimetric water content in the laboratory, the following formula should be applied to convert to volumetric water content:

$$\theta_w = w\frac{\rho_d}{\rho_w} \tag{2.6}$$

In this formula θ_w is the volumetric water content [m3/m3], w is the gravimetric water content [%], ρ_d is the bulk density (dry mass divided by the original volume) [kg/m3] and ρ_w is the density of water [kg/m3].

2.2 Stress states in unsaturated soils

In saturated soils stresses can be determined using Terzaghi's classical effective stress equation. For unsaturated soils, there does not exist one unique formula to determine the stress state. According to Lu and Likos (2006) the unsaturated stress in a soil and the shear strength predicition can be characterized in three categories which will be elaborated in this chapter. First, in section 2.2.1 unsaturated laboraotry tests will be introduced followed by Bishop's modification to the Terzaghi equation in section 2.2.2. Then, in section 2.2.3 the independent stress state variable approach will be discussed and finally in section 2.2.4 the implication on numerical constitutive models will be presented.

2.2.1 Determination of shear strength of unsaturated soil in the laboratory

From conventional laboratory tests such as triaxial, direct shear or direct simple shear tests the undrained shear strength can be easily determined. However, in the laboratory testing of saturated soil samples, the assumption is made that the pore space is completely saturated with water. With unsaturated soil samples, air is present in the pores, and this cannot be neglected. It is therefore of paramount importance that the volume of air is accurately measured during the laboratory tests as the sample may consolidate (reduce in volume) and expel both water and air. The laboratory testing of unsaturated soils has been documented by i.e. Rasool and Aziz (2020) who performed advanced triaxial tests on partially saturated soils under unconfined conditions. The axis-translation technique is described in detail in Tripathy et al. (2012) which is required to measure suction stresses. In principle the main difference with conventional saturated tests is that instead of a porous disk, a High Air Entry Porous Disk (HAEPD) must be used. A HAEPD allows for a water pressure on one side and an air pressure on the other side without the air passing through the HAEPD. Such a disk has a certain air-entry value and thus indicates the maximum suction which can be replicated in unsaturated testing of soils. In addition to the HAEPD, the axis translation method should be employed if samples are tested for a suction larger than 100 kPa. This method is necessary to eliminate cavitation, but also to measure the suction applied to the sample by applying an air pressure to the pore space in the sample. In this method suction is created by the difference in air and water pressure. At first, both are linked, thus if the air pressure increases, the water pressure increases too. Next, the air pressure is increased until the water pressure becomes positive. Note that there is still suction as the water pressure is still lower than the air pressure. For these high levels of suction there are several options available, which are commercially available. These include a direct volume measurement using an air pressure and volume controller, a Hong Kong University of Science and Technology (HKUST) inner cell, a double walled cell or by means of on-sample strain transducers. The type of test that should be performed to match the loading situation of an embankment is called a constant water content test (CW). More information on other types of unsaturated triaxial tests and their interpretation can be found in Fredlund et al. (2012). A schematization of CW test can be seen in Figure 2.5 below.

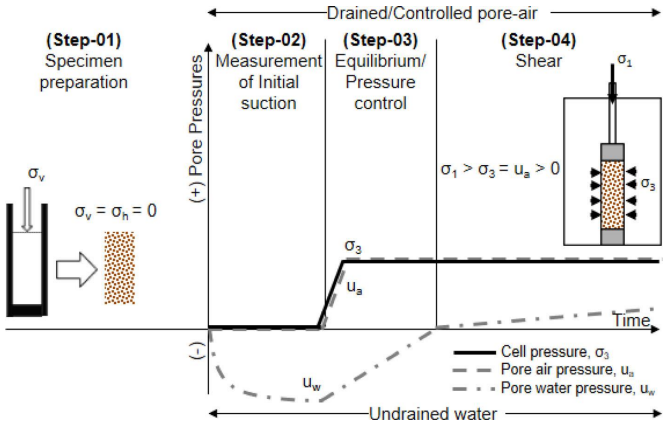

Figure 2.5: Schematic illustration of a constant water content test. Adopted from Rasool and Aziz (2020)

2.2.2 Modified effective stress

Bishop modified Terzaghi's classical effective stress equation to include air pressures as well as a factor χ which is a function of, among others, the degree of saturation. This factor may vary between zero, indicating fully dry conditions, and one, indicating fully saturated conditions. If it is equal to one the relationship reduces to the classical Terzaghi effective stress equation. However, in practice χ is difficult to determine and it has been proven to be non-unique theoretically and experimentally. This can be attributed to the hysteresis effect observed in the SWCC which allows the soil to experience two different possible effective stresses at a given degree of saturation (depending on either wetting or drying conditions).

Bishop's equation for effective stress and followed by the extended Mohr-Coulomb failure criterion for unsaturated soil:

$$\sigma' = \sigma - u_a + \chi(u_a - u_w) \tag{2.7}$$

$$\tau_f = c' + [(\sigma - u_a) + \chi(u_a - u_w)]tan\phi' \tag{2.8}$$

2.2.3 Independent stress state variable approach

In the laboratory the shear strength of an unsaturated soil can be determined using a modified version of the conventional testing apparatus of interest. For instance, but not limited to, by using a modified version of the triaxial apparatus, a modified version of the direct shear apparatus (i.e. Gan et al., 1988) or a modified version of the oedometer test. Experimental studies (i.e. Escario and Saez, 1986; Gan et al., 1988; Vanapalli et al., 1996; Rassam and Williams, 1999) showed that a non-linear relationship exists between shear strength and matric suction.

Fredlund and Morgenstern (1977) proposed an unsaturated shear strength equation where the net normal stress $(\sigma - u_a)$ and matric suction $(u_a - u_w)$ are treated independently in terms of their roles in the mechanical behaviour of unsaturated soil. The equation in the form of an extended Mohr-Coulomb criterion is given below.

$$\tau_f = c' + (\sigma - u_a)tan\phi' + (u_a - u_w)tan\phi^b \tag{2.9}$$

Based on this formula and Bishop's formulation the following can be derived:

$$\chi = \frac{tan\phi^b}{tan\phi'} \tag{2.10}$$

From laboratory experiment both ϕ^b (the angle of increase of shear strength with matric suction) and ϕ' (internal friction angle of a saturated soil) are observed to remain approximately constant at low stresses (and can be said to be stress-independent), but they are stress-dependent for high stresses. At low stresses χ is expected to remain constant. However, as χ is a function of the degree of saturation there is an inherent contradiction.

Fredlund and Morgensterns (1977) ϕ^b defines the rate of change in shear strength with respect to the change in matric suction and it implicitly relates the change between the contact area of the soil particles and the water menisci. Vanapalli et al. (1996) developed a physical model to explain the unsaturated strength behaviour along a SWCC using the three saturation stages: (i) boundary effect stage, (ii) transition stage and (iii) residual stage. Experimental research by i.e. Fredlund and Rahardjo (1987); Gan et al. (1988); Vanapalli et al. (1996); Rassam and Williams (1999); Lee et al. (2005) showed that in the boundary effect stage, ϕ^b, is equal or close to ϕ'. Thus, in this stage, a linear relationship exists between shear strength and matric suction. In the transition stage, a non-linear relationship between shear strength and matric suction exists (i.e. Vanapalli et al., 1996; Bao et al., 1998; Rassam and Willimas, 1999; Lee et al., 2005). In the residual stage, Vanapalli et al. (1996) found that "with increasing matric suction, the shear strength of an unsaturated soil may increase, decrease, or remain constant".

Goh et al. (2010) reviewed existing equations which use the two independent stress state variable approach to predict the shear strength of unsaturated soils. Generally, a distinction can be made between a fitting type (such as Fredlund and Morgenstern, 1977) and a prediction type equation (such as Khalili and Khabbaz, 1998). Goh et al. (2010) concluded that shear strength equations based on the fitting type generally provide a good agreement between measured and estimated shear strength data whereas

prediction type equations were found to provide only moderate agreement and thus can be said to be more site-specific and are less generally valid.

2.2.4 Modified stress variable approach for stress-strain analysis in constitutive modelling

Based on the difficulties associated with the previous two stress definitions numerous researchers came up with a modified stress variable approach for stress-strain analysis. Alonso et al. (1990) expanded Critical State Soil Mechanics (CSSM) theory such that volumetric strain due to matric suction can be included. This led to the creation of the Barcelona Basic Model (BBM). BBM is an extension of the Modified Cam Clay (MCC) model which introduced suction into its formation. Gallipoli et al. (2003) amended this model for elasto-plastic analysis by introducing a stress variable that depends on degree of saturation and matric suction. This means that BBM uses both Bishop stress and suction as state parameters, as opposed to the original formulation which used net stress and suction. This constitutive model switches from a fully saturated model to a partially saturated soil as suction increases. A major advantage compared to other unsaturated constitutive models is that this 'new' version of the BBM model has been implemented for research purposes into the finite element program Plaxis. At the time of this research, the model is not available for widespread use among practicing engineers. Additionally, the model parameters are not straightforward to determine as they require true unsaturated triaxial tests, and currently these are unavailable in the Netherlands.

2.3 The Suction Stress Characteristic Curve

Unsaturated geotechnical tests on cohesive soils can be time-consuming as an equilibrium state has to be reached for a given matric suction between water and air pressure. Lu and Likos (2006) proposed a Suction Stress Characteristic Curve (SSCC) which introduces an effective stress framework for variably saturated soil using a transfer function which describes the macroscopic stress variable at a multiphase air-water-solid representative elementary volume level. The varying interparticle stress can be described using the concept of suction stress. This stress is a result from both physical and chemical phenomena experienced by the soil: (i) Van der Waals attraction, (ii) electric double layer repulsion and attraction, (iii) surface tension, (iv) negative pore water pressure and v) chemical bonding (Lu & Likos, 2006). With SSCC a conventional laboratory set-up can be used to characterize the unsaturated strength of a soil as a function of suction stress. Thus, using this concept, the measurement of matric suction is avoided, and it can be easily applied without major modifications to existing laboratory equipment. This concept was validated by means of true unsaturated test results up to 15 MPa of matric suction (Lu et al., 2010). Xing et al. (2016) were the first to apply this concept to consolidated undrained (CU) triaxial test on loess samples. Their paper shows that it is indeed possible in practice to derive unsaturated strength parameters using conventional geotechnical tests by prescribing a specific water content to a sample and then testing the sample. However, this concept has not been further used on other type of geotechnical tests to date.

The SSCC concept is based on the Van Genuchten-Mualem equation, but in theory, with significant mathematical manipulation, this could be adjusted for other, perhaps more applicable, soil water characteristic curves. Lu and Likos (2006) expanded Bishop's effective stress theory such that the effective stress relationship in terms of suction stress can be expressed as:

$$\sigma' = \sigma - u_a - \sigma^s \tag{2.11}$$

where σ' is the effective stress [kPa], σ is the total stress[kPa], u_a is the pore air pressure [kPa] and σ^s is the suction stress [kPa].

Lu and Godt (2013) showed that the suction stress corresponding to a certain moisture content can be calculated using the effective cohesion and friction angle as determined from Mohr circles described by:

$$\sigma^s = -\frac{c'}{tan\phi'} \tag{2.12}$$

This means that the Mohr-Coulomb criterion can be rewritten as:

$$\tau_f = \sigma' tan\phi' = (\sigma - u_a - \sigma^s) tan\phi' \tag{2.13}$$

Using these equations, the suction stress can be determined. An illustration of how this method is applied in practice can be seen in Figure 2.6. First, the Mohr-coulomb failure lines must be plotted which have been obtained from laboratory tests (which may either be a conventional or an unsaturated one). In the upper part of the Figure, it can clearly be seen that with decreasing volumetric water content, the intercept of the shear strength with the origin is increasing, which conforms to theory. The intercept of the Mohr-Coulomb failure line with the negative horizontal axis is defined as the suction stress. Next, the suction stress versus the volumetric water content can be plotted. If required, it is possible using this information to back-calculate parameters for Bishop's and Fredlund and Morgensterns equation.

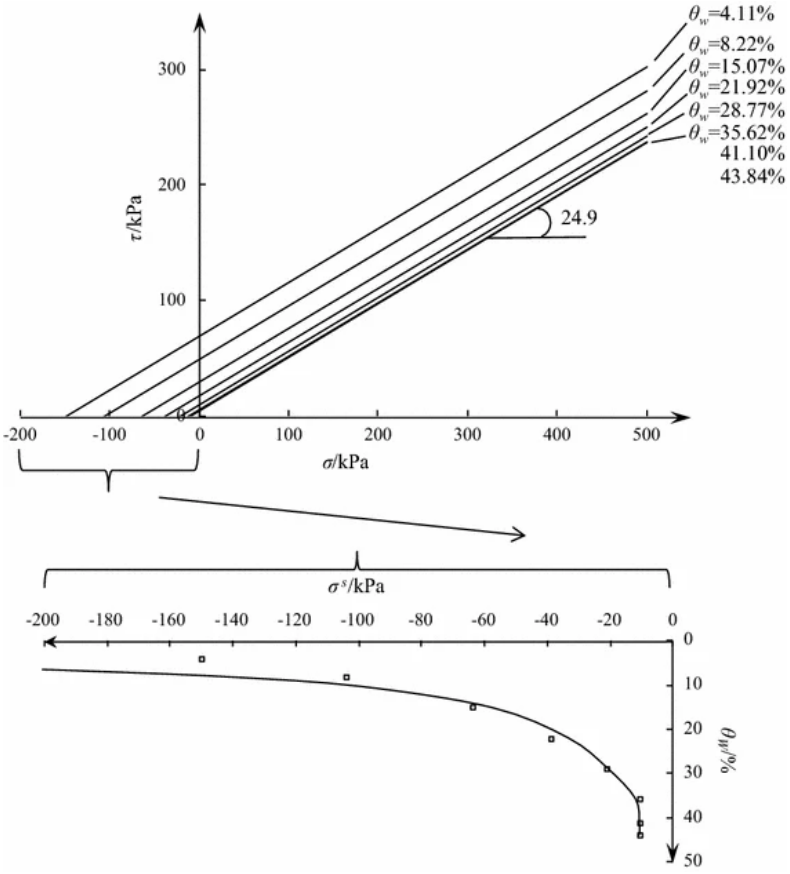

Figure 2.6: Illustrated methodology if the SSCC concept is applied to Mohr-coulomb failure lines obtained from conventional triaxial tests. Adopted from Xing et al. (2016)

2.3.1 A closed-form equation for effective stress in unsaturated soil

The method described in section 2.3 is based on laboratory results. If these are not available, or limited to just the Van Genuchten-Mualem parameters, the suction stress characteristic curve can still be determined. A closed-form expression for the suction stress was introduced by Lu et al. (2010) which is consistent with thermodynamic theory in continuum mechanics. Moreover, Lu (2008) showed that this is a valid stress when scaling up to the representative volume element level in contrast to matric suction.

$$\sigma^s = -\frac{S_e}{\alpha}(S_e^{\frac{n}{1-n}} - 1)^{\frac{1}{n}} \quad \text{for} \quad 0 \leq S_e \leq 1 \tag{2.14}$$

In this equation S_e is the effective degree of saturation, α and n are the empirical Van Genuchten-Mualem parameters. The effective degree of saturation can be determined as follows:

$$S_e = \frac{\theta_w - \theta_r}{\theta_s - \theta_r} \tag{2.15}$$

where θ_w is the volumetric water content of the sample and θ_r and θ_s are the residual and saturated volumetric water content respectively.

An alternative expression for suction stress was introduced by Khalili and Zargarbashi (2010), but unsaturated cyclic DSS tests performed by Jafarzadeh et al. (2020) indicated that the Lu et al. (2010) formulation provides a better match. In addition to this, research by Jafarzadeh et al. (2020) showed that using the suction stress concept it is possible to derive the unsaturated shear modulus if the saturated shear modulus is known and that its magnitude varies non-linearly in the three different regions of the SWCC.

Patil et al. (2020) reviewed the applicability of the closed-form expression by Lu et al. (2010) on different types of cohesive-frictional soils using suction-controlled true triaxial, ring shear and biaxial (where a specimen is tested in plane-strain conditions) tests to determine the SSCC. They observed that in these tests the closed-form expression underestimates experimental results in the case of ring shear and true triaxial tests but overestimates in case of biaxial test results. As a result, they propose a soil-dependent power-fit model to accurately characterize the suction stress. In this research these advanced laboratory tests are not investigated and as such Patil et al. (2020) findings can be ignored, but if in the future further research using these laboratory tests is conducted, it must be considered for a proper interpretation of results.

The Lu et al. (2010) formulation of the closed-form equation considers both adsorptive and capillary forces exerted by the pore water. It assumes that the suction stress in a soil is largely dominated by capillary forces up to the residual water content when the adsorptive regime starts to dominate the suction stress. In this formulation a sharp contrast is made between the capillary and the adsorptive regime whereas in reality this is a much smoother process. The soil of interest for this research is a silty clay which generally has a very low residual water content which will only be reached at high levels of matric suction. As the closed-form equation was proven to be valid for matric suction up to 15 MPa and measurements by Van Duinen (2020) and interpreted by Buiten (2020) showed that suction forces up to at least 80 kPa can be expected in a clay dike in the eastern part of the Netherlands which implies that this formulation is applicable. Zhang and Lu (2020) formulated a different closed-from equation which takes into account the gradual transition between the capillary and the adsorptive regime such that the entire matric suction range can be described in terms of suction stress. They showed that if the soil-water retention is dominated by capillarity the equation can be reduced to Lu et al. (2010) formulation. If capillarity is the only mechanism, the equation reduces to Bishop's effective stress equation and if the soil is fully saturated it reduces to Terzaghi's classical effective stress equation.

3. Determination of geotechnical strength parameters for macro-stability assessment

In geotechnical engineering a wide array of field and laboratory tests is available to characterize a soil. First an overview of the Dutch contemporary practice is presented in section 3.1. In section 3.2 an overview of the available laboratory data can be found as well as an overview of the selected laboratory tests. Although this thesis focuses exclusively on laboratory tests, a short overview of applicable field tests is presented in 3.3. The laboratory tests are then presented in detail in section 3.4 and 3.5. such that these are thoroughly understood and can be interpreted while taking into account both the merits and shortcomings of the respective tests.

3.1 Contemporary Dutch practice

In 2017 new guidelines and regulations were put into practice by the Dutch Ministry of Infrastructure and Environment to assess the macro-stability of water retaining structures. Compared to the previous set of regulations two major changes have been introduced: i) Critical State Soil Mechanics and ii) the SHANSEP method to model soil behaviour. Low permeability soils such as clays and peats are to be modelled using undrained conditions whereas high permeability soils such as sand are to be modelled using drained conditions (Ministerie van Infrastructuur en Waterstaat, 2019). First the different modes of shearing will be explored, followed by an introduction into critical state soil mechanics and the SHANSEP method. Finally this knowledge is combined in how currently, geotechnical strength parameters are determined in the Netherlands.

3.1.1 Modes of shearing

A failure surface could be modelled using sections which represent the active, direct and passive shearing zones as developed by Ladd (1991) and Bjerrum et al. (1974). This can be seen in Figure 3.1. Parameters from triaxial compression (TC) are to be used for the active zone, direct simple shear (DSS) tests for the direct shear zone and triaxial extension (TE) test for the passive zone. Grimstad et al. (2012) state that this concept is especially valid in the case of soft clays for which the undrained stress-strain-strength is generally anisotropic indicating that both the strength and stiffness may have different magnitudes depending on the orientation of the major principal stress to the vertical direction. Anisotropy is believed to be influenced by fabric (particle orientation, structure and layering), the geological history and by the stress path. As such, the principal stress direction may rotate underneath an embankment leading to a varying shear strength depending on the location of interest. This behaviour can be modelled in a so-called directional shear cell test and the varying behaviour according to the zones and which tests adheres best to such a zone was confirmed by O'Neill (1987).

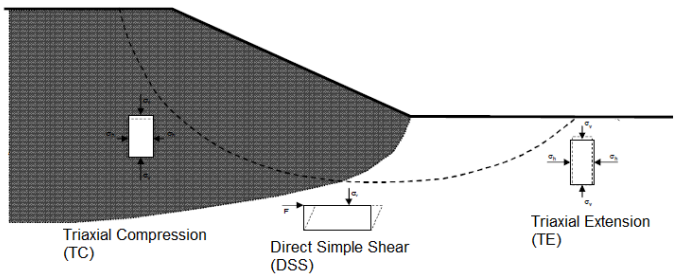

Figure 3.1: Shearing modes in an embankment. Adopted from Ministerie van Infrastructuur en Waterstaat (2019)

3.1.2 Critical State Soil Mechanics

In the Critical State Soil Mechanics (CSSM) framework it is assumed that if a soil is sufficiently sheared, the soil will reach a constant state such that it flows similar to a frictional fluid which contains a turbulent flow of particles in which the shear-strength remains constant and thus is independent of the strain level (Schofield & Wroth, 1968). In this framework it is assumed that the critical state is unique and independent of the initial state of the soil (Lupini et al., 1982; Atkinson et al., 1993). Within the CSSM framework the critical state is reached if during shearing a constant volume can be maintained. CSSM aims to describe the fundamental soil behaviour while incorporating how the shear strength is affected by stress history, compression, dilation, volume change, and how the effective stresses change as a result of shearing and its associated change in pore pressure (Jefferies & Been, 2019). Wood (2017) states that strain softening or hardening of a soil is only dependent on the plastic volumetric strain and hence is equivalent to a situation where deviatoric plastic strain increases, but plastic volumetric strains remain constant. Strain hardening is defined as the increase of the strength of a material while shearing and a reduction in strength is expected in the case of strain softening. Generally, critical state corresponds to the residual state for soils with round particles. A clay may consist of flatter particles and if the orientation of the particles becomes parallel as it resembles laminar flow as opposed to turbulent flow, the critical state may not necessarily correspond to the residual state (Atkinson et al., 1993).

According to CSSM, a soil will reach the same Critical State Line (CSL) independent of the drainage conditions and the OCR, but the critical state strength may be different (see Figure 3.2). The slope of a CSL in compression tests is given by the critical state parameter M and ϕ'_{cs} is the friction angle at critical state. Similar to the critical state strength, the critical state friction angle is unique for each soil. In CSSM a soil is situated on the 'wet side' of critical state when dealing with NC and slight OC soils and it is situated on the 'dry side' if the soil is heavily OC (Atkinson et al., 1993). This terminology originates from the observed soil behaviour during shearing, where a contractive soil expels water during drained loading (and thus becomes 'wet') as opposed to dilative soil (which remains 'dry'). A soil on the wet side of critical state only features strain-hardening, which can be explained as the soil is continuously compressed during shearing such that the interlocking of soil particles is increased before reaching its critical state strength. On the other hand, a soil on the dry side of critical state will reach a peak shear strength rather quickly during shearing after strain-softening behaviour occurs and the soil dilates to its critical state strength.

Pore water cannot dissipate out of the sample during undrained loading as volume change is not permitted and thus the specific volume remains constant. Therefore, a soil on the wet side of critical state develops positive excess pore water pressure and soil on the dry side of critical state develops negative excess pore water pressure. Thus in Figure 3.2 the dry side lies above the CSL and the wet side lies beneath the CSL.

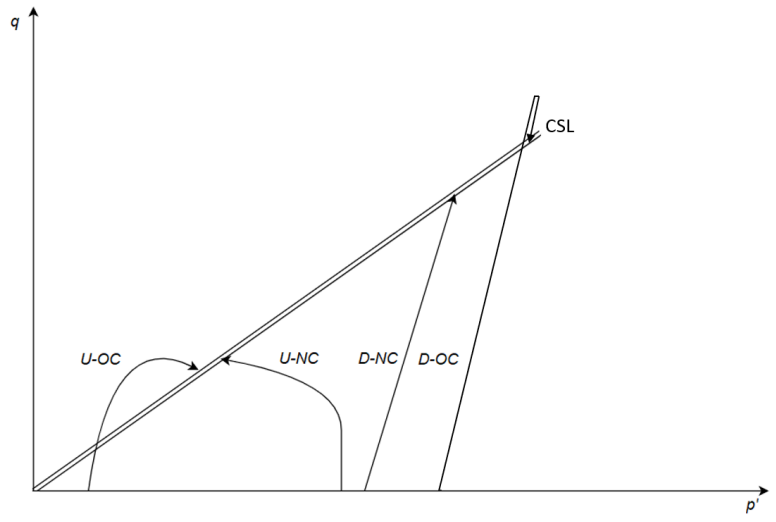

Figure 3.2: Idealized effective stress paths for drained (D) and undrained (U) NC and OC soils. Adopted from Gori (2020))

In case of a NC soil, the initial state is said to be on the so-called Normally Consolidated Line (NCL). The specific volume, or void ratio, can then be plotted as a logarithmic function of the mean normal stress. According to the Modified Cam-Clay (MCC) model, the NCL and CSL are both linear and parallel lines, but the NCL can be found above the CSL as it is located on the wet side of critical state. Using the excess pore pressure development in an undrained triaxial test can determine the critical state too as theoretically the ratio of deviatoric stress to mean effective stress (q/p') must be constant at critical state as well as the incremental changes in this ratio and pore pressure.

$$M = \frac{6sin\phi'_{cs}}{3 - sin\phi'_{cs}} \tag{3.1}$$

$$\frac{q}{p'} = \frac{q}{p-u} = \frac{\sigma_1 - \sigma_3}{\frac{\sigma_1 + 2\sigma_3}{3} - u} \tag{3.2}$$

$$\frac{dq}{dp'} = \frac{dq}{dp - du} = \frac{d\sigma_1 - d\sigma_3}{\frac{d\sigma_1 + 2d\sigma_3}{3} - du} \tag{3.3}$$

The undrained shear strength at critical state found in TC, DSS and TE tests are approximately expected to be similar (Mayne, 1985; Prevost and Høeg, 1976) due to differences in strain rates, initial stress states, the imposed loading and boundary conditions of the respective tests (Ladd, 1991). According to Abelev and Lade (2004) different undrained shear strengths are to be expected for an anisotropic soil as the direction of the major principle stress is vertical in TC, horizontal in TE and is allowed to rotate during a DSS test. Figure 3.3 displays the idealized behaviour during these tests, where the critical state undrained shear strength is expected to be highest in TC, intermediate in DSS, and lowest in TE (Mayne, 1985). The difference is expected to reduce in magnitude for NC clays and silts with a high plasticity index (Mayne, 1985; Ladd, 1991). In TC the sample undergoes axial strain and in DSS the sample undergoes shear strain. In order to compare the results, the normalized shear strength for TC in plane strain conditions can be determined using Equation 3.4 (Koutsoftas & Ladd, 1985). In this equation the plane strain mobilized friction angle, $\phi'_{mob,ps}$, assumes a Matsuoka-Nakai failure criterion (Wroth, 1984) and can be determined from TC using Equation 3.5. The axial strain can be converted to shear strain using Equation 3.6 (Ladd & DeGroot, 2004).

$$\frac{\tau}{\sigma'_{vc}} = qcos\phi'_{mob,ps} \tag{3.4}$$

$$\phi'_{mob,ps} = \frac{9}{8}\phi'_{mob,tc} \tag{3.5}$$

$$\gamma = 1.5\epsilon_a \tag{3.6}$$

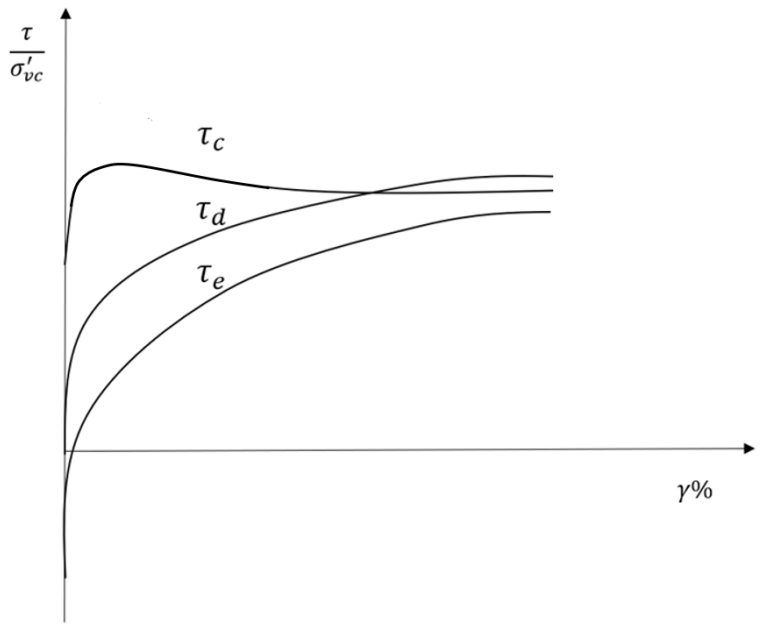

Figure 3.3: Idealised normalised shear stress versus shear strain under plain strain for triaxial compression, direct simple shear and triaxial extension tests. Adopted from Ladd (1991)

3.1.3 The SHANSEP method

In order to determine the undrained shear strength of a soil in line with CSSM the SHANSEP (Stress History and Normalised Soil Engineering Properties) model as originally developed by Ladd and Foott (1974) was introduced. This model is based on the elasto-plastic strain hardening Cam-Clay Model (CCM) which assumes a logarithmic relationship between mean stress and void ratio while adhering to CSSM. In the CCM plastic volumetric strains in the form of preconsolidation pressure are assumed to be represented by overconsolidated behaviour. Ladd (1991) states that this may induce an error if dealing with naturally cemented deposits and highly structured sensitive clays. This also applies to typical Dutch soils such as sand and silt rich clays i.e. loess and boulder clay (Ministerie van Infrastructuur en Waterstaat, 2019). Ladd and Foott (1974) advise not to use the SHANSEP model when dealing with random clay deposits, but it can be used for regular deposits where a well-defined stress history can be obtained. The top of a highly desiccated region often features weathering and it is difficult to determine the OCR accurately which limited the applicability of the SHANSEP method (Ladd & Foott, 1974). In CCM anisotropic behaviour, creep, destructuration and softening are not considered (Wheeler et al., 2003). Using SHANSEP, the undrained shear strength can be described by the equation below:

$$s_u = S\sigma'_{vi}OCR^m \tag{3.7}$$

$$S = (\frac{s_u}{\sigma'_{vi}})_{nc} \tag{3.8}$$

$$m = 1 - \frac{\kappa}{\lambda} = 1 - \frac{a}{b} \tag{3.9}$$

where S is the NC (OCR = 1) undrained shear strength ratio and can be thought to be a friction parameter. σ'_{vi} is the in-situ effective vertical stress, OCR is the overconsolidation ratio and m represents a parameter relating the contribution of the OCR to the undrained shear strength. This parameter can be determined using Equation 3.9 where λ is the slope of the virgin compression line in logarithmic scale and κ is the slope in unloading-reloading in logarithmic scale (Ladd, 1991) and if the Dutch parameter nomenclature is used based on the Isotach method, $\lambda = a$ and $\kappa = b$ respectively (Ministerie van Infrastructuur en Waterstaat, 2019).

3.1.4 Parameter selection and strategy to find the critical state

According to the current guidelines for dike design (WBI 2017) the geotechnical strength parameters (including S) at critical state should be determined at 25% axial strain in a triaxial test and 40% shear strain in a DSS test. Gori (2020) showed that Gorinchem clay is prone to excessive strain softening and if the concept of strain compatibility were to be used, it is possible to determine strength parameters at 15% shear strain in the DSS test and 10% in a triaxial test. As the parameter S is related to a NC soil, the laboratory tests should be performed on NC samples. For this the yield stress needs to be known which can be determined from either constant rate of strain (CRS) test or an oedometer test using the isotach method and selecting point B (Greeuw et al., 2016). A possible disadvantage of this is that the fabric of a sample could potentially be altered resulting in a loss of strength when subjecting the sample to a high yield stress. Theoretically, when using SHANSEP, point A must be used as the yield stress, but this point may lie in a transition zone between normally and overconsolidated samples and therefore is conservative when determining the undrained shear strength. Point B on the other hand, is supposed to correspond to a state of purely normal consolidation and therefore guarantees that the sample in a triaxial or DSS test is subjected to NC conditions.

If only overconsolidated samples are to be used, the parameter S can still be determined if the sample is subjected to the expected vertical effective stress rather than to the yield stress. Although, if a test is performed at lower pressures, the inaccuracies of the measuring apparatus may be more pronounced compared to the same test performed at higher pressures. Moreover, several tests are required in order to establish a correlation with sufficient accuracy as each individual specimen may produce a slightly different S-value (Ministerie van Infrastructuur en Waterstaat, 2019). In a CRS or oedometer test, the parameters λ and κ can be determined for a soil. Although back calculation of the undrained shear strength of an overconsolidated soil using Equation 3.7 is a possibility to determine the parameter m, it may produce a slightly different value compared to those from the CRS or oedometer test and therefore the current guideline advises to determine it using CRS or oedometer tests (Ministerie van Infrastructuur en Waterstaat, 2019).

3.2 Overview of laboratory tests and ongoing research

This section aims to describe which laboratory tests are most suitable using the concept of Lu and Likos (2006) while also taking into account the current Dutch practice presented in 3.2.1 as well as presenting a comprehensive overview of ongoing research into the unsaturated zone in 3.2.2.

3.2.1 Laboratory tests

The aim of this thesis is to characterize the undrained shear strength of partially unsaturated samples. Generally, K0 Consolidated Anisotropic Undrained (K0-CAU) triaxial compression tests are performed on the sand and clay layers, DSS tests are performed on peat layers while triaxial extension tests are rarely performed. The material available for this research can be classified as a silty clay. Recently, extensive laboratory investigation has been conducted for which oedometer test results as well as OC-K0-CAU test results are available in addition to index tests. To the best knowledge of the author the SSCC concept has not been applied to conventional K0-CAU and DSS tests in literature. Moreover, to date there has been little experience in Dutch practice with regular DSS tests on clay. Until a few years ago there were few DSS apparatus available in the Netherlands, but now these are more readily available. As the sample and the duration of the test is shorter than in K0-CAU tests, it would be interesting to investigate whether these tests can be applied in practice. As both laboratory tests conform to the current Dutch practice for characterizing the geotechnical strength parameters in assessing the macro-stability of a dike, these tests were selected for further study. For this research, both NC and OC DSS tests will be performed as well as NC K0-CAU tests on fully saturated but also on several degrees of partially saturated samples. In addition to these tests, several oedometer tests need to be performed in order to determine the appropriate yield strength and index tests such as the Atterberg limits, particle size curves, the amount of organic substance and the amount of dissolved limestone.

3.2.2 Research at Deltares into the unsaturated zone

At Deltares, a Dutch research institute, a research program is currently ongoing into the undrained shear strength in the unsaturated zone (Van Duinen, 2020). For this research two dikes at different locations are available: Oijen and Westervoort (both in the eastern part of the Netherlands). Tensiometers are installed at several locations throughout the dike that were capable of measure suction up to 80 kPa. In summer 2020 several of these sensors malfunctioned due to high suction forces. However, these tensiometers were installed approximately in the top 1.5 m of the dike. As a rule of thumb, a suction force of 1500 kPa corresponds to the change in colour of gras from green to yellow (this indicates the Wilting Point, $pF = 4.2$). As this change in color can be observed in practice, it is likely that strong gradients in suction force exist in the top layer compared to the deeper dike body (where the gradient will be less) in dry periods. This can for instance be done via satellite imagery which forms the input of model which predicts drought-induced cracks using artificial intelligence (Chotkan, 2021). However, these top parts of the dike have little contribution to the overall macro-stability of the dike due to the way the different slices are calculated.

In addition to the sensors, the following laboratory tests have been performed in the saturated zone: UU, Consolidated Anisotropic Undrained (CAU), DSS, DS and oedometer tests on both intact and remoulded samples. Besides this, several index tests have been performed such as the determination of Atterberg limits, particle size curves, the amount of organic substance and the amount of dissolved limestone. For the unsaturated zone, UU, Consolidated Isotropic Undrained (CIU), DSS, DS and oedometer test have been performed on both intact and remoulded samples. For this zone similar index tests as in the saturated zone were performed. CIU tests were performed as opposed to CAU tests on unsaturated clay to correlate samples which have been compacted in different ways or dried to see differences in strength development. Moreover, indirect testing was performed meaning that first a curve was constructed relating the degree of saturation to the suction forces. Then in UU tests, the sample was tested to provide the average undrained shear strength.

3.3 Field tests

Using Field Vane Tests (FVT) and Cone Penetration Tests (CPT) it is possible to determine the in-situ undrained shear strength. For a CPT, a relation exists between the net cone resistance value and the empirical cone factor, N_{kt}, which is highly soil dependent. A recommended value for this factor is in the range of 10-20 (Ladd & DeGroot, 2004) if it has not been calibrated using laboratory tests. Using laboratory tests, it is possible to mimic the expected subsoil loading conditions and hence determine the site-specific N_{kt} such that a more accurate determination of the in-situ undrained shear strength can be found. DeGroot and Lutenegger (2005) showed that if this value is calibrated using laboratory tests that do not suit the subsoil loading conditions, divergent values of shear strength are to be expected. Aas et al. (1986) showed that there is a dependence between the plasticity index and N_{kt} and Karlsrud et al. (2005) showed that there is a relationship with the sensitivity of a clay and the degree of overconsolidation. Practically, this may mean for dike design that this factor is not constant in depth. Besides laboratory test, a FVT can be used to determine the in-situ undrained shear strength by means of a rotating vane. The value produced by this test may need a correction for anisotropy as well as time (Bjerrum et al., 1974). Although, in this way, the N_{kt} is also indirectly determined, it may provide more measurements of the undrained shear strength as laboratory measurements are usually scarcer and especially in cohesive layers, an advantage may be that anisotropy effects can be taken into account better.

Zein (2017) suggests that the N_{kt} is difficult to determine for unsaturated soils, as it depends on the amount of soil suction of which the exact magnitude is usually unknown. In the current Dutch design guideline, for unsaturated soil it is recommended to increase N_{kt} by a factor 3 for the unsaturated zone (Ministerie van Infrastructuur en Waterstaat, 2019). This factor 3 is chosen to account for the unknown magnitude of soil suction stresses at the time of investigation by CPT such that a value for the strength can be found which only accounts for the strength found in normative conditions in which there is not any suction present. This means that a transformation uncertainty is induced into the problem. Although, in theory, it would be possible to determine a depth-varying N_{kt} using the existing CPT and laboratory data in addition to the laboratory data generated by this research, it would only describe the in-situ undrained shear strength at the time the borings were drilled. As this influence of suction on N_{kt} is poorly understood, continuous measurements at the same location would be required to investigate this effect and to determine a possible trend. It is expected that a large number of FVT, CPT and in-situ suction measurements in addition to laboratory data will be needed to determine an accurate factor or procedure which generally holds and is thus not location specific. Currently, ongoing research by Deltares hopes to find a solution to this problem. As such, this topic will not be investigated in this thesis.

3.4 The triaxial test

A triaxial test is a laboratory test which can be executed using different drainage and loading conditions to simulate in-situ conditions and determine strength parameters. Generally, three major parameters can be adjusted depending on the type of test of interest: (i) it can be performed either in compression or in tension, (ii) under drained or undrained conditions (allowing or prohibiting consolidation during shearing) and (iii) before shearing a load can either isotropically or anisotropically (i.e. to K0-conditions) imposed on the sample. If modifications are made to the conventional apparatus, a sample can tested under a specific amount of suction as outlined in section 2.2.1.

3.4.1 Introduction to a triaxial apparatus

In a triaxial apparatus the triaxial cell is mounted on top of a base which is part of a load frame. Between the top of the load frame and the triaxial cell a load cell is situated which measures the force applied to the specimen. Moreover, the load cell has several valves with which the back volume and pressure can be controlled and measured as well as a cell volume and cell pressure controller. The specimen is located on a pedestal on the bottom and a load cell is attached to a cap on top. On both the top and bottom of the sample a porous stone can be found. Filter paper is attached to the sample and it is surrounded by a rubber membrane. Generally, an external displacement sensor can be found on top of the triaxial cell, in addition to a possible measurement from the load frame itself.

3.4.2 Stress-strain inhomogeneities in a triaxial test

The triaxial apparatus imposes boundary conditions due to the end restraints on the specimen which causes stress-strain inhomogeneities in soft soils (Chatzis, 2018; Muraro, 2019). This is related due to the friction at the interface of sample and the porous stone where deformations are restricted and so-called 'dead wedges' are formed in which the sample cannot freely reach failure (see Figure 3.4c). Especially for high frictional and compressible materials these zones may merge and force the specimen to expand laterally around its perimeter with increasing axial strain (Muraro, 2019). Atkinson et al. (1993) observed that for a soil on the dry side of critical state subjected to intense shearing a volume change may occur such that thin distinct discontinuous and slip surfaces may develop.

For high OC soils, strain softening is expected as well as dilation during shearing where stresses and deformations concentrate at any discontinuous which have formed during shearing. In a drained test, uncertainty in the specific volume in and around the slip surface may result in the test being unreliable due to inhomogeneities of shear and volumetric strains. Wood (2017) states that this can be remedied if the deformations are measured internally instead of externally as is generally done in a laboratory. Stress inhomogeneity in an undrained test may warrant additional excess pore pressure development.

For NC to light OC soils strain hardening is expected as well as compression during shearing during a drained test. Similar to a soil on the dry side of critical state, this results in uncertainty in determining the specific volume of the segment of soil at critical state and it may also warrant additional pore pressure development in case of an undrained test which reduces the strength. These effects caused by the friction between the porous stone and the specimen can be largely reduced if the sample is long and slender. A range is prescribed by the Dutch norm (NEN-EN-ISO 17892-9, 2018) where the height to diameter ratio is 1.8-2.2.

3.4.3 Failure modes in a triaxial test

In an undrained test it is inherently implied that the water content remains constant throughout the shearing phase of the test. Although this is valid for the sample as a whole, drainage may still occur locally as there may be an exchange between the more and less intensely sheared zones of the specimen Atkinson et al. (1993) resulting in the incorrect interpretation of laboratory results. Moreover, in clays the effect of undrained creep is entirely neglected, and the axial strain rate is often minimized which influences the interpretation too. As previously explained, the measurement of excess pore-pressure may be unreliable as it is an average of the whole sample and that highly localized shear zones may develop for soils on the dry side of critical state.

At larger axial strain levels, the stress-strain inhomogeneities are more pronounced which means that due to the accumulated deformation of the sample there are greater uncertainties in determining the cross-sectional area on which the load is applied. This means that for a high OC soil, the deviatoric stress may be underestimated due to a reduction in cross-sectional area for a discontinuous sheared sample and an overestimation for a bulging sample. These failure mechanics can be seen in Figure 3.4. A side effect of the long and slender nature of the specimen such that friction between the specimen and the porous stone was limited, is that the bulging mechanism is reinforced. The height over diameter ratio as prescribed in the Dutch guidelines has been optimized to reduce this effect too and research by Chatzis (2018) concurs.

Gori (2020) described the possible failure mechanisms encountered for Gorinchem clay if critical state is approached from the wet or dry side respectively. If the sample approached critical state from the wet side, it was observed to first bulge, during which the cross-sectional area continuously increased, before discontinuities were observed to initiate along the sample near the loading pistons which resulted in a reduction of cross-sectional area. For light OC samples, the failure mechanism showed a mixture of both bulging and discontinuities, in which the latter was not always present. If the sample approached critical state from the dry side, the featured discontinuities were of a different shape in which these may protrude deeply and either feature crossing or single discontinuities.

Numerous techniques to correct for the change in cross-sectional area were presented by Ehrgott (1971) and Muraro (2019), but as the choice for each of these methods is dependent on the stress history, compressibility, deformation mode and strain level of the sample, it is not straightforward to select one that is generally valid. For triaxial tests, strain rate dependency plays a role too, where the undrained shear strength may differ by up to 10% per log cycle of axial strain rate (i.e. Sheahan, 1996; Gens, 1982; Mun et al., 2016). As such, the current Dutch guidelines recommended using an upper limit for the axial strain rate of 1% per hour if the permeability of the specimen is very low (Greeuw et al., 2016).

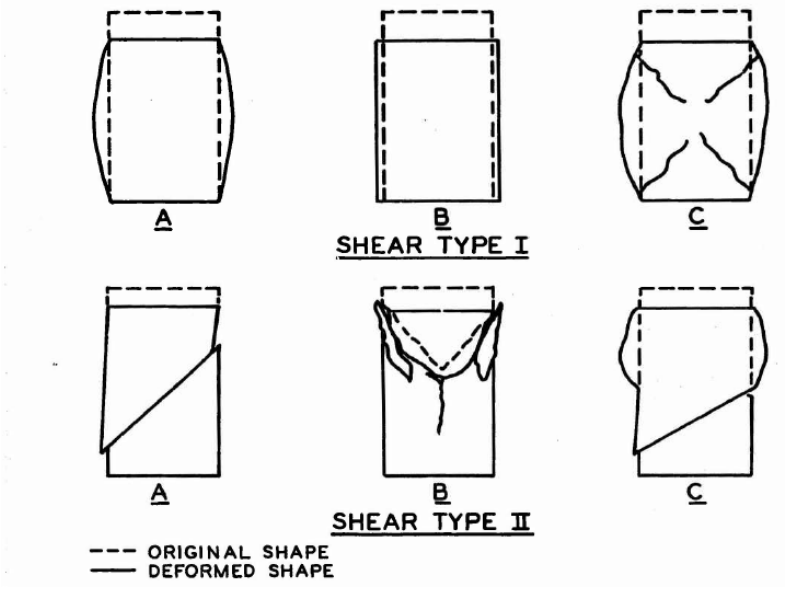

Figure 3.4: Schematized failure shape in a triaxial test. Adopted from Ehrgott (1971)

3.4.4 Interpretation of a triaxial test

In the previous section several causes of stress-strain inhomogeneities were presented and how these are accounted for in the current Dutch norm. Filter paper is attached to the specimen in a triaxial test and enclosed by a membrane. Depending on which norm or guideline is used, different correction formulas exist. In the past, the corrections by Greeuw et al. (2001) were used in the Netherlands. A recent investigation by Konstadinou and Zwanenburg (2019) into membrane and filter paper correction formulas showed that the membrane correction is strain-level dependent and influenced by the friction between the membrane and the specimen and the filter paper correction was found to depend mostly on the wetting of the paper and to a lesser extent on the orientation of it. Currently, the corrections presented in NEN-EN-ISO 17892-9 (2018) are commonly used and as such these will be used in this research.

3.4.5 The Undrained Unconsolidated triaxial tests

The Undrained Unconsolidated (UU) triaxial test is known to yield the lower limit of undrained shear strength as this test is designed to give the short-term undrained shear strength. The advantage of this test is that the sample can be tested as is, is relatively quick and it can be performed on both intact and reconstituted samples. During the formation of the slip circle, but before failure occurs, it could be assumed that the intact clay has sheared in such a way that the particles in these zones have 'mixed'. In such a case the sample could be assumed to behave similar to a reconstituted specimen. In this case the UU strength from reconstituted samples would be a valid approximation of the strength of the dike. Moreover, the result from UU tests can be used to determine a N_{kt} factor for the unsaturated zone, whereas a CPT can provide the respective N_{kt} factor for the saturated zone. However, it should be noted that if this is to be done, the UU test conditions should represent in-situ conditions at the time the CPT was conducted. In that case the effective stress in an UU test is equal to the matric suction. A final remark is that care should be taken as especially UU samples are prone to (significant) sample disturbance.

Ladd and DeGroot (2004) note that "this test relies on the fortuitous cancellation of three errors and therefore one should be cautious, but nonetheless if high quality samples are used, they can give an indication of the average undrained shear strength: (i) the fast rate of shearing can increase the measured undrained shear strength, (ii) but sample disturbance causes a decrease in undrained shear strength and (iii) lastly shearing in triaxial compression causes an increase since it ignores the effects of anisotropy which lowers the undrained shear strength with increase anisotropy". Mun et al. (2016) executed a detailed study into the rate effects on the undrained shear strength while also analyzing the results using the SSCC concept. Ding and Loehr (2019) performed a study into the variability of undrained shear strengths and found that consolidated (anisotropically) undrained tests had a lower uncertainty than UU, pocket penetrometer and handheld torvane tests. Although this test has several advantages if an investigation needs to be performed into the feasibility and applicability of the SSCC concept both in the laboratory and in the field using conventional experiments, it has been successfully applied and studied by Mun et al. (2016) and as Dutch practice is based on the ADP concept, which does not utilize the UU test, this test will not be used in this study.

3.5 The Direct Simple Shear test

A Direct Simple Shear (DSS) test is a geotechnical laboratory test to characterize the undrained shear strength of a sample using a relatively small sample. The mode of shearing of the sample closely resembles the passive failure mode (as can be found in the design of dikes, but also i.e. in offshore structures). In section 3.5.1 the origin of the test will be explained followed by different conditions under which the test can be performed in section 3.5.2. The theory behind the interpretation of a DSS test will be discussed in section 3.5.3. and the stress-strain conditions during such a test will be looked into in section 3.5.4. Finally, contemporary interpretation methods will be discussed in section 3.5.5.

3.5.1 Introduction of a DSS device

The DSS apparatus was originally introduced as it was aimed to improve the direct shear (DS) test. In a DS test a specimen is subjected non-uniform stress and strain condition and as a result it is impossible to characterize the stress-state throughout the test. See Figure 3.5 below for a distinction between a DSS and a DS test). In a DS test the circular or rectangular specimen is encased in a box which can slide over each other. During the test, initially, a normal force is applied to the top of the box in which the sample is allowed to consolidate. In the next phase, a horizontal load is applied to the top (or the bottom) of the box in which horizontal displacement is allowed. During this phase, the shear and vertical stresses are measured. In the resulting stress-strain curve a peak can often be observed as well as a residual condition. Furthermore, this test provides information on the contracting or dilatant behaviour of the soil with the evolution of vertical displacement as a function of horizontal displacement. The stress-strain distribution throughout the sample is in this test highly non-uniform which is caused by a concentration of stresses which develop at the front and rear edges of the specimen. This process causes a progressive failure of the sample and as a result only part of the total theoretical shear strength is mobilized. An implication of this failure process is that the state of stress in the sample remains unknown throughout the test and hence a failure path cannot be determined (Terzaghi et al., 1996).

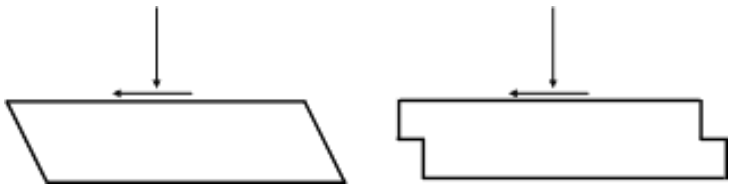

Figure 3.5: Schematic differences in the mode of shear failure direct simple shear test (L=Left) and direct shear test (R=Right)

Various researchers attempted to design a device that would help solve the problems encountered in a DS test. Kjellman (1951) developed an apparatus which formed the basis for a DSS test. In this test a circular soil specimen is enclosed by a rubber membrane and surrounded by aluminium rings. A porous stone is located both at the top and bottom of the sample which allows drainage during consolidation. During the consolidation process the rings can be regarded as imposing a K0-consolidation. Subsequently, the

specimen is sheared from the top plate. This can be done by either maintaining a constant load or a constant height. These porous stones can either be grooved or have little cones or pins to prevent slippage of the sample. To measure the vertical and shear stresses, vertical and horizontal load cells are used and by using displacement gauges, the horizontal and shear displacement can be measured respectively. In contrast to DS test this device imposes a constant area of sliding, but similarities can be found in the direction of the major (vertical) and minor (horizontal) principal stress during consolidation. However, during shearing, these stresses rotate and it remains difficult to trace the amplitude and direction of principal stresses during shearing.

Kjellman's apparatus was subsequently improved by Bjerrum and Landva (1966) at the Norwegian Geotechnical Institute (NGI). In this device the sample is enclosed laterally by a reinforced membrane such it enforces a constant area. This membrane is applied using a vacuum and is therefore supposed to fit perfectly to the lateral boundaries and it must be sufficiently stiff such that it ensures one dimensional consolidation (K0) and to maintain a constant volume during shearing. Other versions of the DSS apparatus have been developed by Roscoe (1953), the so-called Cambridge apparatus, which uses a square sample with straight lateral boundaries, Franke et al. (1979) and Dyvik et al. (1987) designed a DSS test with a pressurized cell such that truly undrained tests can be performed and the Berkeley type apparatus which only uses an unreinforced membrane to confine the sample.

3.5.2 Constant load vs constant volume

For the shearing phase of the DSS test two options exist: i) the vertical load should remain constant or ii) the height of the sample should remain constant. In this case, the former options result in the drained shear strength parameters whereas the latter is used to determine the undrained shear strength parameters. For granular soils, such as sand, drained parameters are usually of interest, and hence DSS tests would be performed with a constant load. In contrast, for soft soils, such as clay and peat, undrained parameters are usually of interest, and hence the test is performed using the constant volume approach during shearing.

Although in practice in Dutch geotechnical laboratories most DSS apparatus cannot perform truly undrained tests, as the testing apparatus is not fully closed and therefore pore water may leak through the apparatus during a test (as opposed to i.e. a triaxial test). Thus, the undrained DSS response is typically investigated by conducting drained tests at constant volume. According to Bjerrum and Landva (1966) there is an equivalence between the two types of tests. This is the case as the observed change in vertical stress in a constant volume test is equivalent to the change in pore pressure that would have occurred during an undrained constant load test. Moreover, if the generation of excess pore pressures is to be prevented, this implies that sufficient time is required for internal equalization inside the sample and thus that the test must be performed at a low rate of strain.

This 'constant volume' hypothesis was validated by Dyvik et al. (1987) who designed a chamber for a NGI-type DSS apparatus. In this device the pore pressure inside a soil specimen could be measured and hence this device is capable of conducting truly undrained tests. With this set-up both truly undrained and constant volume drained tests on NC clay were performed and similar results were obtained. However, their research was limited to saturated NC clay for shear strains up to 10% and thus it was not tested whether for other types of (unsaturated) materials this hypothesis is valid. Using the Modified Cam Clay model and finite element modelling, the evolution of pore pressures in the core of a specimen tested on an NGI-type DSS apparatus could be modelled. This produced results similar to the prediction by Bjerrum and Landva (1966) for similar ranges of shear strain on Speswhite Kaolin.

3.5.3 Theory of interpretation of direct simple shear results

During a DSS test, both load and displacement transducers measure their respective actuation in the vertical and horizontal direction. However, it should be stressed that in a DSS test the measured horizontal and vertical load is not valid for the entire sample due to i.e. rotation of the principal stresses. The vertical load is therefore an average vertical load and hence an average vertical stress too. Although the horizontal load might suggest a relation to a horizontal stress, this is not the case as horizontal stresses cannot be measured directly during a DSS test. The horizontal load is equivalent to the average shear stress which a sample experiences. The principal stress directions continuously change with an increase

in the average shear stress (i.e. Borin, 1973; Arthur et al., 1980; Ochiai, 1981; Joer et al., 1988; Farrell et al., 1999; Doherty and Fahey, 2011; Klar et al., 2019) and the vertical sides tilt. Different methods of interpretation have been proposed as there remain uncertainties on the true stress state inside a specimen throughout the test. de Josselin de Jong (1971) proposed that a soil element can choose between three modes (see Figure 3.6) to select the one which requires the least amount of resistance governed by the boundary condition of the test (and thus of the engineering situation).

1. "The horizontal plane is a plane of maximum stress obliquity such that the mobilized friction angle of the soil can be determined by":
$$tan\phi = \frac{\tau_{yx}}{\sigma_{yy}} \tag{3.10}$$

2. "The horizontal plane is a plane of maximum shear stress such that the mobilized friction angle of the soil can be determined by":
$$sin\phi = \frac{\tau_{yx}}{\sigma_{yy}} \tag{3.11}$$

3. "The vertical plane is a plane of maximum stress obliquity as proposed by De Josselin de Jong (1971). This method assumes a vertical failure combined with a rotation of the specimen with magnitude gamma in the anticlockwise direction where gamma is the amount of engineering strain applied externally to the specimen. The mobilized friction angle of the soil can be determined by":
$$\frac{sin\phi cos\phi}{1 + sin\phi^2} = \frac{\tau_{yx}}{\sigma_{yy}} \tag{3.12}$$

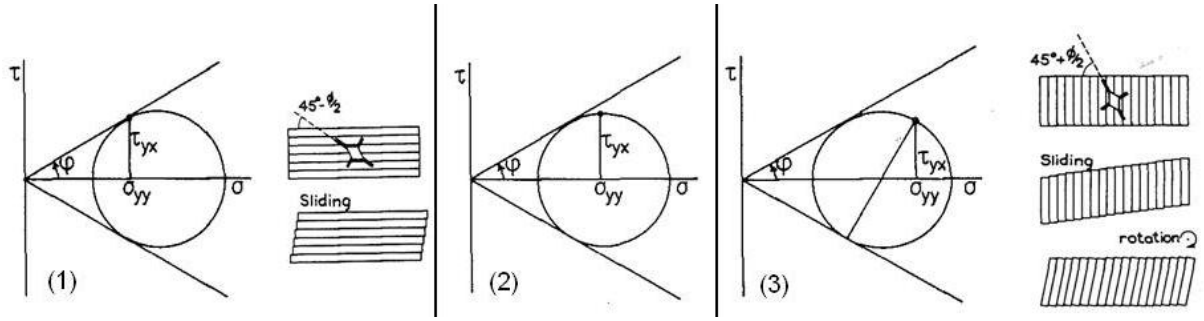

Figure 3.6: Three possible intepretations of a direct simple shear test. Adopted from De Josselin de Jong (1971)

Borin (1973) performed a single test on a kaolin sample with a custom built DSS device in which the sample is completely confined by load cells. This confirmed the hypothesis of De Josselin de Jong (1971) as it allowed for the stress state to be completely defined. Generally, the first hypothesis (Equation 3.10) was used as it provides conservative design parameters.

The magnitude of principal stress rotation during a DSS test was derived by Ochiai (1981) based on the formulation of the principal stress axes as proposed by Oda and Konishi (1974). For a NC clay this results in:
$$tan\phi_{dss} = \frac{\sigma_{xy}}{\sigma_y} = \kappa tan\alpha \tag{3.13}$$

In this equation a linear relationship is proposed between the shear stress ratio on the horizontal axis and the tangent of the angle of σ_1 with the vertical axis. The material constant, κ, was shown by Oda (1975) to be related to the ratio of the initial horizontal and vertical stresses which is equal to the K_0 value.

3.5.3.1 Advanced interpretation of DSS tests

As technology progressed, several authors performed computer simulations of the DSS test to thoroughly investigate this test and its interpretation. A concise overview of some important findings is presented in this subsection. A back-analysis of a DSS test on a peat sample in the finite element program Plaxis

by Farrell et al. (1999) showed that the principal stresses are under an angle of 45 degrees with the vertical and thus it would be in favour of Equation 3.11. Although the approach using this equation is not necessarily conservative, it can be used in a situation where a FEM program such as Plaxis is used to load the material in shear as the back-analysis showed that the material behaviour can be represented correctly.

Doherty and Fahey (2011) performed a three-dimensional finite element analysis of a DSS test and showed that the maximum shear stress simultaneously occurs on the vertical and horizontal planes of the specimen. However, these are not the planes of failure as they are not the planes of the maximum mobilized friction. Their research confirms the experimental observation of Dyvik et al. (1987). Moreover, their research showed that the type of DSS device influences the changes in total stress and excess pore pressure significantly. This is due to the imposed boundary conditions and how the forces to produce constant-volume plane-strain conditions are distributed which can be thought of as a system which has a single degree of indeterminacy. This means that either the vertical stress, the horizontal stress or the pore pressure can be removed without affecting the strain path. However, it will change the value of the two remaining forces. An important practical implication of their work is that it showed that for a drained test in a Kjellman-type DSS device, the total vertical stress will equal the change in pore pressure as experienced in an undrained test and is irrespective of the type of imposed undrained shearing. Finally, their work showed that for tests with a maximum shear strain of 12%, s' and t are located at the top and centre of the Mohr-Circle respectively.

Dabeet (2014) found using discrete element modelling that due to a more uniform stress distribution across the specimen DSS results at small shear strains are more reliable than those obtained at large shear strains. His work showed that at large shear strains, the stresses can be highly non-uniform. This is the case in a narrow zone adjacent to the lateral boundaries, and hence only at the specimen core the sample represent ideal simple shear conditions. Moreover, his research showed that with the development of shear strain, the planes of maximum obliquity rotate continuously. This implies that in order to determine the mobilized friction angle, the appropriate interpretation method should be selected depending on the stress state corresponding to the amount of shear strain.

Klar et al. (2019) showed using fiber optics embedded in 3D printed rings that it was possible to evaluate stress paths during the tests and how the principal stress directions rotate until failure for a drained test on clean sand. Their work showed that for a test performed up to 25% shear strain, Equation 3.10 would be applicable as the stress path reaches the failure envelope at the same point as the tangent to the Mohr circle.

3.5.4 Stress-strain inhomogeneity in direct simple shear

In the interpretation of a DSS test, it is assumed that complementary shear stresses act on the vertical boundaries of the sample. In practice, these boundary conditions cannot be achieved during the test and hence stress-strain inhomogeneities develop. A pure shear state of stress implies that the volume of the specimen remains unchanged while it undergoes, in plane strain conditions, uniform extension in the axial direction and uniform compression in the lateral direction. In simple shear conditions, a constant volume deformation is assumed, while it undergoes, in plane strain conditions, that the sample displaces only in the direction parallel to the axial direction of the specimen. It is therefore equal to pure shear plus a rotation. In both cases stresses need to be applied along all sides to maintain a uniform deformation. In a DSS test the absence of shear stresses along the lateral boundaries of the test create a difference between the pure shear state of stress and the simple shear state of stress (see Figure 3.7). In the right-hand side of the Figure dashed arrows indicate that a pure shear state of stress is only experienced in the core of a specimen as was deduced from tests by i.e. Budhu (1984), Airey and Wood (1987) and in studies by i.e. Doherty and Fahey (2011) and Dabeet (2014).

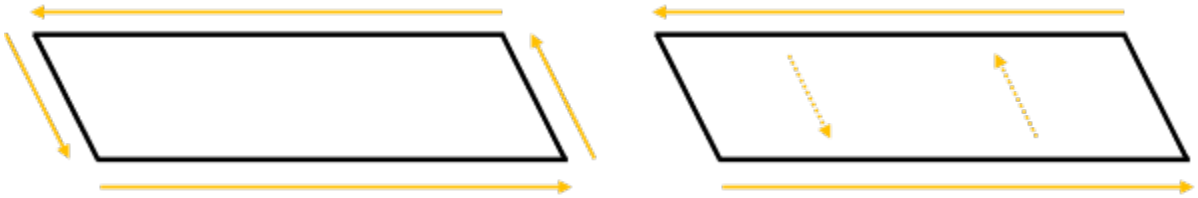

Figure 3.7: A pure shear state of stress (L) and a simple shear state of stress (R)

Besides the lack of complimentary shear forces, an eccentricity may develop between the top and bottom normal forces. As a result, normal forces appear on all faces of the specimen. Roscoe (1953) performed a mathematical analysis assuming a linear elastic material which is approximately valid in the first stages of deformation. The result of this analysis shows that on all faces of the sample both compression and tensile forces act. Moreover, Roscoe (1953) showed that only on the central third of the sample the stress distribution can only be considered uniform. Experiments on a plasticine specimen sheared in a Cambridge apparatus confirmed the analytical hypothesis as a void with an acute angle would develop between the sample and the platen. This phenomenon was more easily observed at lower vertical stress (12 kPa) than at higher vertical stress (495 kPa). Prevost and Høeg (1976) expanded Roscoe's analysis by incorporating this effect which could occur at the platen-soil interface and which is caused by differential displacement. Slippage was found to induce significant variation in normal and shear stresses on the upper and lower face of the specimen. Finn et al. (1971) performed complementary experimental work on plasticine samples. They found that a significant part of the sample remains unrestrained as only a small region near the centre is resisting the shear load if smooth upper and lower plates were to be used. An important implication of their work is that the measured apparent strength would be substantially less than the actual strength of the specimen would be if this phenomenon is not prevented during a DSS test. To avoid this phenomenon most commercially available DSS devices have been equipped with cones or pins on the top and bottom porous stones. Although, as a minimum vertical stress needs to be applied to a specimen such that sufficient grip is created, slippage remains a possibility at low vertical stress (as was observed by Grognet (2011) on peat samples).

3.5.5 Practical interpretation of a DSS test

Traditionally, in the interpretation of a DSS test, complementary shear stresses are assumed to act on the vertical boundaries of the sample. As discussed in the section above, these cannot be imposed in practice. Wood (1990) presented different failure modes during shearing which could occur during a DSS test (see Figure 3.8): "in mode A horizontal rupture planes are generated whereas in mode B inclined rupture planes are formed". Both failure modes are possible to obtain in a Kjellman-type DSS apparatus. This can also be achieved in a NGI-type apparatus where a reinforced membrane is used and in the Berkeley type where the sample is only supported by an unreinforced membrane (Joer et al., 2010).

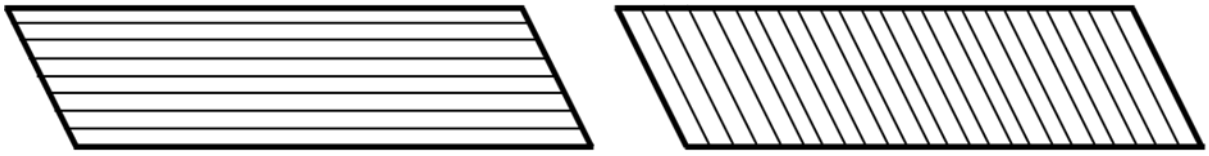

Figure 3.8: Failure modes according to Wood (1990). Type A (L) and Type B (R)

3.5.5.1 'The traditional interpretation method'

According to the current guidelines for dike design (WBI 2017) the geotechnical strength parameters for a DSS test are to be determined at 40% shear strain. Gori (2020) showed using the principle of strain compatibility for Gorinchem clay that it is possible to determine strength parameters at 15% shear strain. As stated in section 3.5.4 it is not straightforward to determine the principal stresses at the end of a DSS test such that the stresses can be plotted by means of a Mohr Circle. Zwanenburg et al. (2019) stated several assumptions in line with earlier work by i.e. Doherty and Fahey (2011) such that this can be done:

1. "Critical state stress conditions are reached at the end of the test."
2. "The measured horizontal stress is equal to the intermediate principal stress σ'_2."
3. "At critical state, the combination of τ and σ'_v correspond to the top of the Mohr Circle."
4. "These stress conditions are reached rapidly for undrained tests while for drained tests it is questionable whether they are reached before terminating the test."

Using these assumptions Zwanenburg et al. (2019) derived the principal stresses at critical state:

$$\sigma'_1 = \frac{\sigma'_{xx} + \sigma'_{yy}}{2} + \sqrt{\frac{(\sigma'_{xx} + \sigma'_{yy})^2}{2} + \tau^2_{xy}} \tag{3.14}$$

$$\sigma'_2 = \sigma'_{zz} \tag{3.15}$$

$$\sigma'_1 = \frac{\sigma'_{xx} + \sigma'_{yy}}{2} - \sqrt{\frac{(\sigma'_{xx} + \sigma'_{yy})^2}{2} + \tau^2_{xy}} \tag{3.16}$$

In these formulas σ'_{xx} represents the horizontal effective stress in shear direction, σ'_{yy} the vertical effective stress, σ'_{zz} the effective out of plane horizontal stresses and $\sigma'_{1,2,3}$ the principal effective stresses. These principal stresses can subsequently be used to determine the mean effective stress and undrained shear strength, s' and t, respectively. They are defined as:

$$s' = \frac{\sigma'_{xx} + \sigma'_{yy}}{2} \tag{3.17}$$

$$t = \sqrt{\frac{(\sigma'_{xx} + \sigma'_{yy})^2}{2} + \tau^2_{xy}} \tag{3.18}$$

3.5.5.2 "The AG method" for a diagonal failure mode

Joer et al. (2010) presented a new interpretation method ("the AG method"). In this failure mode, a diagonal failure plane is formed between the top and bottom of the sample. Generally, the diagonal runs between the back of the top platen and the front of the bottom platen (see Figure 3.9a and 3.9b).

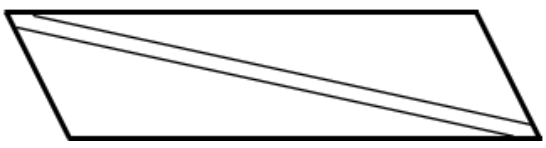

(a) Schematic overview

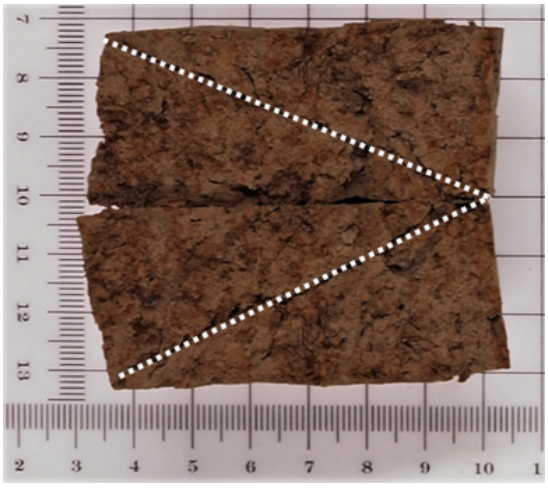

(b) Photo of a vertical cross-section of a typical DSS sample with highlighted white dashed diagonal failure plane

Figure 3.9: Diagonal failure plane in a DSS test

Joer et al. (2010) therefore states that if such a failure plane developed clearly, "it would be more appropriate to consider the stress that act on the inclined failure plane, rather than to focus on the shear stresses applied by the apparatus parallel to the sample ends as is the case in the traditional interpretation method". This interpretation method proposes a linear failure plane based on experimental evidence. A free body diagram, deformation of the sample and the assessment of the friction angle can be seen in Figure 3.10 respectively.

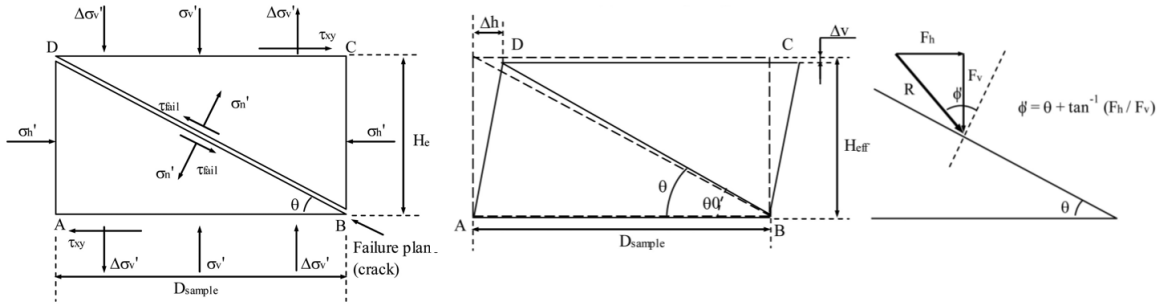

Figure 3.10: Schematic illustration of the boundary conditions of a sample: Free body diagram (L), deformation of the sample (C=center) and the assessment of the friction angle (R). Adopted from Joer et al. (2010)

The normal σ'_n and shear stresses τ_{fail} are determined both on the geometry of the sample and on the stresses on the outside boundary of the sample which are acting on the failure plane. Using the applied effective stresses, the horizontal and vertical load on the failure plane can be estimated:

$$F_h = F_s - \frac{\pi}{4} D_{sample} H_{eff} \sigma'_h \tag{3.19}$$

$$F_v = \frac{\pi}{4} D^2_{sample} \sigma'_v \tag{3.20}$$

In these equations, D_{sample}, represents the diameter of the sample, H_{eff} is the effective height of the specimen and F_s is the horizontal load applied on the sample. Please note, that F_s should be the corrected horizontal load for both the membrane and the slide table friction. Joer et al. (2010) assume that the differential vertical stress averages to zero across the failure plane. This method therefore assumes that the average mobilized resistance along the failure plane is not influenced by this. Thus, during the shearing phase, the specimen only sustains a horizontal displacement of the top platen relative to the bottom platen (δh). Although a possible change in the height of the sample (δv) is theoretically possible, this term is zero in this research as DSS tests are performed using a constant height. The angle of the diagonal failure plane can then be defined as:

$$\theta = tan^{-1}[\frac{H_{eff} - \delta v}{D_{sample} - \delta h}] \tag{3.21}$$

The cross-sectional area of the failure plane can then be determined using:

$$A_{fail} = \frac{\frac{\pi}{4} D_{sample} Heff}{sin\theta} \tag{3.22}$$

The angle between the resulting load and the normal to the failure plane (see Figure 3.10R) is known as the friction angle along the failure plane and can be determined using:

$$\phi' = \theta + tan^{-1}[\frac{F_h}{F_v}] \tag{3.23}$$

The stresses acting on the failure plane can then be estimated using:

$$\tau_{fail} = \frac{\sqrt{F_v^2 + F_h^2}}{A_{fail}} cos\phi' \tag{3.24}$$

$$\sigma'_n = \frac{\tau_{fail}}{tan\phi'} = \tau_{fail} = \frac{\sqrt{F_v^2 + F_h^2}}{A_{fail}} cos\phi' \tag{3.25}$$

The effective friction angle can then be estimated using:

$$\phi' = tan^{-1}[\frac{\tau_{fail}}{\sigma'_n}] \tag{3.26}$$

Joer et al. (2010) concludes that this new method works well for both sands and cemented soils as this method results in post-peak strain softening, but that there is little difference observed with the traditional method for soft clays. Joer et al. (2010)) suggests that "this is possibly caused by the failure mechanism being a combination of both a discrete diagonal shear plane and a conventional type of direct simple shear deformation". Sharma et al. (2017) found in a study between 'flexible' (the sample is only supported by an unreinforced membrane) and 'rigid' boundaries (the sample is supported by a membrane enclosed by concentric rings) that a diagonal shear plane only developed in a DSS apparatus with a flexible boundary on offshore carbonate sediment and at shear strains greater than about 15%.

Part II: Geotechnical laboratory testing of initially unsaturated clay

4. Methodology: set-up of a laboratory plan and test results

This chapter describes the set-up of all laboratory tests, their execution as well as their results. First, a general understanding of the soil characteristics is presented in section 4.1. In section 4.2 the SWCC is determined. Strain compatibility is investigated in section 4.3 which can then be used in the interpretation of the triaxial tests in section 4.4. Preliminary results of DSS on clay are presented in section 4.5 and subsequently in section 4.6 DS tests are used to investigate the occurrence of critical state which can then be used to further investigate the DSS tests in section 4.7. Finally, in section 4.8, it is investigated whether unsaturated soil samples fit commonly used probability distributions in geotechnical engineering.

4.1 Index tests

In this section several key index properties of the soil are investigated which help characterize and identify the soil. Historically, many empirical relationships were developed for a specific area such that without having to perform elaborate laboratory testing, rough estimates of geotechnical parameters would be available. First the Atterberg limits are discussed, followed by the particle size distribution curves and the consistency index.

4.1.1 Atterberg limits

In the plasticity chart (according to NEN-EN-ISO 14688-2 (2019)) soils are designated a symbol consisting of three or four letters. The first two letters identify the primary component of the soil: silt or clay. The third letter second symbol identifies its plasticity characteristics (low, medium, high or very high plasticity). The vertical line at the liquid limit indicates the boundaries of each zone (being 35, 50 and 70 respectively). The fourth symbol is optional if a sample mostly consists of organic material. In this chart both a U-line and an A-line are plotted. The A-line separates clayey soils (above the line) from silty soils (below the line) whereas the U-line can be regarded as the upper boundary which is expected for natural soils. Finally, in this chart there is a zone where both low plasticity silts and low plasticity clays may exists and this is indicated by a zone enclosed by grey lines. Note that NEN-EN-ISO 14688-2 (2019) aims to provide indirectly by means of the Atterberg limits, an approximate indication of the soil characteristics whereas other norms such as the NEN-ISO-14688-1 (2019) describe the characteristics of the soil in detail. In this research the Atterberg limits have been determined 31 times using the Fallcone method on triaxial samples which have been tested to failure. As the samples for the triaxial tests come from different borings, naturally some heterogeneity is to be expected. The results are displayed in Table 4.1.

Table 4.1: Overview of Atterberg limits per boring

Test	Boring	Liquid limit	Plastic limit	Plasticity index	w_n[%]	Ic	A_t
TC1	B012-6	36.16	17.02	19.13	21.85	0.70	0.83
TC3	B012-6	39.94	18.61	21.33	23.39	0.73	-
TC4	B041-3	29.78	15.16	14.62	20.87	0.54	1.12
TC5	B041-3	29.46	16.06	13.40	21.65	0.58	-
TC6	B041-6	34.61	15.70	18.91	22.88	0.57	-
TC7	B012-2	34.01	18.19	15.82	21.98	0.70	-
TC8	B012-3	43.19	21.75	21.43	28.14	0.66	1.02
TC9	B039-1	35.18	17.89	17.29	23.06	0.64	0.69
TC11	B012-4	43.03	22.75	20.29	24.25	0.93	-
TC12	B035-2	59.45	28.43	31.13	43.37	0.49	-
TC13	B038-8	51.59	26.66	28.65	36.71	0.43	1.02
TC14	B012-8	49.02	23.85	25.17	28.70	0.43	-
TC15	B039-2	41.97	20.92	21.05	21.98	0.60	-
TC16	B035-2	40.49	21.36	19.13	37.79	0.78	-
TC17	B038-4	52.35	23.19	29.16	31.56	0.71	1.33
TC18	B015-3	40.32	19.74	20.58	23.15	0.83	2.51
TC19	B012-8	50.88	24.36	26.52	28.47	0.81	-
TC20	B038-8	66.21	27.18	39.04	41.31	0.61	-
TC21	B038-5	42.33	20.33	22.00	25.06	0.74	0.92
TC22	B038-9	62.17	27.23	34.94	45.73	0.47	-
TC23	B015-7	40.01	19.56	20.44	27.16	0.31	-
TC24	B015-8	41.36	18.51	22.85	26.94	0.63	0.71
TC25	B039-6	47.52	22.73	24.79	26.92	0.83	-
TC27	B038-9	57.83	26.35	31.49	41.99	0.50	-
TC28	B015-8	46.86	22.29	24.56	28.79	0.74	-
TC29	B038-6	54.01	24.11	29.90	39.49	0.49	0.96
TC30	B041-6	31.66	14.67	16.99	22.19	0.56	-
TC31	B015-4	29.77	15.89	13.87	22.30	0.54	-
TC32	B038-6	50.96	23.78	27.18	32.27	0.25	-
TC33	B041-6	24.04	13.45	10.59	19.88	0.39	-
TC34	B039-5	48.57	25.75	22.82	31.48	0.75	-
μ		43.70	21.08	22.74	28.75	0.61	1.11
σ		10.17	4.11	6.45	7.42	0.16	0.50

It can be seen in the classification chart (Figure 4.1) that a majority of the samples can be classified as a medium plasticity clay (15), with 7 samples to be classified as low plasticity clays and 9 samples as high plasticity clays. If a linear regression line is plotted through the data points the following formula can be derived with an $R^2 = 0.968$: $PI = 0.623 * LL - 4.527$.

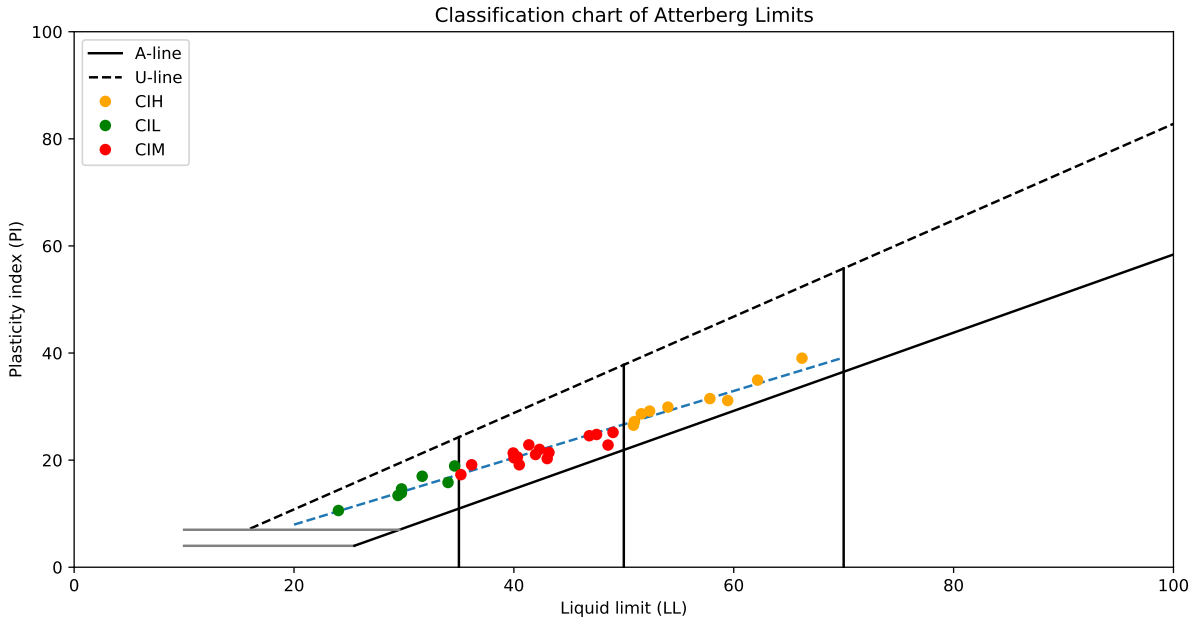

Figure 4.1: Atterberg limits of Ravenstein-Lith and Veessen-Wapenveld

Although there seems to be a clear relationship between the plasticity index and the liquid limit, there is only a very weak relationship between liquid limit, plastic limit, the plasticity index versus the dry density (Figure 4.2c) with an R^2 of about 0.2-0.3. It indicates that if the dry density increases, the soil becomes stiffer (less plastic) which is generally to be expected.

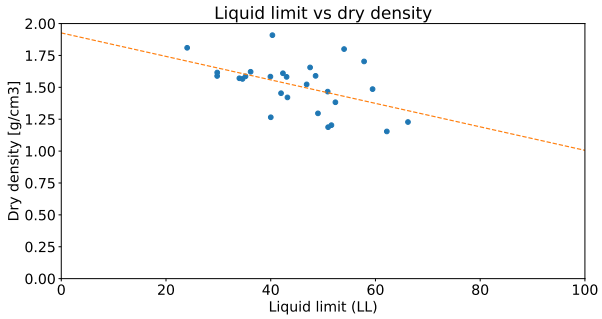

(a) Liquid limit

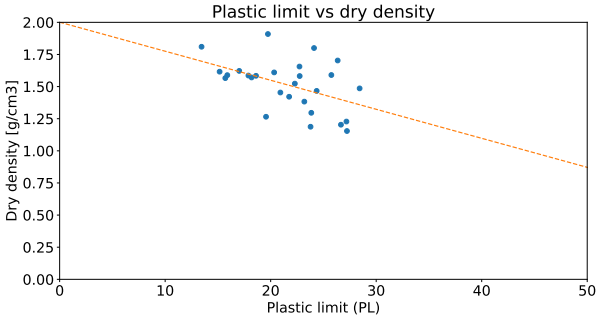

(b) Plastic limit

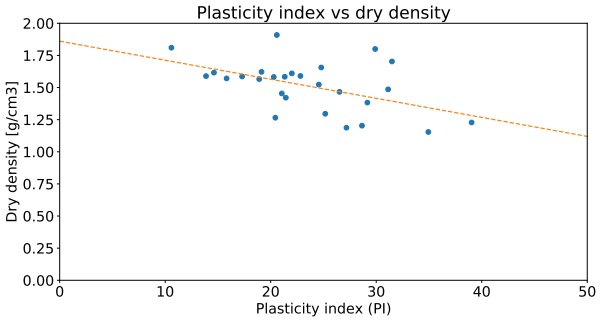

(c) Plasticity index

Figure 4.2: Relationship with dry density

4.1.2 Particle size distribution curves

For this research 16 particle size curves have been constructed. Of these, 15 have been of Ravenstein-Lith and one for the dike section of Veessen-Wapenveld (italicized entry in the table). Table 4.2 indicates per boring, the lutum ($< 2\mu m$), the silt ($2 < x < 63\mu m$), sand content ($63 < x < 2000\mu m$) and organic content.

Table 4.2: Distribution of sieve content per boring

Boring	Lutum [%]	Silt[%]	Sand[%]	Organic Content[%]
B012-3	21.0	69.7	9.3	2.1
B012-6	23.0	46.9	29.8	1.6
B014-3	36.0	60.5	2.8	1.9
B015-3	8.2	61.0	29.9	2.9
B015-5	16.0	54.3	28.9	0.8
B015-8	32.0	55.3	12.7	1.5
B036-4	36.0	62.6	1.4	2.2
B036-5	34.0	64.5	1.5	5.0
B038-4	22.0	40.9	36.7	3.4
B038-5	24.0	43.8	32.2	1.2
B038-6	31.0	66.9	2.1	1.2
B038-8	28.0	50.9	20.8	1.5
B039-1	25.0	64.8	9.9	1.5
B039-4	21.0	67.7	11.3	0.8
B041-3	13.0	47.7	38.3	1.2
B027-2	19.0	21.5	59.5	1.2
μ	24.7	57.2	17.8	1.9
σ	8.0	9.0	13.2	1.1

Note: The italicized entry in the table is a sample from Veessen-Wapenveld. As such it was disregarded in the calculation of the average and standard deviation of the respective content. The particle size distribution can be seen in Figure 4.3 and the textural plot of soils can be seen in Figure 4.4 respectively.

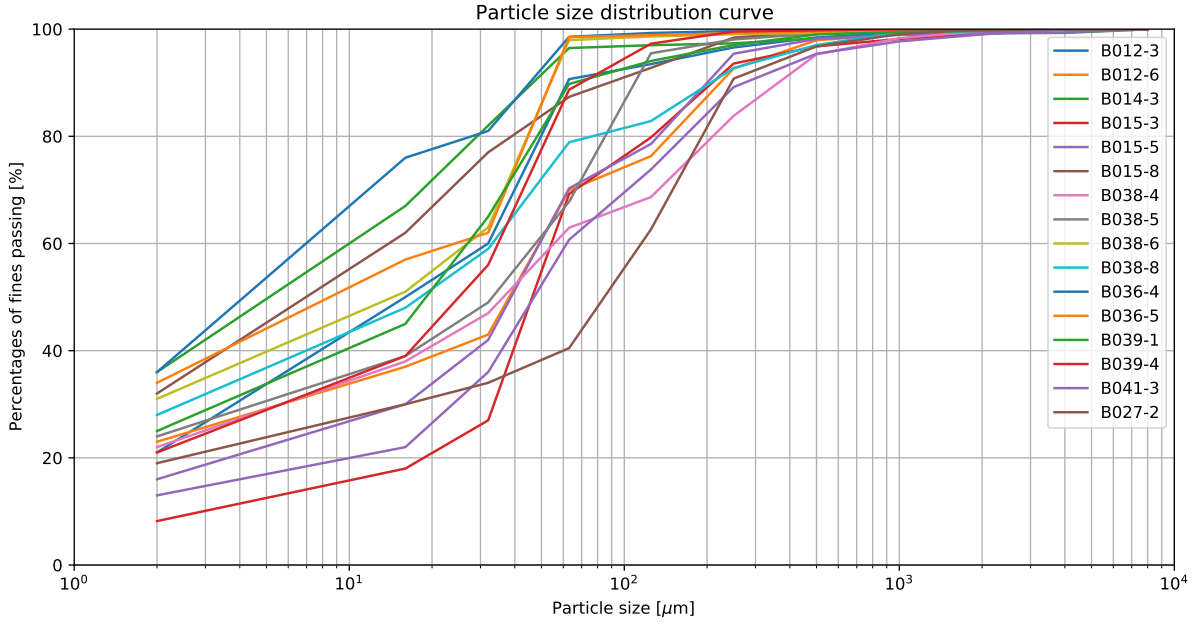

Figure 4.3: Particle size distribution curves of Ravenstein-Lith and Veessen-Wapenveld

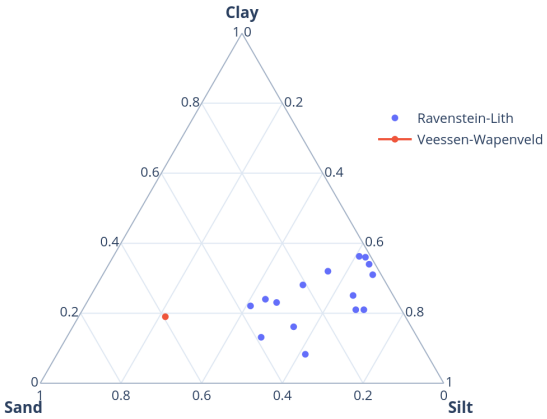

Figure 4.4: Textural plot showing the various fractions per boring

It is interesting to note that while the textural plot clearly shows that the soils are dominated by silt, the plasticity chart indicates that the soils are being dominated by clay. As the soils have a significant silt and sand component, their physical properties in laboratory testing may deviate from a typical clay. If the soil is to be correctly characterized as a silty clay or a clayey silt, it raises the question whether dilatancy is sufficiently considered in the plasticity chart. However, when the lutum, silt and sand content are plotted versus the plasticity index it is impossible to establish a trend (Figure 4.5). According to NEN-EN-ISO 14688-1 (2019) all samples in this research can be classified as weak calcareous homogeneous silty clay with a colour range of lightgrey to darkbrown.

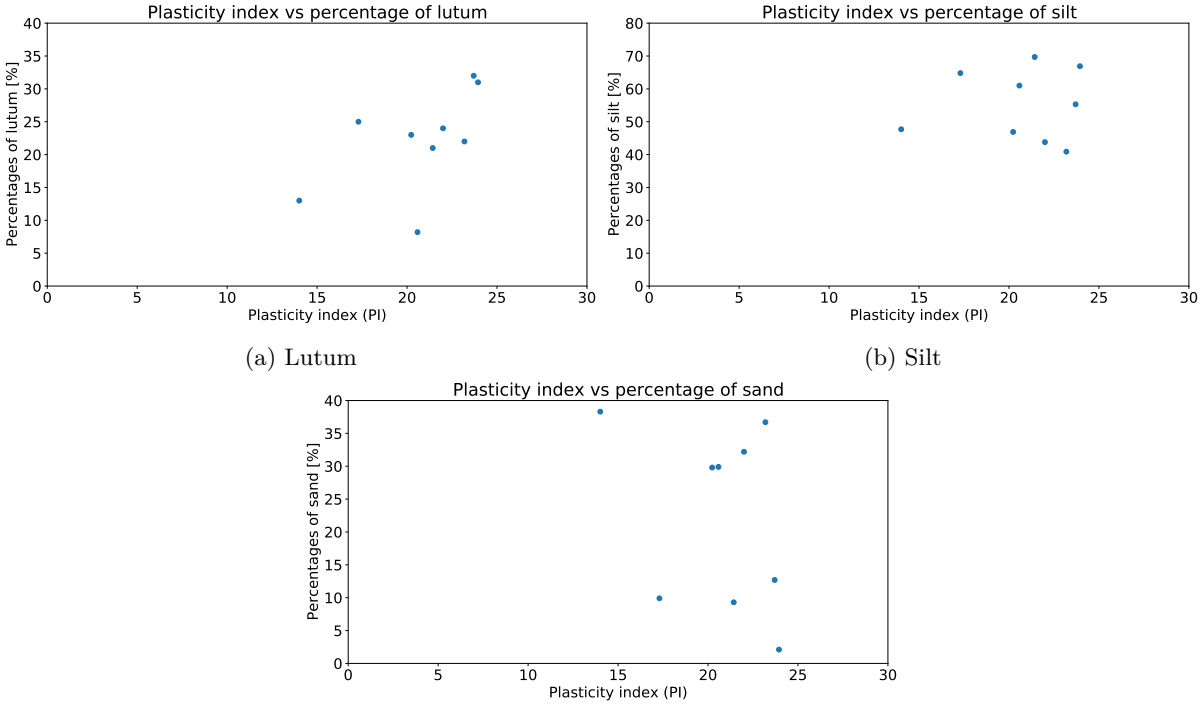

(a) Lutum

(b) Silt

(c) Sand

Figure 4.5: Relationship with dry density

4.1.3 Consistency index

The consistency index of a soil ((Liquid Limit- Natural Moisture content)/PI) can be used as an estimate of the firmness of a soil. An overconsolidated soil with natural moisture content less than the plastic limit will have an $Ic < 1$, whereas a sensitive clay may have an $Ic > 1$. Based on 31 samples for which the Atterberg limits where determined, the soil can be classified as medium stiff (Ic = 0.25-0.50) to very soft soil (Ic = 0.75-1.0) with most samples classified as soft soil (Ic = 0.50-0.75). The activity of a soil indicates whether a soil is prone to swelling and shrinkage behaviour. To calculate this, for each sample the plasticity index must be divided by the lutum content. For 10 samples this information was available and this classified the soil as a normally active clay (between A_t = 0.75-1.25). This means that some swelling and shrinkage behaviour is expected.

4.2 SWCC

In this thesis the SWCC is measured using a tensiometer (Hyprop; Decagon devices) to measure suction forces up to 100 kPa and a WP4C (Decagon devices) which measures suction forces between 100 kPa and 300 MPa using the dew point chilled mirror technique. The latter technique is the easiest as it only requires a cup with a few grams of soil to measure the amount of matric suction. For each datapoint three independent measurements were taken and then averaged. Per data point this process takes approximately half an hour and afterwards the sample is put in the oven for at least 24 hours at 105 ° C to determine the gravimetric water content. This analysis used these specific methods as opposed to others as the TU Delft geotechnical laboratory was equipped with only these.

The Hyprop on the other hand, is a more complex measurement device, and it takes approximately one week to obtain a measurement curve. Half of this time can be attributed to the proper set-up of the experiment as it requires that all air bubbles in the measurement cell and tensiometers have been removed by means of applying a vacuum, and the other half can be attributed to the actual measurement and the oven drying after the test. As there is a risk of cavitation in the tensiometers in the Hyprop, the results should be carefully analysed to see until which value of matric suction the measurement data is valid. The WP4C measures the total suction which is the sum of matric suction and osmotic suction. If a wet sample is measured in the WP4C, the corresponding value can be assumed to be the contribution of the osmotic component and hence all measurement data can be corrected using this value. Figure 4.6a displays the sample that was used in the Hyprop device and Figure 4.6b displays several samples that were measured using the WP4C (note that the darker colour of the sample indicates a wetter sample which experienced less matric suction).

(a) Hyprop sample (b) WP4C samples

Figure 4.6: Some of the samples used for the determination of the SWCC

The Van Genuchten-Mualem equation was fitted to the measurement data and optimized using the non-linear optimization Nelder-Mead algorithm (Nelder & Mead, 1965). The result of this method and the measurement data based on a soil sample of boring B036-4 of the Ravenstein-Lith trajectory can be seen in Figure 4.7 and the parameters can be seen in Table 4.3.

Table 4.3: Optimised Van Genuchten-Mualem parameters

θ_r	θ_s	α	n
$8.6216e^{-11}$	0.5266	0.0284	1.3180

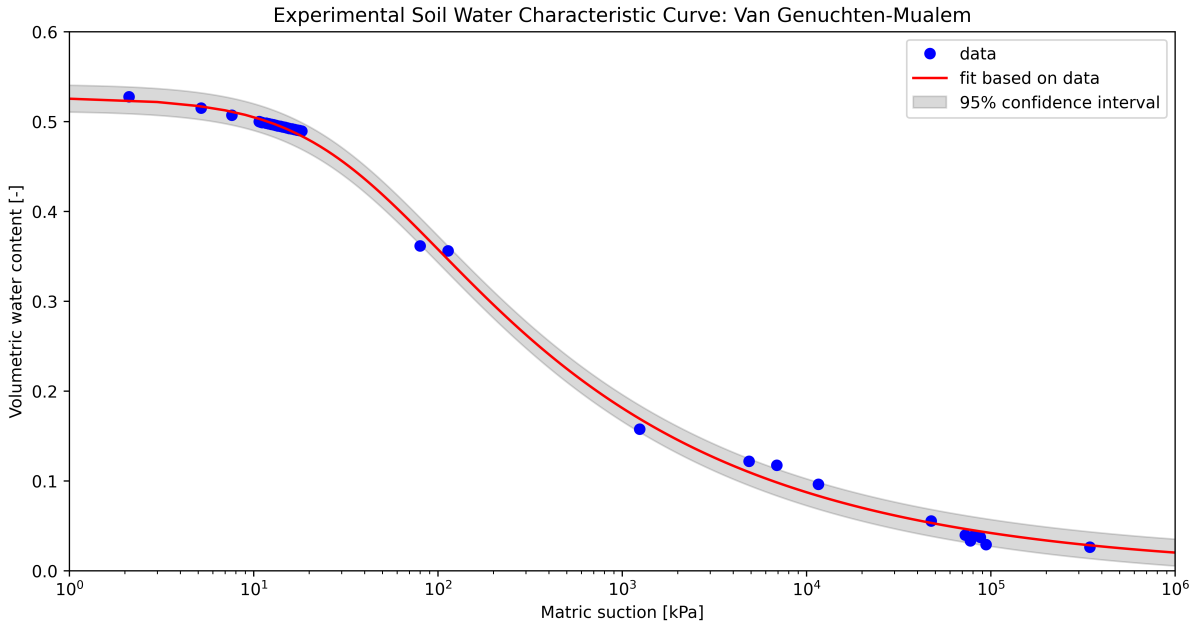

Figure 4.7: Experimental SWCC measurements fitted to Van Genuchten-Mualem

Based on the particle size distribution curves it can be noted that the soil characteristics of this boring (BO36-4) deviates as opposed to the mean values. This boring deviates approximately 1.5 x the standard deviation from the mean lutum percentage, is within one standard deviation from the mean for the silt percentage, is more than 1 standard deviation from the mean sand percentage and is within one standard deviation from the mean organic content. It must therefore be noted that locally, the shape of the SWCC may be slightly different, as its shape mainly depends on the make-up of the soil.

4.2.1 The Staring Series

In literature there are several databases to determine Van Genuchten-Mualem parameters. One of these databases is the Staring series developed by Heinen et al. (2020) for the Netherlands. It classifies both top soils (code starting with a B) and lower soils (code starting with a O) based on both the soil particle gradation and the organic content of the soil. If the Staring series approach for soil quantification is followed, the mean organic content is 1.2%, lutum content (all particles smaller than 2 μm) of 24.7 % and a silt content (all particle smaller than 63 μm) of 81.9 %. Based on these characteristics three soils in the Staring series would be an acceptable match to the soil used in this research. The Staring characteristics are displayed in Table 4.4.

Table 4.4: Staring parameters

	Parameters			
Staring series	θ_r	θ_s	α	n
B04	0.02	0.462	0.0149	1.397
O08	0.00	0.454	0.0113	1.346
O09	0.00	0.458	0.0097	1.376

The possible matches are plotted over the experimentally determined SWCC (see Figure 4.8).

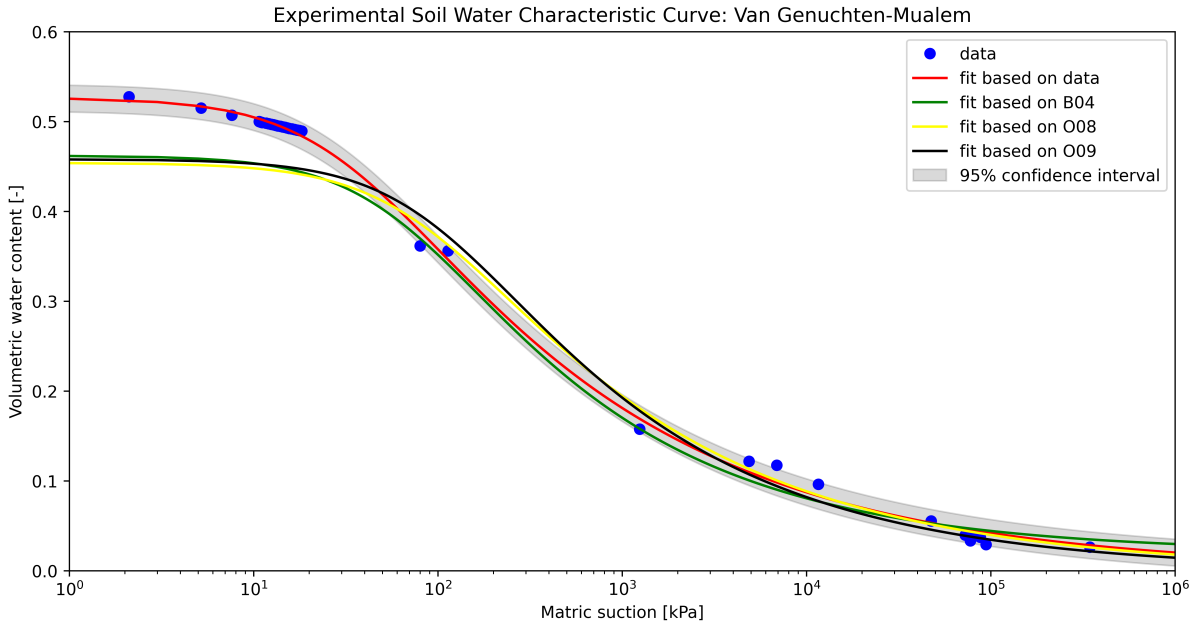

Figure 4.8: Experimental SWCC measurements fitted to Van Genuchten-Mualem with Staring series

It should be noted, that although the initial behavior is not matched well, the behavior matches quite closely beyond 100 kPa. Measurements by Van Duinen (2020) and interpreted by Buiten (2020) showed that suction stresses up to at least 80 kPa can be expected in a clay dike in the eastern part of the Netherlands (at Oijen and at Westervoort). This implies that the initial part of the SWCC is of importance and hence a good match would be required. This means, that although the Staring series can be used to give an indication of the expected SWCC, a unique SWCC should be determined for each distinctly different layer in a dike section if unsaturated behaviour is to be accounted for. Moreover, the Staring series was developed for agricultural soils and not for man-made dikes, explaining one of the reasons why discrepancies may occur. As the unsaturated hydraulic conductivity was not measured in the laboratory, the respective value of the closest Staring series will be considered when modelling the time- and spatially dependent distribution of matric suction.

4.3 Strain Compatibility

Gorinchem clay was shown to be prone to excessive strain softening and used the principle of strain compatibility to recommend that geotechnical strength parameters are to be determined at lower strains than currently are recommended in the Dutch guideline (Gori, 2020). The concept of strain compatability facilitates a comparison of the results of different geotechnical laboratory tests using the equations presented in section 3.1.2. The soil used in this research bears similarities to Gorinchem clay and therefore it is expected that strain compatibility can be applied too such that strength parameters can be determined at lower strain levels. Normally, for this analysis, DSS, triaxial compression and triaxial extension tests are to be used on NC samples with approximately the similar plasticity index and yield stress. In this research an attempt was made with several tests to show that this principle may be useful

too in the Ravenstein-Lith dike section. Please note that for this fully saturated samples are used to limit the influence of possible unsaturated effects, and thus this limits the number of adequate tests. Nonetheless, three NC DSS tests (DE1, DE2 and D20) and two NC K0-CAU triaxial tests (TC13 and TC14) were found to fulfill these conditions. The procedure outlined in section 3.1.2 was used to convert the axial strain in a triaxial test to shear strain such that results from both tests can be compared. The friction angle for triaxial tests is 26.38 degrees determined from the set of triaxial tests and subsequently fitted to a Mohr-Coulomb failure envelope (see section 4.4.4). The resulting graph can be seen in Figure 4.9.

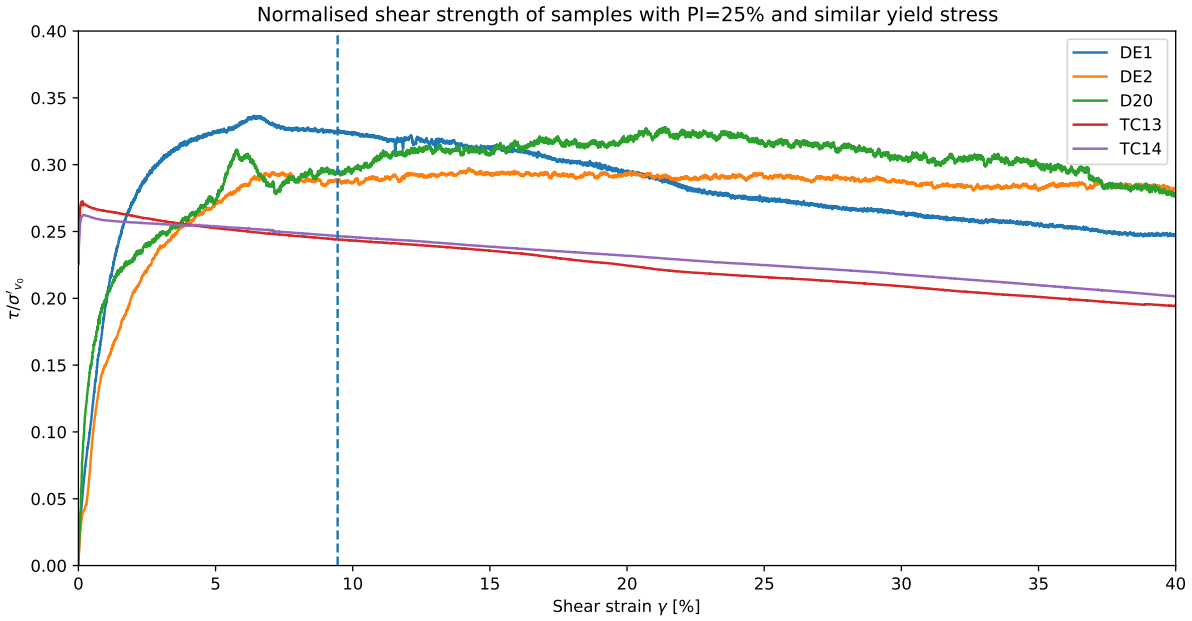

Figure 4.9: Strain compatibility using DSS and Triaxial compression tests

For Dutch soils the normalised shear strength is expected to be about 0.3 for NC soils, which is approximately reached. The dotted blue vertical line (at 9.45% shear strain) indicates the maximum stress ratio for triaxial tests. In the concept of strain compatibility, this should approximately coincide with the maximum of the respective DSS tests. Although limited tests are available for this analysis, these indicate that determination of geotechnical strength parameters at the recommended strain levels is conservative, but that these should be determined closer to those specified by Gori (2020). It could be argued that based on these few tests, that parameter determination can be done at even smaller strains, but as only few tests are available the recommended values by Gori (2020) will be used as a conservative approach. Therefore, in thesis, geotechnical parameters will be determined at 15% shear strain in DSS tests and at 10% axial strain in triaxial tests.

4.4 Triaxial tests

4.4.1 Set-up of the triaxial test program

In this research triaxial tests have been performed on a GDS shearbase system with either a 1 or 5 kN loadcell subject to availability. The tests have been conducted in accordance with the latest version of the relevant Dutch protocol - Protocol Laboratoriumproeven voor grondonderzoek aan waterkeringen (Greeuw et al., 2016). The aim of these tests was to (i) to determine whether the SSCC can be succesfully applied to K0-CAU tests and (ii) to determine geotechnical strength parameters in accordance with the SSSC concept. For the latter, the objective was to perform approximately 3-5 tests for at least three different levels of water content at varying stress levels.

4.4.2 Specimen preparation

For this test an undisturbed sample from for e.g. an Ackerman tube is trimmed to its predetermined height and diameter. Currently, in the Netherlands (but also in the international version of the norm), a sample of 100 mm in height and 50 mm in diameter is prescribed. In the past, smaller samples were used (with a diameter of 38 mm) but these were found to suffer from more pronounced sample disturbance compared to larger samples. Due to the trimming process, the sample often deviates slightly (depending on the skill of the technician this may be a tenth of a mm to several mm at most) from the prescribed height and diameter, but nevertheless it is still a valid sample a long as the height to diameter ratio is between 1.8 and 2.2. Figure 4.10a displays the temperature controlled storage room required for preservation of soil samples and Figure 4.10b displays a device which is used to trim triaxial samples.

(a) Temperature-controlled storage room (b) Trim device

Figure 4.10: Preparing a triaxial sample

At this stage, the water content of the sample can be determined, and the choice can be made to air-dry the sample to a specific water content. Practically this meant, that the sample should be turned every 1-2 hours such that the sample dries evenly, and that crack formation does not occur. Once the sample has reached its target mass, it is wrapped in plastic and placed in the fridge at 7 ° C for at least 24 hours such that the pore water in the sample will again be homogeneously distributed. The exact time can be calculated if the consolidation coefficient of the soil is known.

After trimming, the sample is weighed and is installed on moist porous stones. If dry stones were to be used, in which air is present within the pores, this in turn may result in incorrect measurements from the volume controllers due to air bubbles. On the other hand, completely wet stones, would result in the sample absorbing an unknown amount of water due to the suction forces inside it. If the stones are moist, meaning that on the side of the sample the stone is tapped dry with a piece of paper, the volume measurements of the back pressure volume controller will be more accurate, while at the same time minimizing the amount of water being absorbed by the sample. However, this does mean that there is an inaccuracy in the measurement of the mass (and therefore the water content) of the sample, but this inaccuracy is approximately equal for all samples. Another inaccuracy, inherent to this technique, is when testing increasingly dryer samples that air bubbles may infiltrate the volume controllers. These measurements are used to determine the diameter of the sample and in turn all stresses and therefore directly influence the test results. One of the ways that this could be reduced, is by using special volume controllers that can also measure the amount of air or by using a custom set-up where the existing volume controller is attached to a scale such that the mass displaced can be measured more accurately.

The next step is to attach so-called paper consolidation strips to the sample. The function of these strips is to speed up the consolidation process inside the triaxial cell. These strips influence both the vertical and horizontal stresses in the sample and thus must be corrected according to NEN-EN-ISO 17892-9 (2018). Similarly, a correction factor is required due to the influence of the membrane on both the vertical and horizontal stresses in the sample.

If the sample is properly installed inside a triaxial cell, it can be filled with de-aired water and installed on the load frame. An example of the triaxial set-up used in this research can be seen in Figure 4.11. The first step in a K0-CAU test, is to isotropically consolidate the sample to a cell pressure. In this thesis, NC triaxial test have been performed, which means that according to the Greeuw et al. (2016) a K0 value of 0.45 for this type of clay can be used. The cell pressure can then be calculated by multiplying the K0-value by the so-called B Value which is retrieved from a CRS test. If instead of a CRS test an oedometer test is used, the B Value can be approximated as 2.5 x the yield stress (Greeuw et al., 2016). In 2020 an exhaustive laboratory research has been performed on the dike section Ravenstein-Lith by Inpijn Blokpoel ingenieurs and for most of the borings oedometer tests had already been performed. In addition to this, two oedometer and four CRS tests have been performed. The additional oedometer tests were performed on the same boring as two of the CRS tests and this showed a difference in the yield stress. However, this is often seen in geotechnical practice and currently a topic of research. For all triaxial test, this B-value was determined to be at least 2.5 times the yield stress, but if permitted by the load cell, this value was increased to 3-4 times the yield stress. The advantage of this, is that one with more certainty could state that the test is executed normally consolidated and thus virgin soil behavior can be observed in the tests.

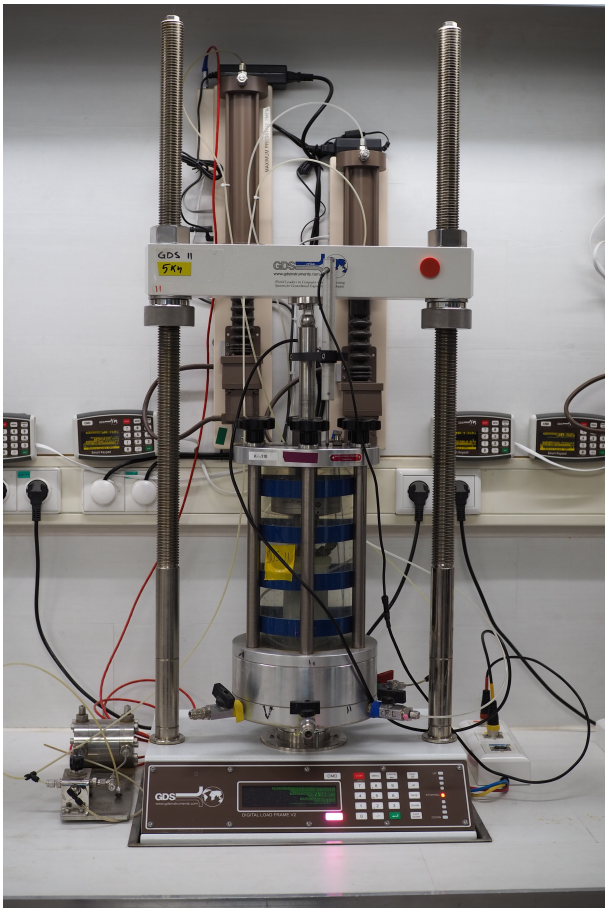

Figure 4.11: A triaxial apparatus

To check whether the consolidation phase is finished (often after about 24 hours), a check is performed by setting the back volume controller to hold volume. If the difference in pore water pressure is not more than 3 kPa per 30 minutes (Greeuw et al., 2016), the sample can be stated to be consolidated. The next stage is to anisotropically consolidate the sample. This can be done by slowly applying a load to the sample. This load can be determined by taking the difference of B-value stress and the cell pressure divided by the surface area of the sample. A practical rule-of-thumb states that this load is applied in 10 x the pressure difference minutes. This means that if this difference is 100 kPa, the load will be applied in 1000 minutes to the sample. Again, it must be checked whether the sample has finished consolidating after the load has been applied (typically 24 hours after the load has been applied).

Finally, the sample can be sheared to at least 25% strain to determine its strength parameters. The shearing rate is determined according to NEN-EN-ISO 17892-9 (2018), but in practice this meant for all samples that the shearing rate is 1% per hour. After this stage, the sample can be removed from the triaxial cell. After several tests, it was observed that the calculated volume based on the measurements of the volume controllers did not closely match the actual volume of the sample. For the relatively moist samples (θ_{vol}> 33.50%), this difference between the calculated and the measured volume of the sample was at most approximately 1-5 cm^3 (0.5%-2.5% of the total sample volume), whereas for dryer samples this difference was potentially up to 30 cm^3 (15% of the total sample volume). This difference can likely be attributed to the nature of the unsaturated samples which have a (large) amount of air entrapped inside the sample. As air is compressible, this means that the volume measured by the volume controllers is not necessarily correct. As the volume is used to determine the diameter of the sample, which is in turn used in the calculation of the different pressures on the sample, this directly impacts the interpretation of the respective test too. It was therefore decided to determine the volume of the sample at the end of each test by means of wet weighing according to NEN-EN-ISO 17892-2 (2014). If linear interpolation is assumed to be valid in both the isotropic and anisotropic consolidation phase, the difference in volume measurements could be corrected such that after the shearing phase the calculated volume matched the measured volume. A comprehensive guide describing how an unsaturated K0-CAU triaxial test should be performed can be found in Appendix B.

4.4.3 A guide to performing conventional K0-CAU triaxial tests using the SSCC concept

In literature no clear description is available how conventional laboratory tests are to be conducted using the SSCC concept. Although Xing et al. (2016) presented their test procedure, some questions were raised over which valves were closed during which phase during the test. This meant that several triaxial tests had to be used to determine how this method works in practice, and more importantly, to make sure that indeed that all possible ways of interpretation of their test procedure were checked. Especially the following two italic sentences were open to debate: *After the excess pore water (air) pressure generated by the application of confining pressure was completely dissipated, the axial stress with the axial deformation rate 0.04 mm/min was applied to the specimen. During the shearing phase, the drainage valve was kept closed and the excess pore pressure was monitored at the bottom of the specimen (Xing et al., 2016).* This is an inherent contradiction as during conventional triaxial testing the drainage valves are open during the consolidation phase to allow dissipation of pore pressures before being closed during the shearing phase (in an undrained test).

One test was performed where drainage was allowed during consolidation before being shearing (TC1) and one test was performed where drainage was prohibited during consolidation before being sheared (TC16) (see Figure 4.12). It clearly showed that for a test performed such as TC16 that the K0-value can never truly be reached as due to the constant suction force in the sample, the horizontal effective stress is constantly increasing throughout the test. Normally, this value would remain approximately constant throughout the test as it can be directly related to the prescribed cell pressure minus several correction factors for the membrane and filter paper as described above. Thus this test showed, that the test procedure as described above, is in fact the correct one and should be used.

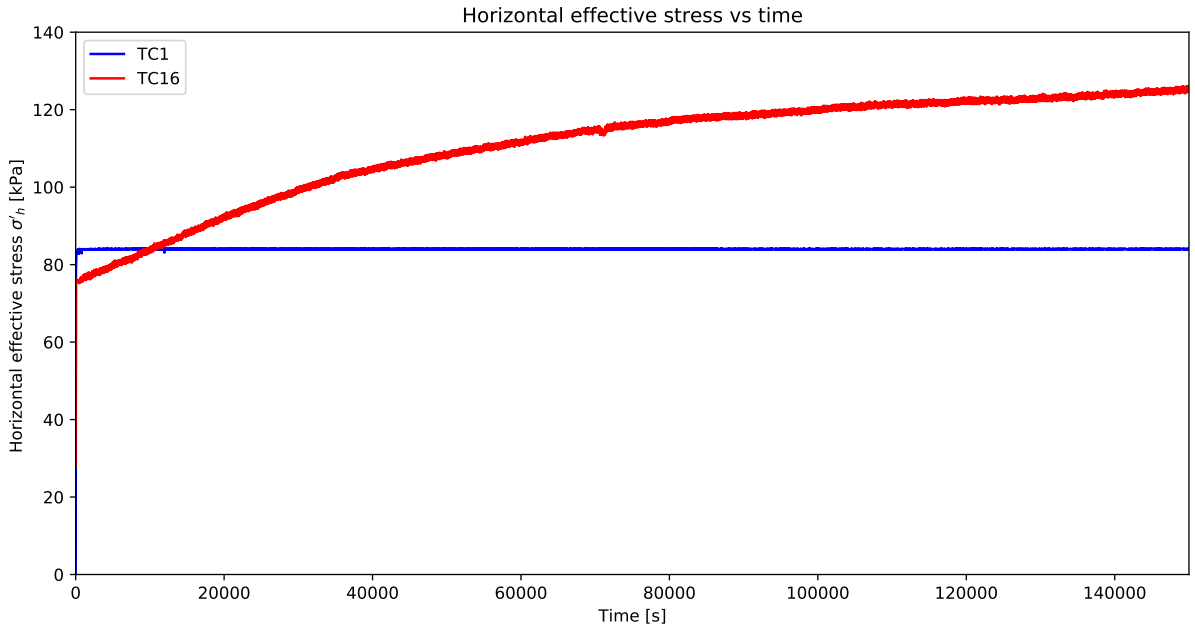

Figure 4.12: Check to see which method should be used to perform a K0-CAU triaxial test

4.4.4 Interpretation of results

In the SSCC concept it is of importance that for analysis the tests are grouped per volumetric water content respectively. In this section only the final results of the conventional K0-CAU triaxial tests will be presented and a complete overview of graphs displaying the soil behaviour can be found in appendix A for each volumetric water content. Figure 4.13 displays the failure mode of a triaxial sample for each volumetric water content. A complete overview of the 27 tested specimens and relevant parameters is displayed in Table 4.5.

Figure 4.13: Overview of the failure mode corresponding to the driest specimen (L) to the fully saturated (R)

Table 4.5: Geotechnical strength parameters at 10% axial strain

Average θ_{vol}	Test	θ_{vol} [-]	s' [kPa]	t [kPa]
51.50	TC13	51.60	140.06	68.93
	TC14	49.49	182.41	87.94
	TC20	51.13	200.81	99.25
	TC22	52.78	219.96	102.47
	TC32	52.49	183.31	79.82
42.05	TC8	39.99	240.54	124.26
	TC12	41.90	176.97	91.63
	TC15	42.70	227.37	115.91
	TC19	43.20	220.47	108.81
	TC21	41.90	172.33	91.54
	TC23	42.60	321.60	160.07
35.87	TC1	35.41	184.90	105.99
	TC3	37.05	153.52	83.56
	TC6	35.80	242.16	120.99
	TC7	34.53	238.18	126.67
	TC9	36.57	246.00	122.99
33.50	TC4	33.73	270.40	158.26
	TC10	34.18	306.70	174.55
	TC17	32.60	317.78	181.23
26.01	TC11	26.31	326.81	193.04
	TC18	25.70	380.47	204.07
	TC25	27.20	629.76	289.76
	TC27	26.90	271.02	133.45
16.09	TC28	15.30	673.81	278.72
	TC29	16.22	331.32	186.08
	TC31	16.66	381.05	199.72
	TC34	16.19	541.15	240.17

For each volumetric water content, based on the s' and t values, Mohr Circles were plotted to which a Mohr-Coulomb failure line was fitted. The complete overview of all Mohr-Coulomb failure lines is shown in Figure 4.14. Please note that although the volumetric water content differed slightly for each group of triaxial tests, the different distinctions were based on the measured SWCC such that at most the difference was 50 kPa between the lowest and the highest value of volumetric water content within a group, and then averaged.

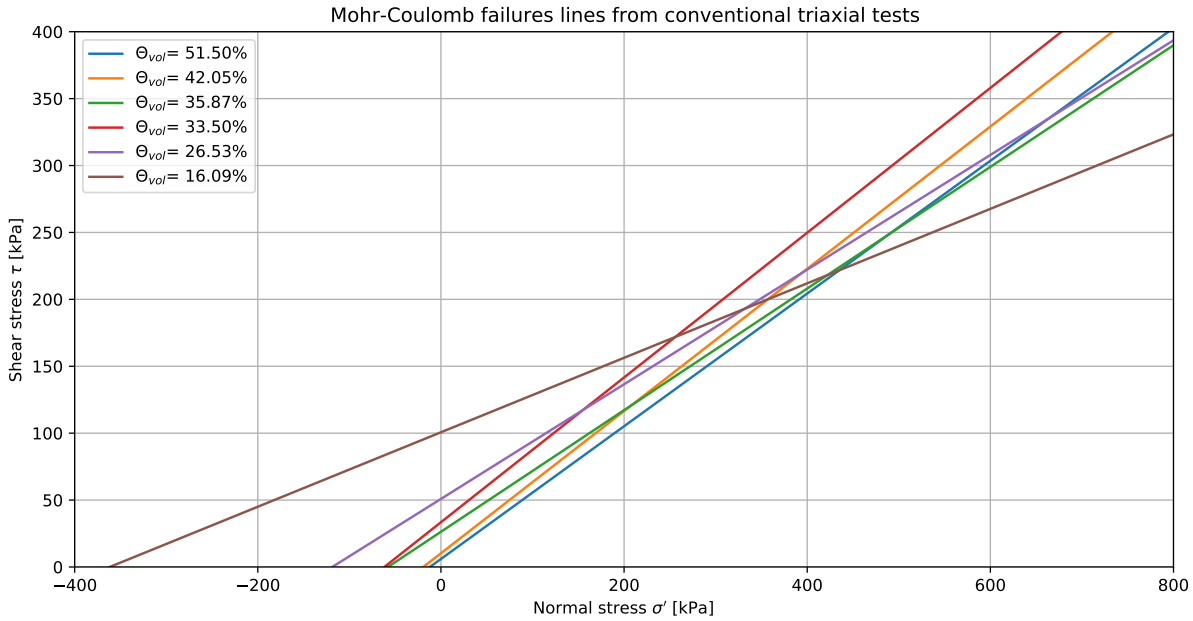

Figure 4.14: Mohr-Coulomb failure envelopes for varying volumetric water content

It can be observed that all lines roughly have the same slope, except for the two driest samples, as opposed to findings by Xing et al. (2015). This can most likely be attributed to the presence of air particles in the volume controllers as well as by imperfections in the dimensions of the sample due to uneven shrinkage. An overview of relevant parameters can be seen in Table 4.6.

Table 4.6: Average geotechnical strength parameters at 10% axial strain

θ_{vol}	w [%]	c' [kPa]	ϕ' [°]	σ_s [kPa]	ψ [kPa]	τ_{SSCC} [kPa]	τ_{Bishop} [kPa]	$\tau_{Fredlund}$ [kPa]
51.50	41.20	5.97	26.38	-12.04	5.97	6.08	7.38	7.43
42.05	29.00	10.26	27.99	-19.30	48.86	9.75	17.48	17.93
35.87	22.42	26.30	24.44	-57.89	99.02	29.25	29.29	30.20
33.50	20.94	33.44	28.41	-61.82	128.60	31.23	36.25	37.43
26.53	16.58	50.86	23.19	-118.71	290.51	59.97	74.38	77.05
16.09	10.06	100.66	15.55	-361.70	1456.96	182.74	349.06	362.44

The suction stress characteristic curve is presented in Figure 4.15. In this figure both the closed-form SSCC is plotted based on the experimentally determined Van Genuchten parameters and the values determined which were found as a result from conventional K0-CAU triaxial tests. It should be noted that the triaxial samples in this study come from different in-situ borings, and hence heterogeneity in the properties is expected (which can be verified using the Atterberg limits and the particle size distribution curves). Nonetheless, the experimental results seem to match the theoretical closed-form SSCC remarkably well and thus it can be concluded that this method seems to work well for anisotropic triaxial tests and that the tests were executed with sufficient precision.

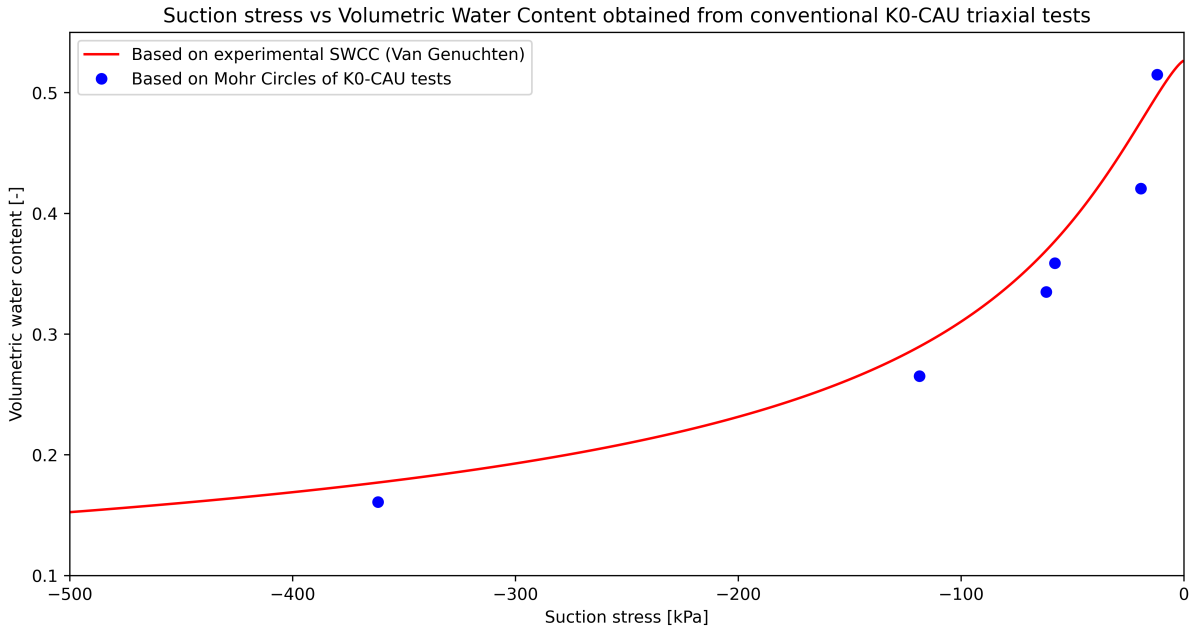

Figure 4.15: Suction stress characteristic curve

Using the SSCC, relevant design graphs can be determined being both the volumetric and the gravimetric water content versus the effective cohesion in Figure 4.16 and 4.17 respectively. In these figures three horizontal lines are plotted which display, (i) 80 kPa being the maximum amount of suction measured in field experiments by Deltares at the time of this research, (ii) 150 kPa and (iii) 200 kPa which are most likely attainable but these have not been independently verified with field measurements and are solely meant to illustrate what the effect is on the effective cohesion which could be attributed to a soil layer if this amount of suction is verified to exist in the field. In the SSCC effective cohesion can be determined directly from the laboratory experiments, but it should be noted that this is the sum of fully saturated cohesion and the apparent cohesion due to matric suction. Thus if these graphs were to be used in critical state design (such as those used in the Netherlands), the fully saturated cohesion (which is the cohesion at the maximum volumetric water content) should be subtracted to form a curve of solely the apparent cohesion versus either the volumetric or gravimetric water content.

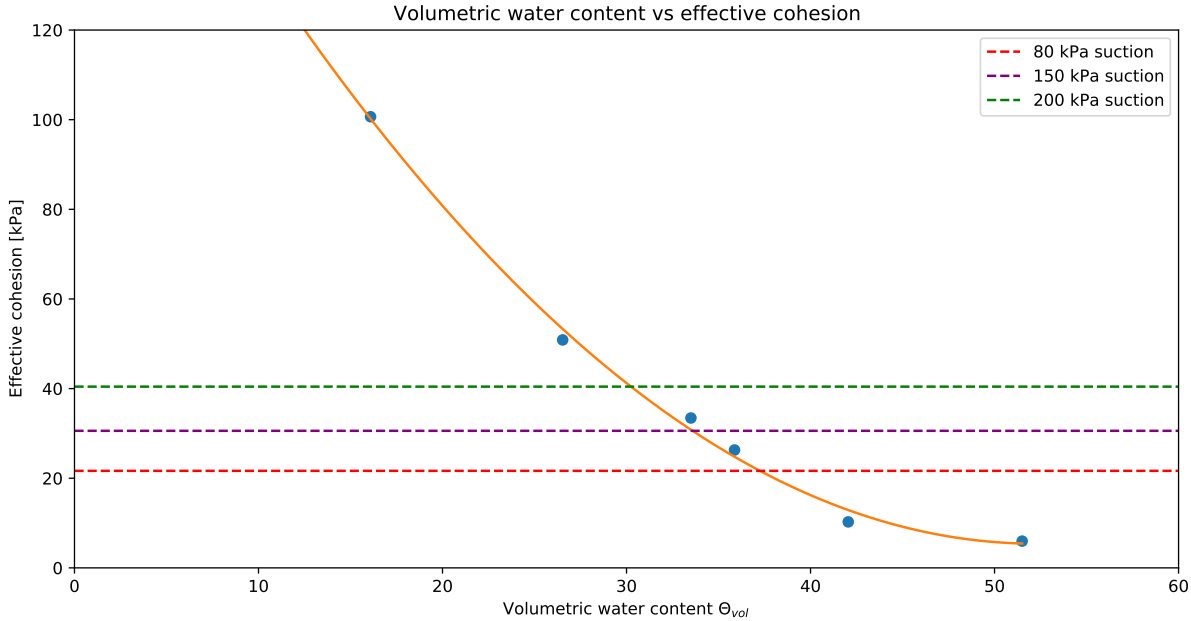

Figure 4.16: Volumetric water content versus effective cohesion

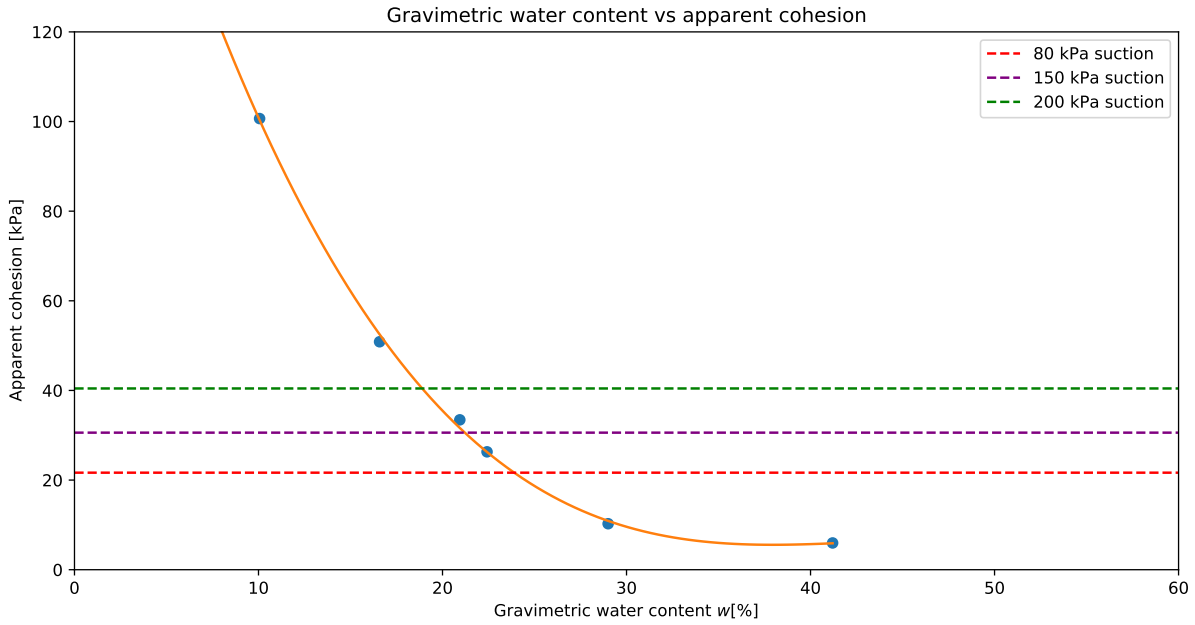

Figure 4.17: Gravimetric content versus effective cohesion

A general overview of how effective cohesion seems to develop versus suction is displayed in Figure 4.18. Please note that there is reason to believe that the two measurement points for which effective cohesion is highest deviates from the expected value and hence that only the first four measurements are accurate as concluded from Figure 4.14.

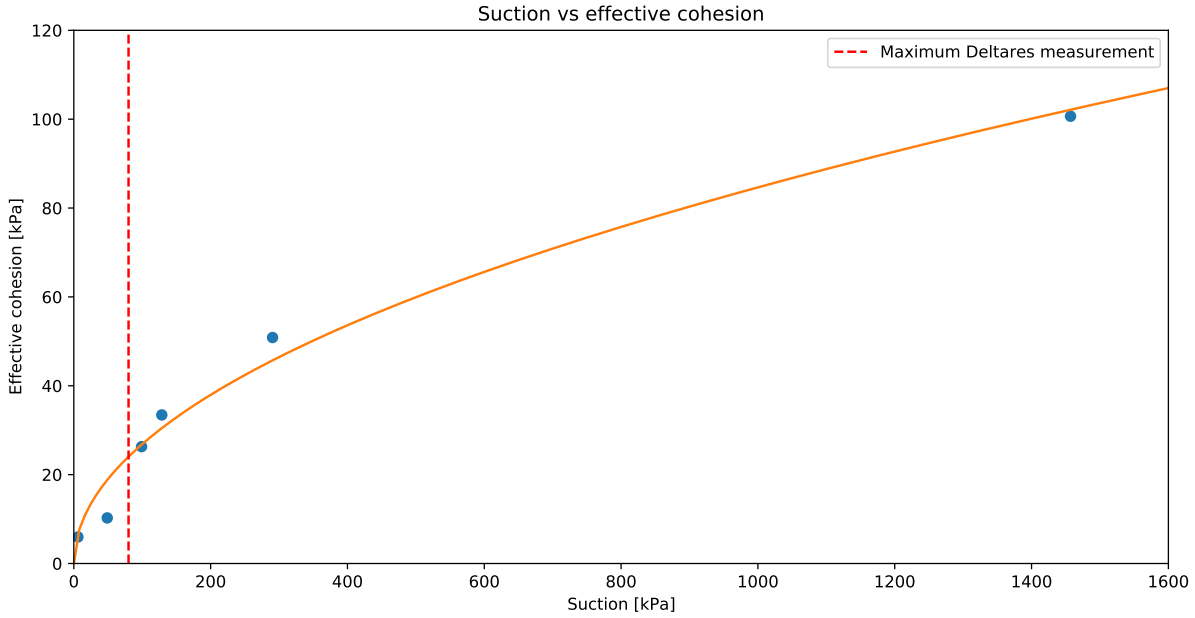

Figure 4.18: Suction versus effective cohesion

4.4.4.1 Determination Bishop and Fredlund and Morgenstern parameters

Using the experimental results an attempt is made to determine both Bishop's and Fredlund and Morgenstern shear strength parameters which culminates in a comparison of calculated shear strength versus matric suction. These parameters are determined in a similar fashion as is done in Xing et al. (2016). The effective friction angle, ϕ', is assumed to be the average of the results found from the Mohr-Coulomb failure lines. In this thesis, the first four measurement points are assumed to be approximately valid, and hence $\phi' = 26.3°$. The tangent of the slope of the regression line in Figure 4.19 is used to determine $\phi_b = 13.7°$.

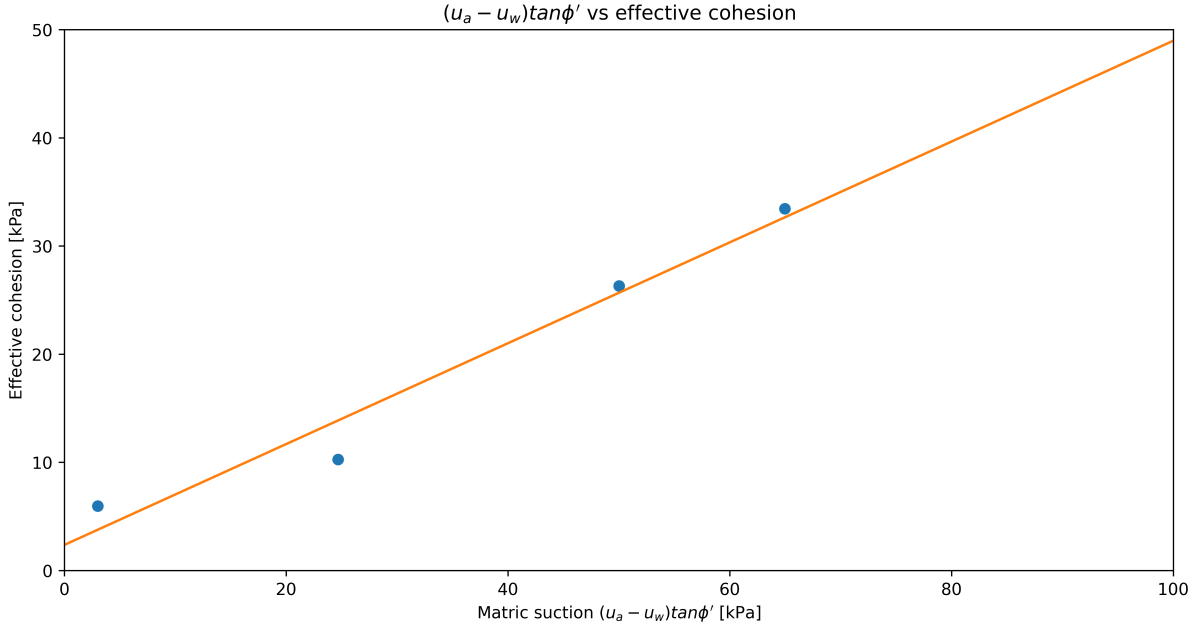

Figure 4.19: Determination of Fredlund and Morgenstern shear strength parameters

The slope of the regression line in Figure 4.20 is $\chi = 0.466$. Using the theoretical definition of $\chi = tan\phi_b/tan\phi'$ using the previously determined values, $\chi = 0.484$. This indicates good agreement between the two methods.

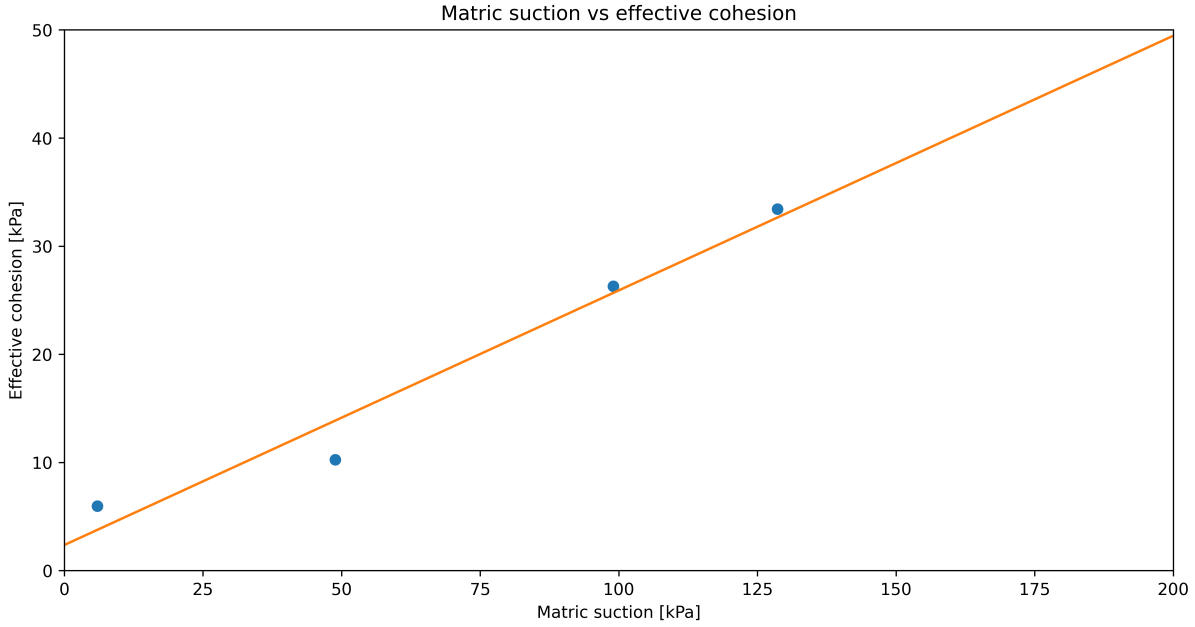

Figure 4.20: Determination of Bishop shear strength parameters

Figure 4.21 displays the shear strength versus matric suction based on the SSCC, Bishop and Fredlund and Morgensterns approach (see Equation 4.1, 4.2 and 4.3 respectively) and the respective input parameters can be found in Table 4.6.

$$\tau_f = (\sigma - u_a - \sigma^s)tan\phi' \tag{4.1}$$

$$\tau_f = c' + [(\sigma - u_a) + \chi(u_a - u_w)]tan\phi' \tag{4.2}$$

$$\tau_f = c' + (\sigma - u_a)tan\phi' + (u_a - u_w)tan\phi^b \tag{4.3}$$

It can be observed that both Bishop and Fredlund and Morgensterns approach are quite similar, whereas the SSCC starts to deviates from matric suction of 200 kPa. In part this is due to the the previously error in volume measurements for the extremely dry samples resulting in a very low friction angle. Moreover, it was assumed that χ, and thus both ϕ_b and ϕ', remain constant with increased matric suction in both Bishop and Fredlund and Morgensterns approach, whereas it is known that this is only true for low stress levels. For higher stress levels this is variable depending on the degree of saturation of the sample. Although, in Dutch conditions, if Deltares measurements are expected to be the upper boundary (or even 200 kPa as mentioned), all three methods produce similar results which deviate at most by 17.5% (which is to be expected due to the origin of the different shear strength formulations). Another reason why the deviation is greater for larger values of matric suction, becomes apparent from Equation 4.1 and Figure 4.15. As the equation of the curve in this figure originates from a Van Genuchten formulation, the impact of a deviation for drier samples is greater than for more saturated samples. This can clearly be observed from Figure 4.7 where especially a dry sample, with a relatively low volumetric water content, may be strongly impacted by the nature of the logarithmic curve if an uncertainty exists in the determination of the volumetric water content of the respective sample. This uncertainty is propagated through Equation 4.1. The large deviation in shear strength for the last data point in Figure 4.21 can likely be attributed to this error.

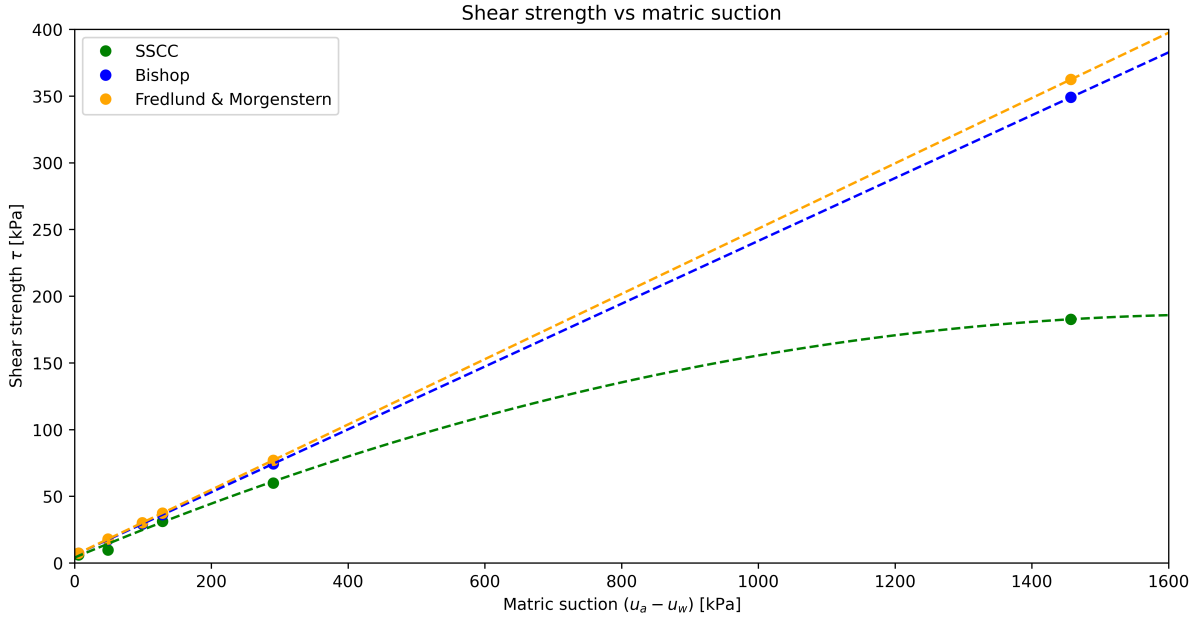

Figure 4.21: Shear strength for unsaturated soil using varying methods

4.5 Direct Simple Shear tests and preliminary results

In this section the set-up of the test program will be discussed followed by the presentation of the initial laboratory results as well as interesting observations.

4.5.1 Set-up of the DSS test program

In this research DSS tests have been performed on a GDS shearbase system with a 1 kN loadcell. The tests have been conducted in accordance with the latest version of the relevant Dutch protocol - Protocol Laboratoriumproeven voor grondonderzoek aan waterkeringen (Greeuw et al., 2016). The sample is enclosed by an unreinforced rubber membrane surrounded by concentric rings. On both sides of the sample, a porous stone with protruding cones is used. The aim of these tests was to (i) determine geotechnical strength parameters in accordance with the SSCC concept and (ii) obtain operational knowledge of DSS tests on clayey samples at low vertical stresses (<100 kPa).

The objective for the first aim was to perform approximately 3-5 tests for at least three different levels of water content. Especially the latter point is of interest as in Dutch geotechnical practice relatively few DSS tests are performed on clay samples. In dike design DSS tests are most often performed to determine geotechnical strength parameters of peat samples.

4.5.2 Specimen preparation

Similar to the triaxial tests, DSS tests samples were tested at saturated, in-situ water content and dryer conditions. For in-situ water content samples, the relevant Dutch protocol could be followed (Greeuw et al., 2016). For drying samples, the sample was taken with a cutting ring and then air dried to the specified mass before being covered with several layers of foil and left for at least 48 hours before testing would commence. For fully saturated samples, the sample was taken with a cutting ring, but then a porous stone was placed both on top and at the bottom of the sample before being placed in a container of water. Results in section 4.1.3 indicated that some swell could possibly occur and therefore on top of this an extra mass of 1 kg was placed such that the swell would be prevented. Please note that at this time the sample is still inside the cutting ring and thus the additional mass is carried by the cutting ring only and hence it does not impact the integrity of the sample. Moreover, the vertical stress that would be applied during the DSS test would be higher than any swell force that would be generated by 1 kg, implying that no significant changes in stress-strain behaviour would be expected due to swell. After 48 hours the sample was taken out of the container of water, covered in several layers of plastic foil and then, again with the additional mass on top, rested for at least 48 hours before testing would commence. As a final check, the height of the sample before saturation was measured, and just before installation into the DSS apparatus and there was no observable difference in height (within the 1 mm measurement accuracy of the measurement device). Figure 4.22a shows an example of a DSS apparatus used in this research and Figure 4.22b shows a sample in the process of saturation. An overview of the DSS specimens can be found in Table 4.7.

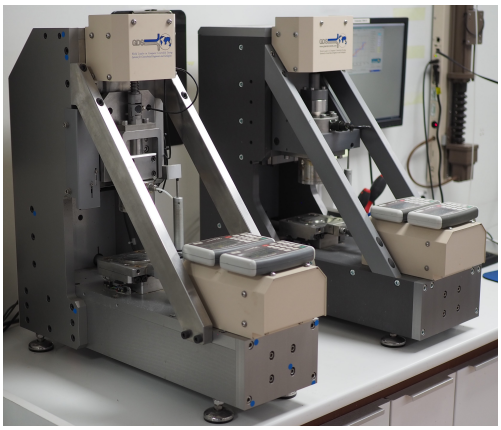

(a) A DSS apparatus

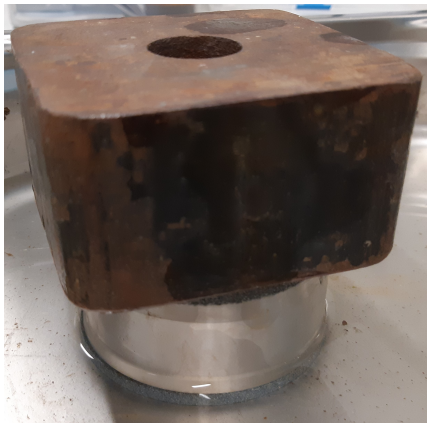

(b) Saturating a DSS sample

Figure 4.22: Set-up and preparation of DSS tests

Table 4.7: Characteristic parameters for each Direct Simple Shear test

Test	Boring	σ_{vo} [kPa]	Yield stress [kPa]	OCR	θ_{vol}	Strain rate [%/hr]	Note
D01	B014-2	22	62	2.82	0.45	5.0	
D02	B036-4	69	106	1.54	0.435	5.1	
D03	B014-2	22	62	2.82	0.445	5.0	
D04	B036-4	69	106	1.54	0.452	5.0	
D05	B036-5	75	115	1.53	0.458	5.0	
D06	B036-5	75	115	1.53	0.454	5.1	
D07	B014-1	13	36	2.77	0.422	1.1	
D08	B014-1	13	36	2.77	472	2.2	
D09	B014-1	13	36	2.77	0.452	2.0	
D10	B014-1	13	36	2.77	0.306	2.0	Very sandy
D11	B012-4	64	70	1.09	0.366	2.0	
D12	B014-1	13	36	2.77	0.135	2.0	Too dry
D13	B014-1	13	36	2.77	0.167	2.0	Too dry
D14	B038-4	31	103	3.32	0.395	2.0	Fully saturated
D15	B038-8	51	76.5	1.50	0.498	2.0	Fully saturated
D16	B015-5	77	163.4	2.12	0.402	2.0	Fully saturated
D17	B015-5	77	163.4	2.12	0.126	2.0	Too dry
D18	BO39-4	66	194.8	2.95	0.232	2.0	Too dry
D19	BO39-4	66	194.8	2.95	0.413	2.0	Fully saturated
D20	BO12-8	101	84.4	0.84	0.426	2.0	Fully saturated
D21	BO12-8	101	84.4	0.84	0.239	2.0	Original porous stone
D22	BO12-3	55	76.8	1.40	0.147	2.0	Original porous stone
D23	B038-5	39	107	2.74	0.086	2.0	Too dry
D24	B035-2	22	61.6	2.80	0.455	2.0	
D27	B012-2	46	54.9	1.19	0.417	2.0	
D28	B038-6	44	95	2.16	0.434	2.0	Fully saturated
D29	B038-6	44	95	2.16	0.434	1.9	
D40	B039-2	48	115	2.40	0.37	2.0	Stopped early
D41	B039-2	48	115	2.40	0.37	2.0	
DE1	B038-8	268	76.5	1.00	0.552	2.0	NC
DE2	B038-6	285	95	1.00	0.386	2.0	NC
V01	B027-2	60	-	-	-	2.0	Veessen-Wapenveld
V02	B027-5	32	-	-	-	2.0	Veessen-Wapenveld

Note: In this context, 'too dry', meant that these samples were unsaturated to such a degree that the DSS test could not be performed accurately and within the prescribed boundary conditions. The pins on the porous stones were unable to penetrate the sample and the stack of rings was unable to provide sufficient restraint due to excessive shrinkage of the sample. Please see section 4.7.3 for further details.

4.5.3 Preliminary DSS test results

Initially, several DSS test were performed samples from borings of Ravenstein-Lith (a complete overview of parameters can be seen in Table 4.5.2). These tests showed signs of slippage between the tests and the platens as well as diagonal failure surface. This prompted the author to execute a strain rate study to investigate its effect on the DSS tests in section 4.5.3.1, but also the interpretation method was studied and presented in section 4.5.3.2

4.5.3.1 The slip phenomenon

The initial test were sheared at a strain rate of approximately 5%/hr and then both the slip phenomenon and the diagonal failure plane were observed. All samples discussed in this section were performed at in-situ water content (and thus were unaltered) The results of these tests are shown below were Figure 4.23a displays the shear strength versus the shear strain and Figure 4.23b shows the normalised shear strength versus the normalised vertical stress.

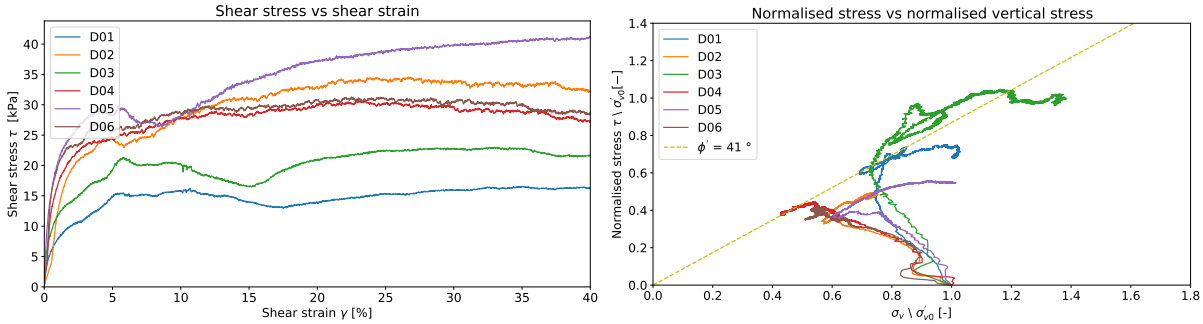

(a) τ vs γ

(b) τ/σ_{vo} vs σ_v/σ_{vo}

Figure 4.23: DSS tests performed at 5% /hr

Figure 4.23(a) displays striking behaviour for what is theoretically expected in a DSS test. Normally, in a DSS test, the sample is sheared such that the measured shear strength gradually increases, until a plateau is approximately reached. At this point the sample is normally said to have reached the so-called critical state. Samples on Gorinchem clay by Gori (2020) showed softening such that a plateau was never reached at the end of the test. However, these samples show an initial peak around 5% shear strain after which the shear strength diminishes until a minimum is reached at 10-15 % shear strain before increasing to a second peak. It is thought that at the minimum, the sample has (partially) failed and after this point membrane effects start to play a role. At large strains, some of the load may be carried by the membrane, and therefore a value for shear strength may be measured which does not occur in the sample. Based on this hypothesis, it would be recommended to disregard any part of the test after this point as the results are unreliable. When considering the normalised shear strength versus normalised vertical stress, odd behaviour can be observed too. Normally such a line is expected to curve to the right for an OC soil (which are performed in this research) and to the left for an NC soil. Generally, this behaviour occurs, but approximately halfway the line seems to follow a circular trajectory before continuing. This behaviour seems to approximately coincide with the minimum in the shear strength versus shear strain graphs.

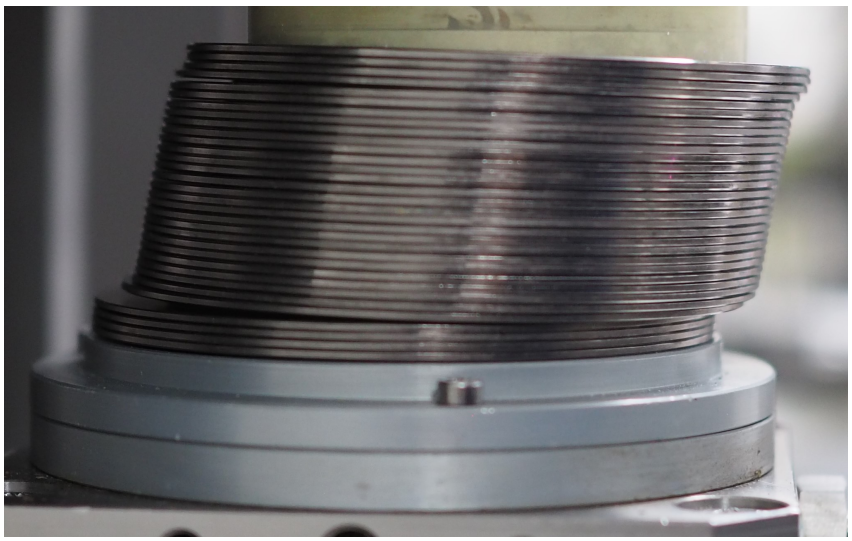

Figure 4.24: A DSS test in which slippage has occurred

The slip phenomenon can clearly be observed in Figure 4.24 where it can be seen that the stack of rings has not homogeneously sheared during the test and approximately three separate zones can be distinguished. After these initial tests in which the slip phenomenon was observed, it was decided to test whether the strain rate at which the test is performed potentially has any unwarranted effects. It was hypothesized based on Le Meil et al. (2016) that the clay may be sufficiently stiff. In this case, the metal pins on the porous stones would be dragged through the sample, and thus creating signs of slip. If the sample would be very stiff, applying a lower strain rate may reduce and or limit the magnitude of these effects.

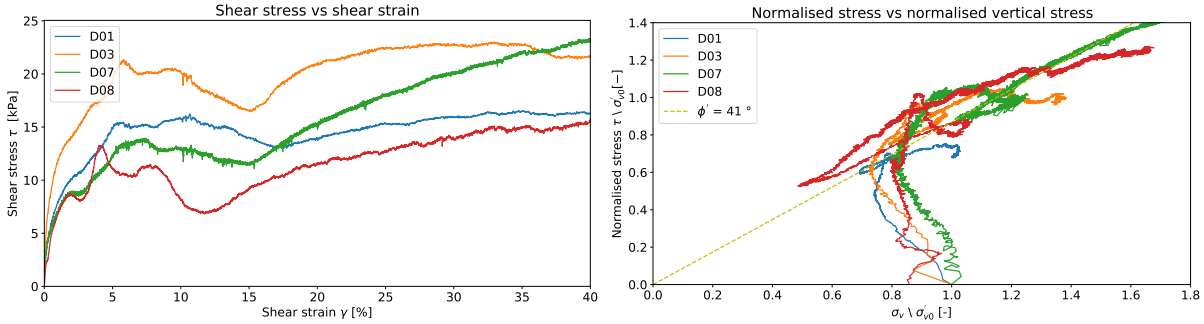

(a) τ vs γ (b) τ/σ_{vo} vs σ_v/σ_{vo}

Figure 4.25: DSS tests performed at varying strain rates

In Figure 4.25 the results from varying the strain rate can be observed. At a first glance, generally similar behaviour can be observed. However, when qualitatively investigating the top and bottom of the sample, it showed that at lower strain rates the length of the slippage gaps was lower too and more consistent over the entire sample as compared to those performed at 5%/hr. Little difference could be seen between the test performed at 1%/hr and the test performed at 2%/hr (although this could be related to soil heterogeneity and the limited number of tests too). To try and limit any adverse affects caused by a too high strain rate, it was decided, that all further DSS tests would be performed at 2%/hr. This strain rate was chosen for practical reasons such that the number of DSS test being able to be performed would not be affected.

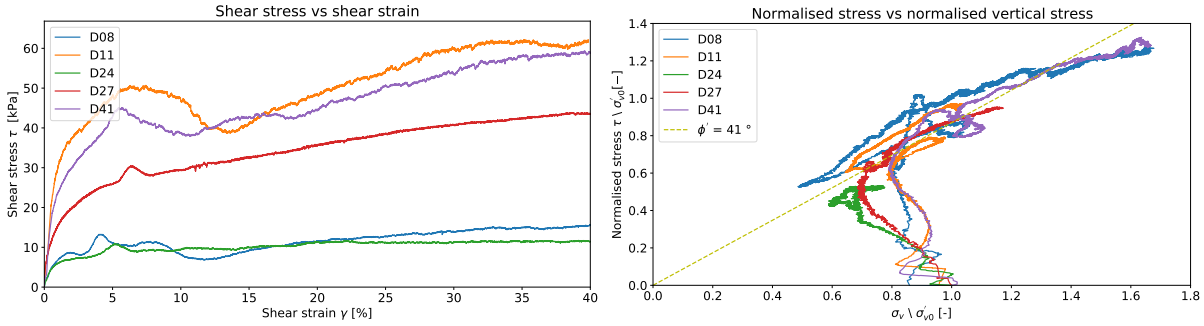

(a) τ vs γ (b) τ/σ_{vo} vs σ_v/σ_{vo}

Figure 4.26: DSS tests performed at varying vertical stress levels at 2% /hr

Figure 4.26 displays DSS tests performed at varying vertical stress levels while at 2%/hr. Generally the behaviour seems quite similar, but it should be noted that for samples tested at a higher vertical stress, less slippage was observed. As discussed in the literature study, this is to be expected, as a larger vertical stress creates more confinement at the soil-platen interface.

4.5.3.2 Traditional vs "AG method" interpretation

In these samples in which slip occurred, a clear diagonal failure pattern originating at the front of the top part of the specimen running to the back of the bottom of the specimen was observed in all samples. In section 3.5.5 two methods were discussed on the interpretation of the DSS test: one being the traditional method and the second one being the AG method (which was developed for samples with a diagonal failure plane). To the best knowledge of the author a comparison has not been made in literature between the two methods and therefore it would be interesting to see how they compare. Both methods have been applied and visualised to the results of two DSS tests of which one has been performed NC and one OC (see Figure 4.27).

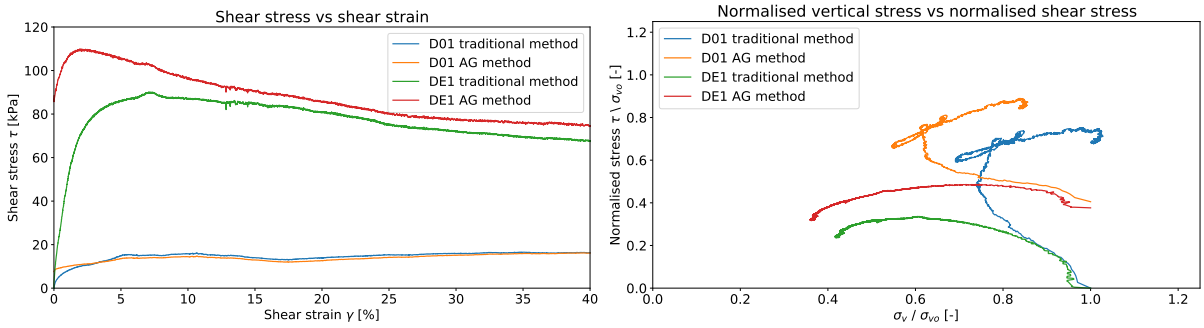

(a) τ vs γ

(b) τ/σ_{vo} vs σ_v/σ_{vo}

Figure 4.27: Comparison of results of DSS tests using different interpretation methods

Although both methods produce acceptable results, at this time, it is unclear which method represents best the conditions during the test in case of diagonal failure plane. The test can be modelled using Discrete Element Modelling such that the exact rotation of principle stress axis is known which enables accurate determination of the stress paths.

4.6 The Direct Shear test

In the previous section it was shown that slippage occurred at a relatively early stage in the test and concerns were raised pertaining to the validity of the DSS tests if slip occurs. Currently, Dutch design standards suggest that the geotechnical strength parameters should be determined at a shear strain of 40%. To determine the strength parameters for clay at this amount of strain does not make much sense given the obtained laboratory results, as (i) slip has occurred and (ii) membrane effects will play a role which will artificially increase the measured maximum shear strain. It was therefore suggested to check whether critical state would have been reached before slip starts to occur.

Although the Direct Shear tests inherently has a different shear plane, it would be possible to have a first order estimation at which percentage of shear strain, critical state would be reached. This has been investigated by means of 9 (of which 8 were valid) tests at the geotechnical laboratory of Deltares. Another important difference is that in this test the sample is submerged, meaning that is possible for the pore fluid to freely communicate with the water surrounding the shear box as opposed to the DSS tests. It was performed submerged, in accordance with section 6.5.3 in NEN-EN-ISO 17892-10 (2018) , as the objective of the DS test was to determine when critical state would occur as opposed to determining unsaturated strength parameters. Moreover, a substantial increase in the degree of saturation is not expected if a back pressure is not applied during the test (Borden & Putrich, 1986).

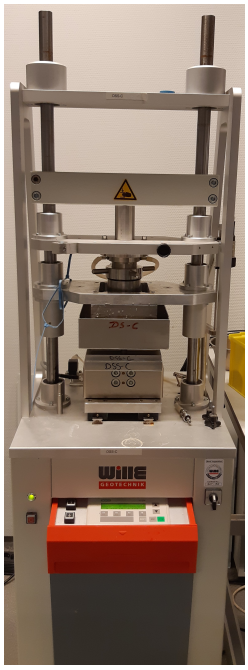

(a) A DS apparatus

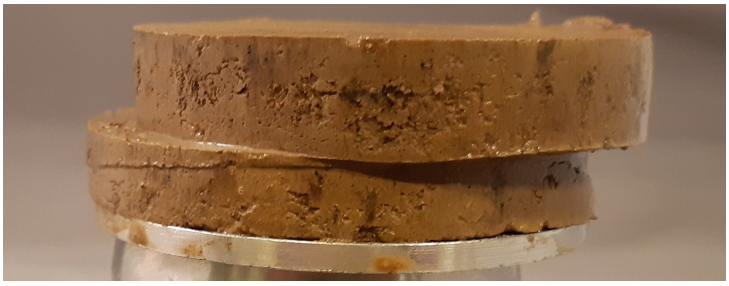

(b) Failure mode in a DS test

Figure 4.28: Set-up and failure mode of a DS test

Figure 4.28a displays a DS apparatus and Figure 4.28b shows the failure mode of a DS test. An overview of the tests and relevant parameters can be found in Table 4.8 below.

Table 4.8: Characteristic parameters for each Direct Shear test

Sample	DS1	DS2	DS4	DS5	DS6	DS7	DS8	DS9
Boring	B14-1	B12-4	B12-7	B12-5	B12-8	B38-5	B14-2	B12-7
σ_{vo}[kPa]	13.0	64.0	88.0	74.0	101.0	39.0	22.0	93.0
τ_{max} [kPa]	17.8	66.4	67.7	68.0	77.4	41.6	31.6	133.9
$\tau_{residual}$ [kPa]	15.2	64.5	66.8	68.0	73.8	41.6	29.1	130.0
$\tau_{max}/\tau_{residual}$	1.17	1.03	1.01	1.00	1.05	1.00	1.09	1.03
e_0	0.684	0.736	0.679	0.659	0.618	0.957	0.731	0.701
ρ_{dry} [kg/m3]	1584.7	1539.3	1584.8	1613.9	1548.3	1354.3	1530.7	1682.8
$w_{initial}$ [%]	21.3	21.6	15.6	19.5	28.7	27.1	25.6	17.5
w_{final} [%]	23.8	23.8	21.4	22.5	29.2	30.2	30.6	23.5

Note: Test DS3 was determined to be invalid as it was performed with a load cell with insufficient maximum measurement capacity.

An area correction to the measurements has been applied according to Bareither et al. (2008):

$$A_c = A_i \left[\frac{1}{90} cos^{-1}\left(\frac{\delta h}{D}\right) - \frac{2}{\pi}\frac{\delta h}{D}\sqrt{1-\frac{\delta h}{D}^2} \right] \tag{4.4}$$

where A_c is the corrected area, A_i the initial area, δh is the horizontal displacement and D is the diameter of the shear box. The normal and shear stress are then calculated by dividing the vertical and horizontal force by the corrected area.

It can be observed in Figure 4.29 which displays the stress-strain graph for each individual test, that there is sometimes a clear peak and residual shear stress visible, but for most tests this is not the case.

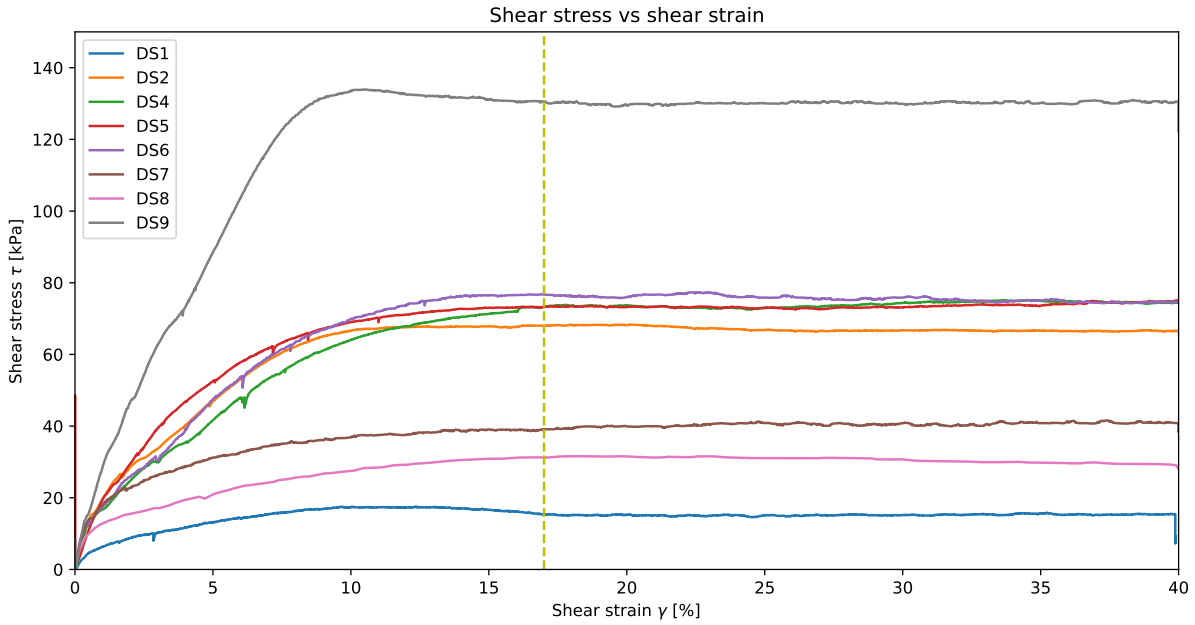

Figure 4.29: Direct shear test results

If then the normalized stress versus shear strain is plotted, where the normalized stress is the shear stress divided by the initial normal stress, Figure 4.30 is obtained. This figure also clearly shows that normally consolidated samples (with a peak expected around 0.2-0.3 for Dutch soils) as well as overconsolidated samples have been tested.

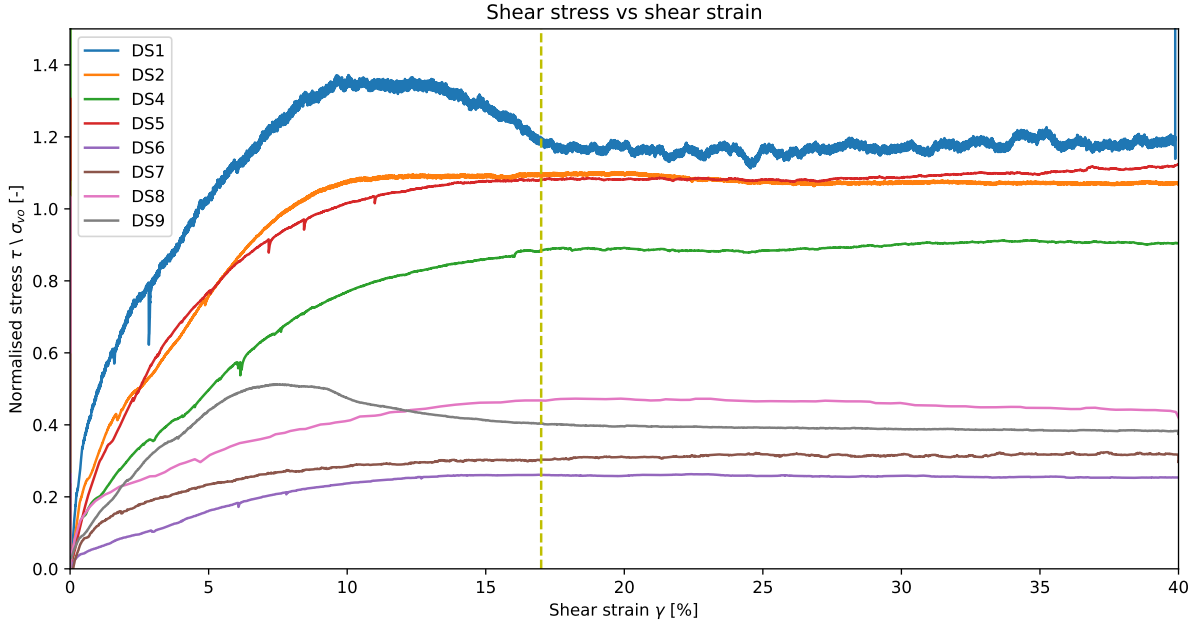

Figure 4.30: Normalised direct shear test results

In general, these graphs show, that critical state is reached at approximately 15-17% shear strain (where the curves flatten out). In the DSS tests slip was found to occur around this range of shear strain too. Considering that the failure surface of both the DS and DSS are not 1-to-1 comparable, it is a reasonable assumption to conclude from these DS tests that critical state will indeed be reached just before slip occurs in DSS tests.

4.7 DSS test results continued

In the previous chapter it was established that critical state has been reached before slippage occurs and therefore the test program can be continued by varying the degree of saturation. Test on samples with a gravimetric water content below 15% proved to be difficult to perform and as such different porous stones, without protruding cones, were used to investigate whether those could be of use in section 4.7.3. Additionally, DSS tests on clays with a higher organic content from two different locations were conducted to investigate whether similar failure mechanisms would be observed in section 4.7.5.

4.7.1 Behaviour of saturated samples

The behaviour of fully saturated samples can be observed in Figure 4.31. The shear strength vs shear strain graphs have a less pronounced minimum as opposed to samples performed at in-situ water content. However, minor signs of slippage could still visually be observed on the samples, but no signs of the diagonal failure surface could be found.

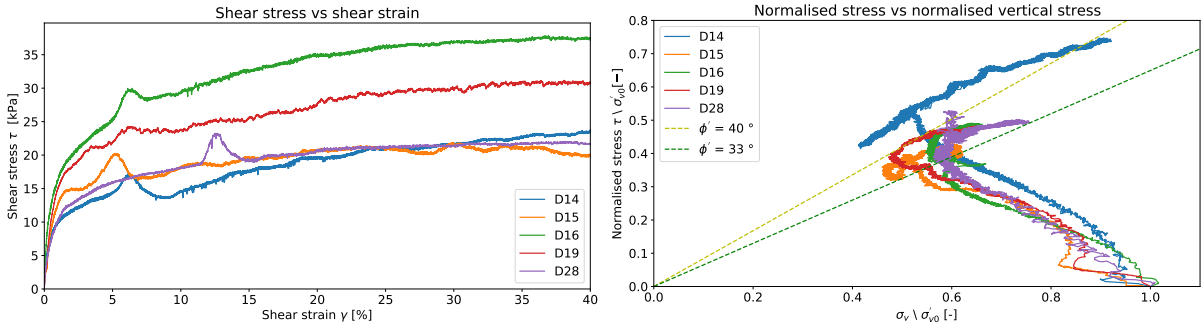

(a) τ vs γ (b) τ/σ_{vo} vs σ_v/σ_{vo}

Figure 4.31: Saturated DSS tests

4.7.2 Behaviour of NC samples

Normally consolidated soil samples in the DSS test behaved as expected (see Figure 4.32). No signs of either slip or the diagonal failure surface could be observed. As a result of the higher vertical stress under which the test is performed, it is less likely that the soil-platen interface looses grip and develops slippage.

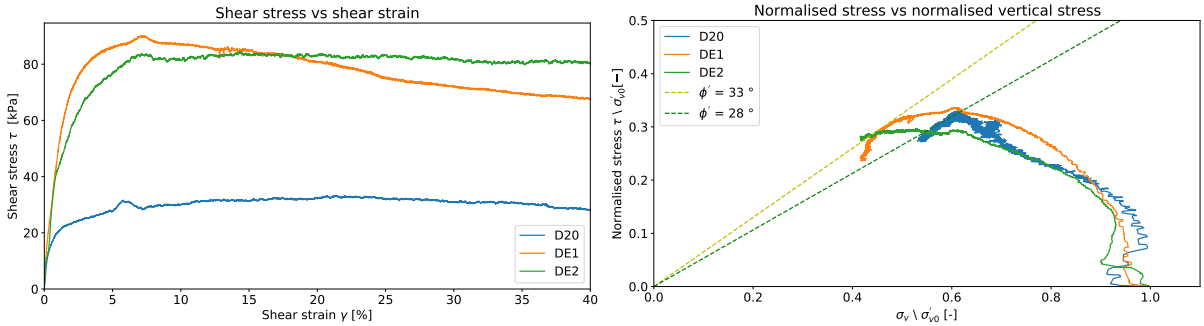

(a) τ vs γ (b) τ/σ_{vo} vs σ_v/σ_{vo}

Figure 4.32: NC DSS tests

4.7.3 Effectiveness of (protruding) porous stones on air-dried samples

For the SSCC concept, it is essential that samples are tested at lower volumetric water contents too, such that a curve (similar to Figure 4.14) can be derived. Figure 4.33 displays the soil behaviour of air-dried samples. As expected from theory, the shear strength increases with increasingly dryer samples (as suction creates apparent cohesion and therefore an increase in measured shear strength). However, when investigating the sample after the test, it is clear that the protruding pins on the porous platens were unable to penetrate the sample both on the top and bottom of the sample. Furthermore, no diagonal failure surface could be detected. Similar to the behaviour of NC samples, no circular behaviour seemed to occur when the normalised shear strength versus the normalised vertical stress would be plotted.

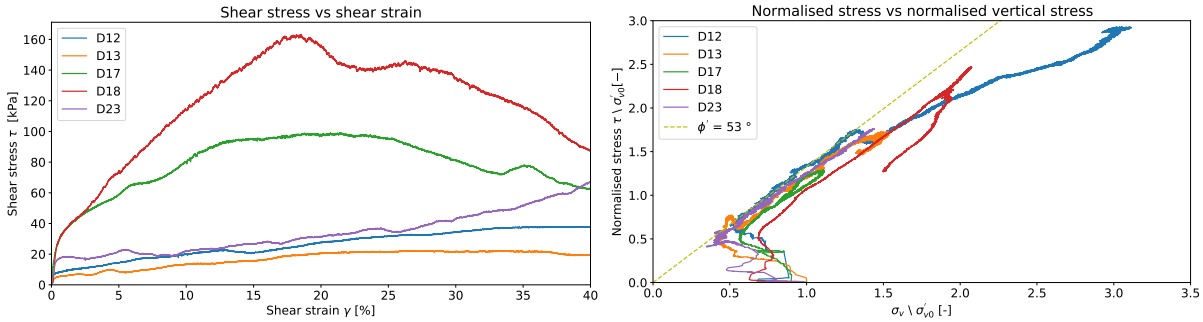

(a) τ vs γ

(b) τ/σ_{vo} vs σ_v/σ_{vo}

Figure 4.33: DSS tests at low volumetric water content

Figure 4.34a displays the platens with protruding pins and Figure 4.34b shows platens without protruding pins but with grooves.

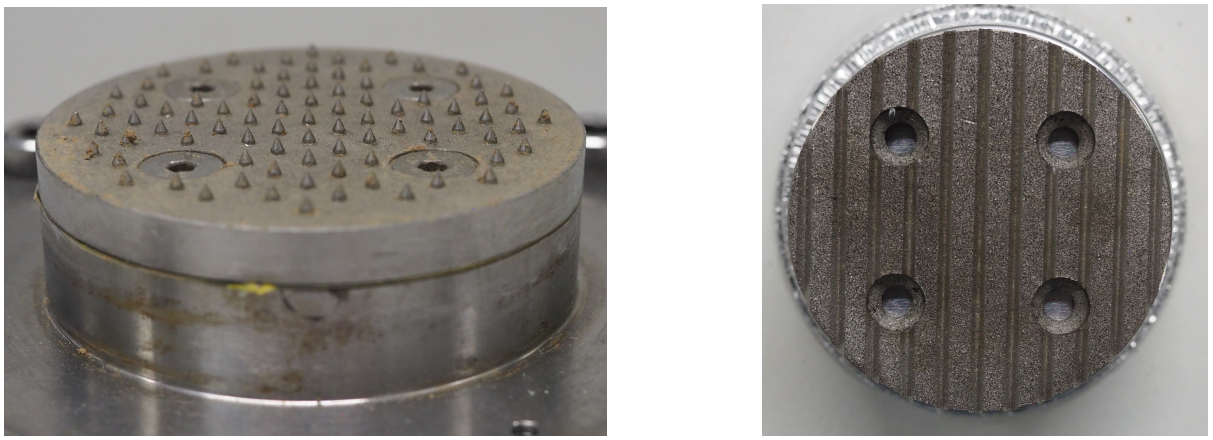

(a) With protruding pins

(b) Without protruding pins

Figure 4.34: DSS porous platens with and without protruding pins

As the porous stones with protruding pins were unsuitable in penetrating the sample such that sufficient grip is created, it was tried to see if the original platens without protruding pins could offer a solution on dry samples. Figure 4.35 displays the soil behaviour of two DSS tests that have performed using these type of platens. A double peak can be observed in shear strength graph early in the test before the shear strength diminishes. From these graphs, it is thus clear that this type of platen does not offer a solution.

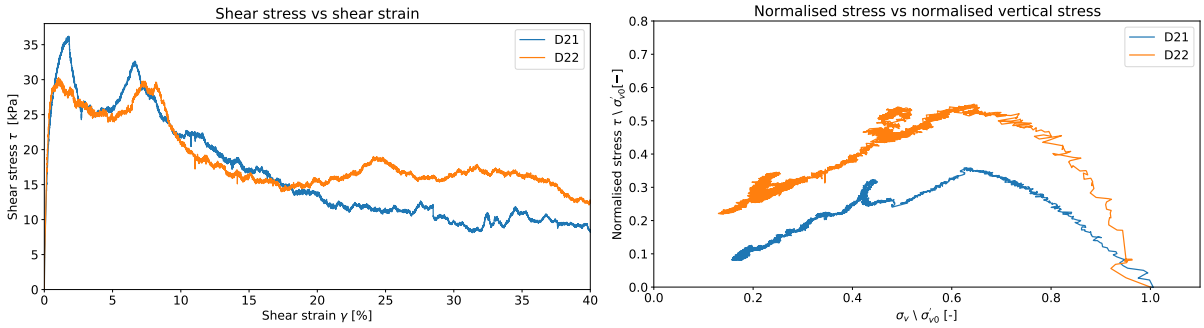

(a) τ vs γ (b) τ/σ_{vo} vs σ_v/σ_{vo}

Figure 4.35: DSS tests using porous stones without protruding pins

DSS tests on dry samples have insufficient ability for the protruding pins to penetrate the sample and create sufficient grip. Moreover, as the sample has decreased in diameter due to shrinkage in the drying process, insufficient restraint by the membrane and the stack of rings can be provided, resulting in unknown stress and strain effects. It is therefore recommended that DSS tests are not be performed on dry samples.

4.7.4 Formation of the diagonal failure surface

Based on DSS tests on NC and air-dried samples, a hypothesis was formed that both slip and the formation of a diagonal failure surface would be caused by the loop in the normalised shear strength versus normalised vertical stress graph. A time-lapse using a GoPro camera has been made for eight DSS tests which showed both signs of slip and had a diagonal failure surface. Using these, it could be observed that at the end of the circular behaviour, slip was visually observed to occur. To validate this hypothesis, two DSS were performed on samples from the same boring at in-situ water content. One of these test was stopped early and one would be performed fully. The results of these test can be seen in Figure 4.36 and visual comparison of both samples after the test can be found in Figure 4.37.

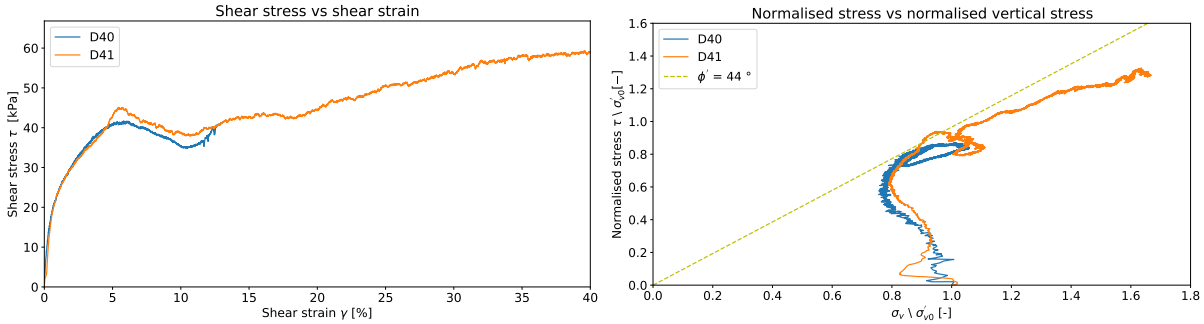

(a) τ vs γ (b) τ/σ_{vo} vs σ_v/σ_{vo}

Figure 4.36: Comparison of DSS tests for which the diagonal failure surface forms

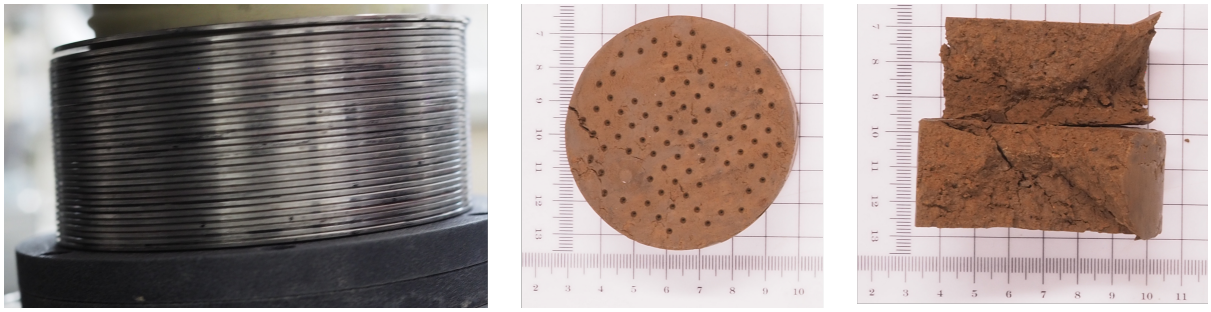

(a) D40

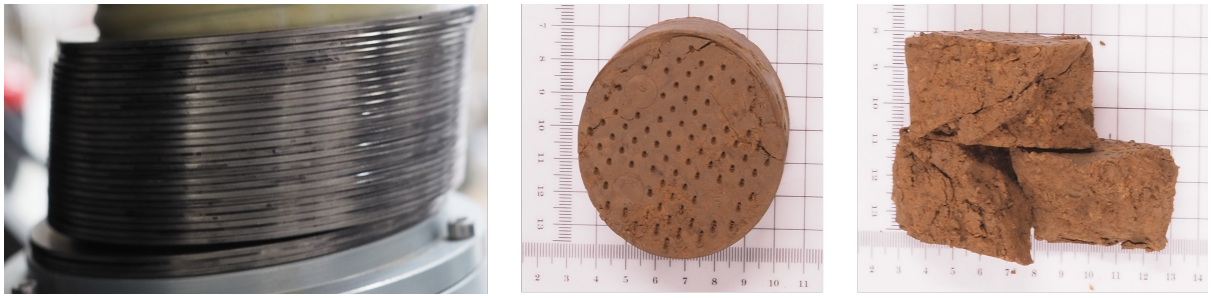

(b) D41

Figure 4.37: Comparison of DSS test to confirm the formation of the diagonal failure surface

In sample D40 the test was stopped early and no signs of slip could be observed, but it did show signs of a diagonal failure surface. Sample D41 showed both signs, and therefore the hypothesis is likely true. However, this also leads to speculation about the interpretation method, as sample D40 was executed slightly after the minimum in shear strength was observed. This means that most likely the traditional interpretation method for a DSS test can be used in the part that the DSS test is considered to be valid.

4.7.5 Samples with other compositions

The slip phenomenon and the diagonal failure surface were observed in sample with a different composition too. Samples from the Haarlemmermeerpolder (Figure 4.38) and from Veessen-Wapenveld (Figure 4.39) were available for this. As opposed to sample from Ravenstein-Lith which were often classified as either a clayey silt or a silty clay, samples from these regions could also be classified as peaty clay or clayey peat (indicating a much higher organic content). Both showed similar behaviour to the previously discussed results on samples from Ravenstein-Lith. Please note that the indicated test numbers in the figures below are not related to any information regarding the composition of the samples previously stated in this chapter as the Atterberg limits and the particle size distribution curves were unavailable.

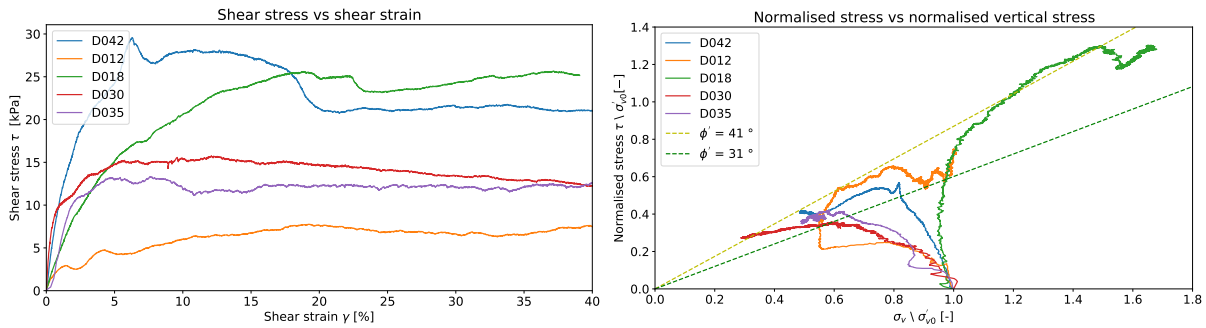

(a) τ vs γ

(b) τ/σ_{vo} vs σ_v/σ_{vo}

Figure 4.38: DSS tests performed on Haarlemmermeerpolder samples

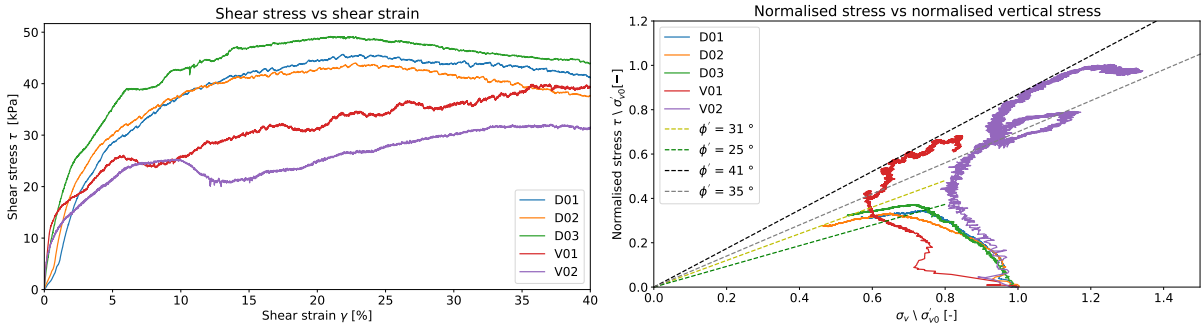

(a) τ vs γ

(b) τ/σ_{vo} vs σ_v/σ_{vo}

Figure 4.39: DSS tests performed on Veessen-Wapenveld samples

4.8 Probability distribution

In geotechnical engineering, soil parameters (i.e. c', ϕ', undrained shear strength) are generally assumed to follow the normal or lognormal distribution. This section verifies whether this also holds if the dataset contains unsaturated samples.

If the parameters of a Probability Density Function (PDF) are unknown, a frequentist procedure called Maximum Likelihood Estimation (MLE) can be used. As these estimators are generally consistent and asymptotically normally distributed with increasing sample size, a reliable estimate demands that sufficient observations are available. Assuming that the data X contains n independent and identically distributed (i.i.d.) observations $x_i, i = 1, ..., n$ and that the distribution parameters are represented by θ, the join density of the data $f(x|\theta)$. This joint density is commonly known as the likelihood function $\mathcal{L}_x(\theta)$ and is constructed based on the product of the marginals $f(x_i|\theta)$.

$$\mathcal{L}_x(\theta) = \prod_{i=1}^{n} f(x_i|\theta) \tag{4.5}$$

The maximum likelihood estimate is the maximum of this function. Since finding the maximum likelihood estimate can be computationally expensive, it is often more convenient to work with the logarithmic transformation of this function, known as the log-likelihood function.

$$l_x(\theta) = \sum_{i=1}^{n} log f(x_i|\theta) \tag{4.6}$$

The unknown distribution parameters can then be found by differentiating with respect to the unknown parameters and setting this equal to zero. The solution is known as the maximum likelihood estimate.

If the observed variables $x = x_1, ..., x_n$ are i.i.d. log-normal random variables given parameters μ and σ^2 then:

$$f(x|\mu, \hat{\sigma}^2) = \frac{1}{x\sigma\sqrt{2\pi}} exp\left\{ -\frac{(ln(x) - \mu)^2}{2\sigma^2} \right\}. \tag{4.7}$$

For convenience a logarithmic data transformation is applied which allows for working with a normal distribution. This is achieved by setting $Y_i = ln(X_i)$, $i = 1, .., n$ which leads to a normal distribution with parameters μ and σ^2. The likelihood of the normal distributed random variables Y can be written as

$$p(y|\mu, \sigma^2) = \sum_{i=1}^{n} \frac{1}{\sigma\sqrt{2\pi}} exp\left\{ -\frac{(y_i - \mu)^2}{2\sigma^2} \right\}. \tag{4.8}$$

This likelihood function is transformed to its log-likelihood variant such that:

$$l(\mu, \sigma^2|y) = -\frac{n}{2} ln(2\pi) - \frac{n}{2} ln(\sigma^2) - \frac{1}{2\sigma^2} \sum_{i=1}^{n} (y_i - \mu)^2. \tag{4.9}$$

The derivative with respect to μ and σ^2 and setting them to zero leads to the maximum likelihood estimates of:

$$\hat{\mu} = \frac{1}{n}\sum_{i=1}^{n} y_i \tag{4.10}$$

$$\hat{\sigma}^2 = \frac{1}{n}\sum_{i=1}^{n} (y_i - \hat{\mu})^2. \tag{4.11}$$

Figure 4.40 displays the empirical cumulative distribution function (ECDF) based on the experimental measurements and the fitted Cumulative Distribution Function (CDF) of the normal and lognormal distribution based on MLE with a sample size of 27 (see valid triaxial test results and their undrained shear strength).

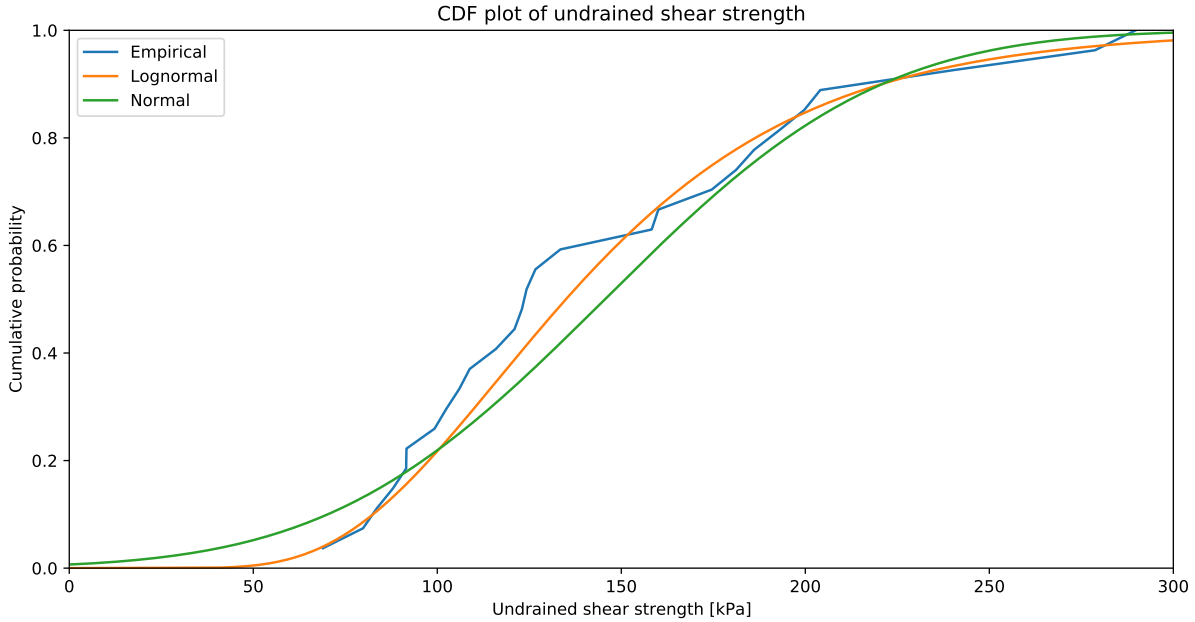

Figure 4.40: Cumulative distribution function of undrained shear strengths retrieved from triaxial tests

To compare if a distribution actually fits the data, a Kolmogorov-Smirnov (K-S) test is performed. In this test, the sample is compared with a reference probability distribution and subsequently it determines the distance between the ECDF and the CDF of the respective distribution. If the K-S statistic is below 0.05 the lack of fit is significant and thus the higher the statistic, the better the fit to a supposed probability distribution is. For the lognormal distribution a K-S value of 0.182 is found and for the normal distribution a K-S value of 0.121 is obtained. Although this means that both distributions are acceptable, the lognormal distribution has a better fit to the data.

Another method based on an unbiased probability distribution called the maximum entropy distribution which uses probability-weighted moments can be opted for (i.e. Deng et al., 2004; Kanwar and Deng, 2019). This method has been applied to the data gathered in this research, but successful convergence could not be achieved such that the appropriate Langrangian multipliers could be found. It must be noted that the current safety philosophy is based on the normal and lognormal distribution and therefore it may not be desirable to use a different probability distribution.

Part III: The application of unsaturated soil parameters for macro-stability

5. The macro-stability modelling of an initially unsaturated dike

In this chapter the results from the geotechnical laboratory tests described in chapter 4 will be used to determine the influence on the factor of safety in D-Stability calculations. In section 5.1, the dike trajectory will be examined and relevant assumptions required to model the initially unsaturated zone are stated before a cross-section of dike trajectory Ravenstein-Lith is modelled in section 5.2.

5.1 Outline & Assumptions

If the strength associated to the initially unsaturated zone is to be taken into account for macro-stability calculations, as opposed to a calculation following the WBI2017 approach which does not take these effects into account, the following aspects are especially of importance:

- The geometry of the dike
- Spatial and time-dependent distribution of apparent cohesion (due to suction forces) throughout the dike

5.1.1 General overview of the dike trajectory

Figure 5.1 depicts a typical part of the dike trajectory Ravenstein-Lith. Generally, in this trajectory there is a road on the crest of the dike and buildings near the inner slope. Moreover, in ordinary conditions, the crest of the dike is situated approximately 100 m from the main river channel. The crest of the dike is typically covered by relatively large (at least 10 m tall) trees along the length of the dike trajectory. At the western end of the dike trajectory, at Oijen, a Deltares test site is located (white arrow). At this site, amongst others, suction is measured for a prolonged period of time. In this research, a cross-section (orange arrow) will be investigated which is located approximately 1 km south of this test site. Therefore, it can be assumed that the suction measurements are reliable and representative for this cross-section.

Figure 5.1: Overview of dike trajectory Ravenstein-Lith with a featured zoom of the Deltares test site and cross-section DP 604. Adopted from Hoogewerf and Leemkuil (2019) and Google Maps (2021)

A recent schematization made by Witteveen+Bos for waterboard Aa & Maas corresponding to the location depicted in Figure 5.1 was provided for use in this thesis and is shown in Figure 5.2. Generally, this cross-section is approximately the same throughout the trajectory. A clay dike is situated on top of a clay layer. Below this often a silty (sandy) clay layer can be found which is situated on top of a deep sand layer. The groundwater level in this model is located underneath the Clay_EC formation. Model parameters can be found in Table 5.1.

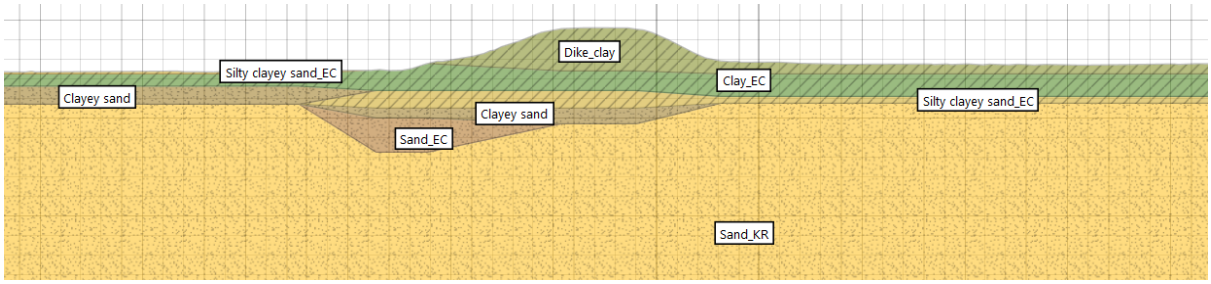

Figure 5.2: D-Stability schematization

	Above the phreatic surface			Below the phreatic surface			
Layer	Shear strength model	γ_{dry} $[kN/m^3]$	ϕ [°]	Shear strength model	γ_{wet} $[kN/m^3]$	S [-]	m [-]
Dike clay	MC drained	19.4	30.9	MC drained	19.4	-	-
Clay_EC	MC drained	16.6	33	SHANSEP	16.9	0.24	0.8
Silty clayey sand_EC	MC drained	19	30.9	MC drained	19.3	-	-
Clayey sand	MC drained	18	29.9	MC drained	20	-	-
Sand_EC	MC drained	20.2	28.6	MC drained	20.7	-	-
Sand_KR	MC drained	17	32.4	MC drained	19	-	-

Table 5.1: Input parameters for each soil layer in D-Stability

5.1.2 Modelling assumptions

5.1.2.1 Geometry

The dike and blanket layer consist of a clay layer on top of a sand layer. Especially this clay layer can develop an apparent cohesion due to matric suction. During a high-water event, the moisture content of both the dike body and the blanket layer may increase, thus decreasing the amount of apparent cohesion. However, this may not necessarily be the case in practice, as during a high-water event of short duration little influence was found by Calabresi et al. (2013) for a dike in Italy along the Po river with an approximately similar characterisation of soil layers.

5.1.2.2 Cracks

Dikes in the Netherlands are typically assumed to be monitored frequently enough such that cracks are discovered early in the process and that those cannot grow into significant cracks. This assumption is powerful as it means that the full geotechnical strength can be attributed to that specific soil layer instead of a possible strength reduction due to crack formation. Van den Akker et al. (2014) investigated the nature and response of cracks in the dikes of the waterboard of Hoogheemraadschap Delfland and found that most cracks in clay dikes are formed in August/September and are not closed naturally due to precipitation until November/December. This means that infiltration is possible and thus it is likely that locally the magnitude of suction will be altered compared to areas of the dike further away from a crack. Moreover, inspections suggested that swollen cracks tend to reopen during the next dry spell and that the magnitude depends on the lutum content in case of clayey soils. A simplified model was proposed by Bronswijk (1988) based on the behaviour of Dutch clays to take into account all of these factors, but at this time it is unavailable in models and programs available to practicing engineers who deal with dikes.

This dike trajectory can be characterised by trees growing on top of the dike. Although one would initially think the roots would hold the soil somewhat together, locally they can influence the magnitude of

suction (Bakker et al., 1995). In Dutch practice the influence of trees is usually neglected due to various reasons but an extensive report exist (Stowa, 2001) which deals with all relevant aspects depending on the type of tree and its influence on each specific failure mode in a dike.

A conservative approach that takes reduced strength due to desiccation cracks into account, would be to model a soil layer of the dike with a reduction of strength over a specific depth. Research by Molenaar (2020) showed that the crack depth could vary between 0-2 m with a reduced strength of 20-50% compared to the original strength parameters (the friction angle in a Mohr-Coulomb shear strength model) of the layer as the reduction in geotechnical strength parameters was found to increase with increasing crack length and depth. Research by Bakker et al. (1995) showed that for a measurement location in Lith in a relatively dry year the depth of desiccation cracks did not exceed 80 cm. Therefore, in this research it assumed that desiccation cracks only play a role in the top 1 meter of both the dike body and the blanket layer. In this research scenario's will be investigated in which desiccation cracks occur in either the dike body, the blanket layer or both with a reduction in strength of 25% and 50% respectively.

As opposed to the dike body, it is not immediately clear how the blanket layer should be modelled as it can be moister than the dike body at the time of a normative event. Therefore, a sensitivity study is required such that insight is provided into the influence of the aforementioned effects. From a conceptual point of view, one could argue that 'preferred' pathways may originate which influence the local characterization of water content. As such two modelling situations are suggested: 1) where only the dike is given an apparent cohesion (based on cracks and reduced strength), and 2) where both the dike and blanket layer are given an apparent cohesion (again with cracks and reduced strength as described earlier).

5.1.2.3 Spatial characterization of apparent cohesion

If there has a been dry period before a high-water event occurs, the dike body will be at its driest near the crest and become moister towards the phreatic line situated inside the dike. Deltares measured at least 80 kPa of suction in a dike near Oijen (at the western end of the dike trajectory) and Westervoort (about 50 km to the North East). Both locations approximately have a similar cross-section as well as similar soil characteristics. The measurements showed that suction only completely disappeared in early March. Figure 5.3 shows that if 80 kPa is taken as conservative limit, this would correspond to 25 kPa of apparent cohesion (at 23% gravimetric water content) for the soil investigated in this thesis for this specific dike trajectory. As the soil becomes wetter, the apparent cohesion decreases cubicly following a trendline of $c' = -0.0029x^3 + 0.3715x^2 - 15.647x + 217.08$ with $R^2 = 0.999$ where x is the gravimetric water content.

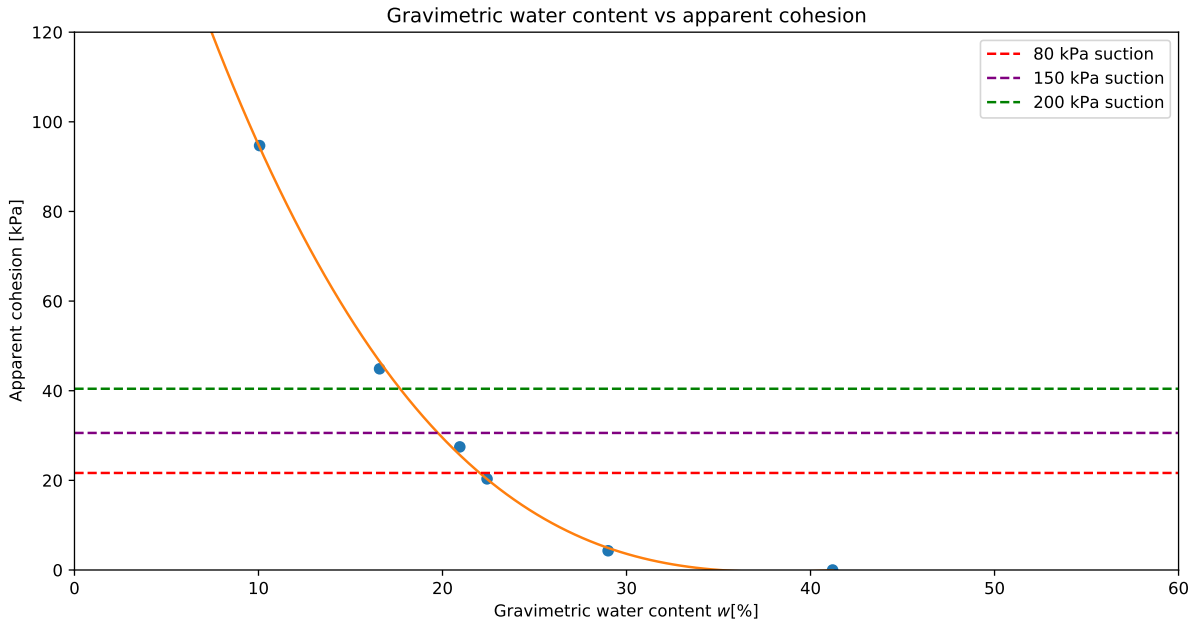

Figure 5.3: Gravimetric content vs apparent cohesion corrected based on CCSM assumptions

In the Dutch guidelines on dike stability assessment (Ministerie van Infrastructuur en Waterstaat, 2019), CSSM is applied. In Critical State it is impossible for cohesion to exist as the soil has been sheared to a state critical state conditions (where volume change no longer occurs). In CSSM cohesion can only exist if the soil is in an overconsonlidated state, meaning that the specimen has not been sheared to the critical state yet. The soil in this thesis can be classified as a transitional soil. For such a soil, it seems that each test converges to a different critical state line depending on the initial volume of the sample (i.e. Ponzoni et al., 2014; Ponzoni et al., 2017). This is the case for the current interpretation of where critical state is expected to occur in laboratory tests, but in principle critical state can be reached if sheared to very large strains. However, this poses then the question how transitional soils fit within the framework of CCSM. Earlier in this research, using the concept of strain compatibility it was shown that critical state conditions are reached at 10% axial strain and 15% shear strain respectively. The Dutch guideline Ministerie van Infrastructuur en Waterstaat (2019) mentions the following causes as to why cohesion can be found in fully saturated sample: (i) as an artefact of applying a best-fit procedure of a Mohr-Coulomb line to multiple Mohr Circles and (ii) due to soil heterogeneity. Irrespective of this guideline, one could argue that using the current interpretation of where to determine strength parameters in a transitional soil using CSSM should be altered for this specific type of soil. Results from the triaxial tests (see Table 4.5) indicated that, when using the SSCC concept, fully saturated samples produced a cohesion of 5.97 kPa. It could be argued that this should be the minimum value of cohesion applied to a soil layer modelled with the Mohr-Coulomb model in D-Stability in which strain compatibility is an intrinsic requirement. However, as currently it is unclear, whether transitional soils fit the current interpretation of CSSM, or whether there is an unknown effect in laboratory testing for these specific type of soils, as a conservative measure, this effect is not taken into account in the model in this thesis. Thus, at fully saturated conditions, the cohesion is assumed to be 0 kPa in line with the current interpretation of CSSM. Figure 4.17 was therefore corrected by shifting down all values by 5.97 kPa such that Figure 5.3 is obtained and can be used in a design.

5.1.2.4 Time-dependent characterization of apparent cohesion

Moreover, this is a highly time-dependent problem. If a dry spell is followed by a few wetter days followed by again a dry spell this would mean that there would be a layering of apparent cohesion in the soil: dry -> moister -> very dry. There are many possible combinations where one could use KNMI data as modelling input and it would be recommended to further explore these modelling mechanisms in another study.

Besides this, there is another important point to be considered. In Figure 5.4 a schematization is shown for a typical dike with several zones indicating the spatial distribution of suction within the dike. Zone 4 is assumed to become saturated during a high water event and zone 5 is assumed to be always saturated as it lies under the average lowest groundwater table. Zone 3 becomes more saturated over time and thus can change its amount of apparent cohesion during a high-water event. Zones 1 and 2 remain unsaturated, where zone 1 is the zone affected by potential cracks or by such high matric suction. High matric suction may cause to the numerical problem to become unstable due to the very sharp gradients throughout the dike. The sharp transition between zone 2 and 3 in this figure may not occur as this is only expected if a steady state is reached.

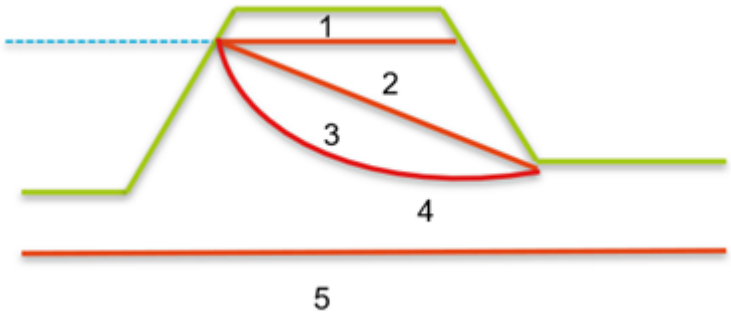

Figure 5.4: Schematised zones of suction within a dike

Ideally, one would like to perform a simulation where both weather data and river water levels are used to predict the distribution of water content throughout the dike such that an apparent cohesion can be assigned before a macro-stability calculation is performed. This would require an extensive FEM calculation on the scale of a PhD thesis. Preferably, this is also complemented by a field test similar to the one performed in Calabresi et al. (2013).

5.2 D-Stability

Using the assumptions and input of the previous section, the existing D-Stability model provided by waterboard Aa & Maas was adjusted to account for suction and cracks. In this model it was assumed that if a layer is cracked, that the entire layer in D-Stability reduces its geotechnical parameters by a certain percentage. This is a valid approach as the cracked soil would generate a driving moment, but it would not provide any strength to resist this driving moment. In this thesis, the Uplift-Van method is chosen which assumes an equilibrium of forces between the active and passive slip circles.

If the water content is assumed to linearly increase with depth, a conservative option would be to model a linear reduction in cohesion over the depth between 20.3 kPa at 22.4% and 0 kPa at 30% (as can be seen in Figure 5.3). Although, this cannot be modelled directly in D-Stability version 20.1 (Deltares, 2019). It is possible to define several zones within each initially unsaturated soil layer within the dike body in which each layer is assumed to have an average gravimetric water content. The value for the gravimetric water content of each zone corresponds to an apparent cohesion which can be calculated using the trendline in section 5.1.2.3. Ideally, one would use the s_u-table option, but in the expressions (see Equation 4.1, 4.2 and 4.3 respectively) to determine unsaturated shear strength of a soil, a variable describing the net normal stress $(\sigma - u_a)$ is introduced of which the magnitude is unknown.

Figure 5.5 displays the phreatic line within the dike according to the Dutch guidelines. It can be seen that this schematization assumes that the phreatic line inside the dike assumes steady-state conditions and that aforementioned zone 3 displayed in Figure 5.4 does not occur. In this thesis the phreatic line as prescribed by the Dutch guidelines has been adopted.

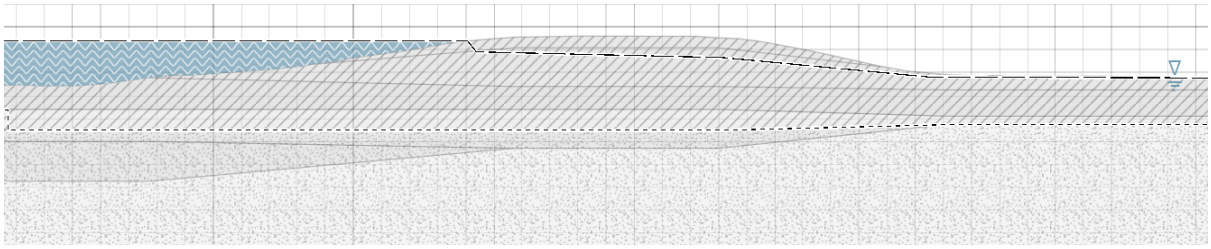

Figure 5.5: Schematization of the phreatic surface in a normative scenario

The cross-section of the dike was split into various sections: (i) the left slope of the dike body was is assumed to be unaffected by both matric suction and desiccation crack formation, (ii) the upper 1 meter of the dike body and the blanket layer could potentially have reduced strength as a result of desiccation cracking and (iii) the core of the dike body would be subdivided in multiple layers depending on their location respective to the steady state phreatic line. Clay layer 1 and 2 are situated above the steady state water line in the case of a high water event and can thus be assumed to remain unsaturated during such an event. Both layers were assumed to be of similar thickness of 0.4 m. It is likely that clay layer 1 experiences higher levels of matric suction during a high water event than clay layer 2 as it lays higher above the steady state phreatic line.

Clay layer 3, 4, 5 are located below this phreatic line and are expected to increase in volumetric water content and thus have lower matric suction (or perhaps even none) during the duration of a high water event. The thickness of these layers has been assumed to be 0.8 m. This value resulted from a Plaxis calculation which simulated 2018 weather data of the KNMI Volkel weather station on this cross-section and as a trade-off between average gravimetric water content and ease of modelling in D-stability. Clay layer 6 is assumed to contain zero additional strength as due to the interface of the different layers on

both sides of the dike body, this layer may become saturated faster than the layers situated above it as it is situated above a sand layer similar to results from field measurements by Calabresi et al. (2013). Figure 5.6 displays a schematic overview of the location of the different zones and Figure 5.7 shows a zoom of the dike core.

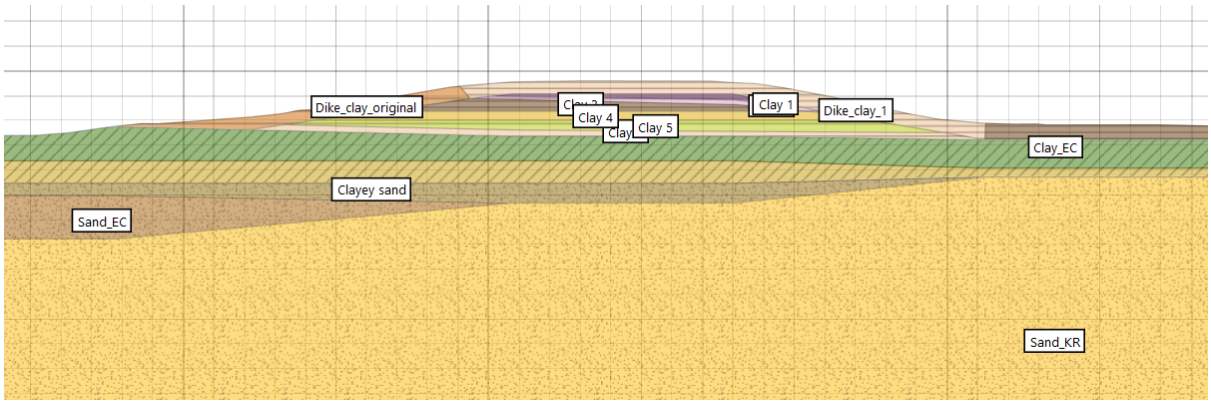

Figure 5.6: Overview of the adjusted cross-section in D-Stability

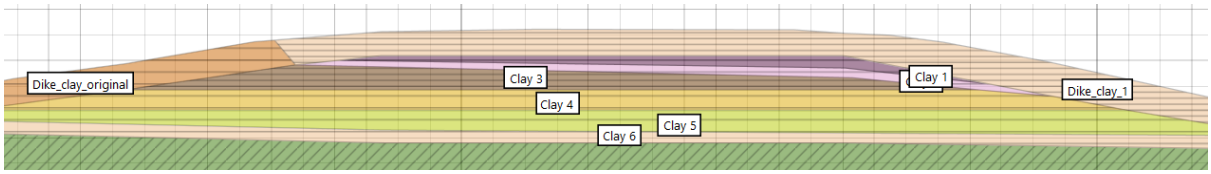

Figure 5.7: Close-up of the adjusted cross-section in D-Stability

As the exact magnitude of suction during a high water event is unknown, a sensitivity study is performed to investigate the effect of initially unsaturated soil layers at the time of a high water event. In this study several scenario's have been simulated. Each scenario represents a different initial condition in which the magnitude of suction in each initially unsaturated clay layer is different too. As previously mentioned, suction can be modelled by means of an apparent cohesion in D-Stability. In order to accurately predict the corresponding magnitude of cohesion for each respective layer, a confidence interval is required. In section 4.8 it was found that both normal and lognormal distributions may be used to describe the laboratory tests. The normal distribution has been selected to construct a 95% confidence interval. Table 5.2 displays the values of this confidence interval and it is visualised in Figure 5.8.

Table 5.2: Overview of 95% confidence interval parameters based on the normal distribution

θ_{vol} [-]	c' [kPa]	Sr (μ) [%]	σ [%]	Sr ($\mu - 2 * \sigma$) [%]	Sr ($\mu + 2 * \sigma$) [%]
51.50	0.00	98.54	1.28	95.96	101.11
42.05	4.29	96.96	2.27	92.41	101.50
35.87	20.33	93.69	1.18	91.32	96.05
33.50	27.47	88.36	5.24	77.86	98.85
26.53	44.89	73.40	5.81	61.76	85.02
16.09	94.69	49.67	4.68	40.30	59.03

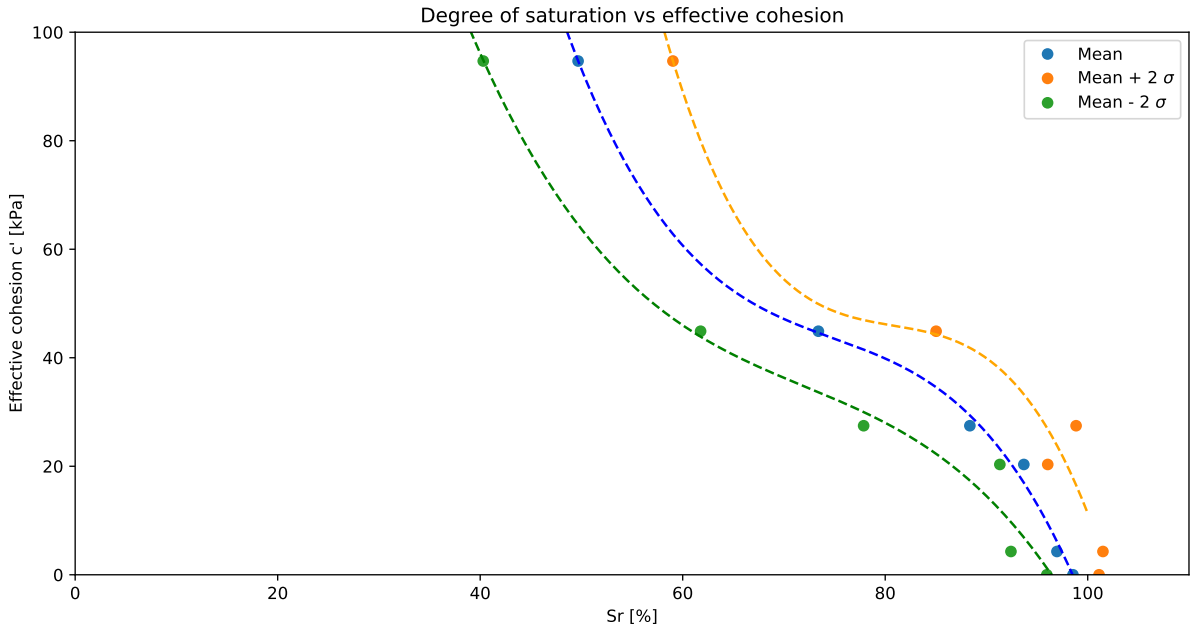

Figure 5.8: 95% confidence interval of the degree of saturation versus effective cohesion

Using the aforementioned assumptions, thirteen scenario's were calculated in which the cohesion for each zone was variable depending on the confidence interval. Moreover, depending on the scenario a zone could be influenced by desiccation cracks with varying strength reduction. Detailed input parameters and results for each zone can be found in Table 5.3 and are meant to serve as an indication of what the effect of the initially unsaturated zone is on the macro-stability of a clay river dike during a high water event. An example of the slip circle at failure can be seen in Figure 5.9.

Scenario	1	2	3	4	5	6	7	8	9	10	11	12	13
Layer	Cohesion [kPa] or strength reduction [%] due to desiccation cracking												
Clay 1	0	20	40	20	20	20	20	20	20	20	20	20	20
Clay 2	0	10	20	10	10	10	10	10	10	10	10	10	10
Clay 3	0	6	6	0	0	0	0	6	6	6	6	6	6
Clay 4	0	4	4	0	0	0	0	4	4	4	4	4	4
Clay 5	0	2	2	0	0	0	0	2	2	2	2	2	2
Clay 6	0	0	0	0	0	0	0	0	0	0	0	0	0
Dike Clay 1	-	-	-	-	- 50%	-	- 50%	- 50%	-	- 50%	-25%	-	-25%
Blanket	-	-	-	-	-	- 50%	- 50%	-	- 50%	- 50%	-	-25%	-25%
FoS	1.014	1.073	1.121	1.045	1.041	1.036	1.031	1.072	1.068	1.064	1.074	1.071	1.069
w.r.t.to #1 [%]	0.0	5.9	10.7	3.1	2.7	2.2	1.7	5.8	5.4	5.0	6.0	5.7	5.5
β	4.03	4.42	4.74	4.23	4.21	4.17	4.14	4.41	4.39	4.36	4.43	4.41	4.39
P_{fa}	2.8E-05	4.9E-06	1.1E-06	1.2E-05	1.3E-05	1.5E-05	1.7E-05	5.1E-06	5.8E-06	6.5E-06	4.8E-06	5.2E-06	5.6E-06
x P_{fa} of #1	-	5.7	26.5	2.5	2.2	1.9	1.6	5.6	4.9	4.3	5.9	5.4	5.1

Table 5.3: Input and results from D-Stability for various scenario's in macro-stability assessment

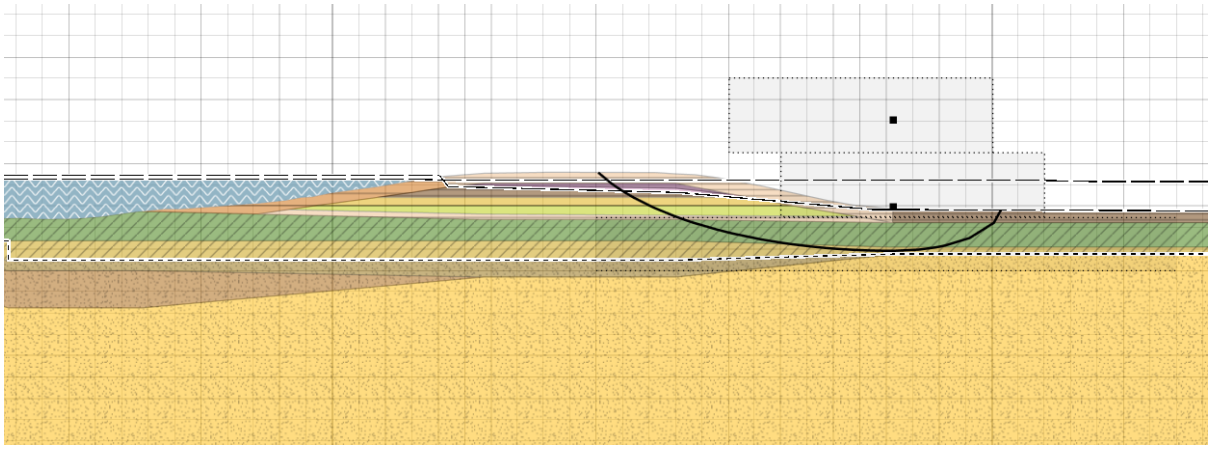

Figure 5.9: Results of a simulation with scenario 11 in D-Stability

The current design approach yielded a factor of safety of 1.014 (scenario 1). If cohesion was given to the zones based on the measurements by Deltares and the corresponding amount of cohesion found as a result of the SSCC concept applied to K0-CAU triaxial tests, the factor of safety increased to 1.073 (scenario 2). If the measurements in the field were not limited by 80 kPa due to sensor issues, and if it assumed that 200 kPa would have been attainable, the factor of safety would have increased further by another 4.8% to 1.121 (scenario 3). Moreover, it is interesting to note that the relative influence of desiccation cracking on the factor of safety is limited - even if both the dike body and the blanket layer are exposed to this. If either the blanket layer, the dike body or both were found to contain at least 50% cracks, the increase in factor of safety was smaller if suction was assumed to only appear above the phreatic line, but was still 1.7% higher (scenario 7) compared to the current design approach. If suction is present below the phreatic line too, the factor of safety may increase with 5.0% and possibly more if cracks are not present in the dike body and blanket layer.

Although it is currently unclear which of these scenario's represent reality best, it indicates that even in the most conservative case which can be supported by field measurements (scenario 7), that a 1.7% increase in factor of safety can be found compared to the current design approach. For a cross-section which is slightly below the minimum factor of safety, this may have just been sufficient to avoid costly upgrades. This is especially of importance as the budget for dike reinforcements is limited compared to the shear amount of dikes that need to be reinforced and any reduction in conservatism in the determination of the factor of safety may be useful to obtain a more efficient design.

Part IV: Conclusion & Discussion

6. Conclusion

6.1 Answer to the main research question

"What is the influence of initially unsaturated clay on the macro-stability of river dikes in the Netherlands and is it possible to quantify this soil behaviour using conventional laboratory experiments?"

In this thesis it is shown that when the initially unsaturated behaviour of clay is accounted for the macro-stability of clay river dikes in the Netherlands increases. Moreover, it is shown that initially unsaturated soil behaviour can be accurately quantified using the SSCC concept for K0-CAU triaxial tests, but that it is unable to be applied to DSS tests due to the inherent constraints of the testing apparatus and in the assumptions that are required for the interpretation of the test.

The current design philosophy is conservative in assuming that there is no additional strength due to matric suction. The design guidelines can be improved by taking initially unsaturated behaviour into account. Potentially there is some increase compared to the current determination of the factor of safety during a high water event that currently is unaccounted for in the design process. In the future this might be utilised to make a more efficient dike design or a more realistic prediction of the actual factor of safety of the respective dike. At this time, there is insufficient measurement data available to quantify the respective additional strength to each zone during a high water event. In this thesis assumptions were based on the limited number of field observations of Van Duinen (2020) and a field test in similar geological conditions conducted by Calabresi et al. (2013) which may lead to a conservative design approach. However, as it is unclear how the additional strength should be taken into account in a practical yet safe way for the determination of a factor of safety, care should be taken in applying this concept. It is however, encouraging to know that applying this concept will only lead to a higher factor of safety, and that the current method of determining the factor of safety can be seen as a lower-bound if suction is not taken into account.

In addition to a favorable influence on the macro-stability, the triaxial test results would make it possible to determine a N_{kt} factor for a given amount of suction. Thus, if a CPT were to be performed in the summer period when there is a possibility for suction to exist, the measured strength can be corrected to current design conditions stated in the guidelines were suction is assumed to be non-existing. Practically, this would mean that it would be possible to correct for the additional strength as a result of suction as measured by the CPT. Therefore, this will ensure correct parameter determination in a design condition without suction based on CPT results which may have been performed when suction existed within the dike.

6.2 Answer to the sub-questions

"Which of the methods to determine undrained shear strength is most suitable for initially unsaturated soil in the Netherlands?"

Based on this thesis it would be advised to use triaxial test to determine the undrained shear strength of initially unsaturated soil. It is likely that in the future this can be done with in-situ tests such as the Field Vane Test, but this was not further investigated in this thesis, and for this to work, it would be required to know the corresponding matric suction or the suction stress. The latter can be found accurately using conventional laboratory tests.

"How can the strength parameters of clay under variable degrees of saturation be determined using conventional laboratory tests?"

Using conventional laboratory experiments it is recommended to make use of the SSCC concept developed by Lu and Likos (2006). It was found that it can be successfully applied to K0-CAU triaxial tests, but that due to shrinkage and boundary effects it is unsuitable to DSS tests. Moreover, if only a first-order calculation has to be made or limited funds are available, it possible to use the closed-form

expression of Lu et al. (2010) for which only the Van Genuchten parameters of the soil need to be determined.

"Do geotechnical laboratory test which are performed in line with the SSCC concept, allow the determination of an optimal parametric probability distribution that represents the laboratory data"

It can be concluded that both the lognormal and normal probability distribution fit the unsaturated data gathered in this thesis and therefore no exotic distribution has to be developed or used.

"How does the degree of saturation change within a dike subjected to changing atmospheric conditions and changing ground- and river water level and can this be simplified to several zones for each relevant design condition using site specific laboratory tests? "

Although a Plaxis calculation has been performed to visualize the effect and the magnitude of the atmospheric conditions (evaporation and precipitation) to the degree of saturation, it was not possible to do the same with variable ground- and river water level. The basis of this visualisation together with a 95% confidence interval based on the K0-CAU triaxial tests formed the input for the various scenarios in the D-Stability calculations. This is a simple and practical approach to model additional strength due to changes in the degree of saturation, but it does not take into account time-dependence, which is of paramount importance in these type of simulations.

"What is the influence of unsaturated clay on the macro-stability in relevant design conditions and can this be quantified?"

A positive influence of unsaturated soil behaviour on the macro-stability in design conditions was found to exist. Using the SSCC concept and conservative assumptions based on field measurements by Deltares a minimum increase of 1.7% in the factor of safety was found. More likely, scenario 10, would exist in the field, which would produce an increase of 5.0% in the factor of safety. Even if during a high water event it is found that the additional strength due to matric suction completely disappears, the current design philosophy remains valid, and thus can be seen as the minimum factor of safety.

7. Recommendations & Further research

In this thesis it has been shown that it is possible to determine geotechnical strength parameters of unsaturated samples using conventional laboratory equipment as well as the influence of this in contemporary modelling of macro-stability as used in the Netherlands. Both in the laboratory tests as well as in the modelling, several assumptions were required which ideally should be further refined and verified before this method can be applied in practice. Recommendations and possible options for further research concerning laboratory tests are discussed followed for the modelling phase.

7.1 Geotechnical laboratory testing

1. Unsaturated soil properties

    - It is recommended to determine the SWCC for each distinctly different soil layer which is expected to be unsaturated for each dike section. Using the closed-form equation of the SSCC, an accurate representation can be found for the unsaturated strength which then in turn can be used in stability calculations.
    - Any effects due to shrinkage and swelling of the samples have been neglected, but these are known to for example have an effect both in the formation and in the dissolution of cracks. Additionally, if a sample is prone to shrinkage, samples should be carefully monitored such that uniform samples are created. This is especially important as even little deviations can create stress and strain inhomogeneities throughout the sample and therefore directly affect the validity of the geotechnical laboratory test of interest.

2. Applicability of the SSCC concept

    - The SSCC approach described in this thesis has been applied to K0-CAU tests for the first time and generally seems to work well and match the unsaturated shear strength formulations of Bishop and Fredlund and Morgenstern. It was found that especially for relatively dry samples with a volumetric water content lower than 26%, major discrepancies in the measurements by the two respective volume controllers were introduced. The majority of the discrepancies occurred in the anisotropic consolidation phase, with the isotropic consolidation phase only being a minor source. As the volume measurements are used in the back-calculation of the diameter of the sample, this is of significant importance. If volume measurements are thought to be distorted by air bubbles, a practical approach should be used to determine the correct diameter of the sample. As the sample does not have a uniform diameter directly after shearing, it is advised to determine an average diameter by measuring the diameter after shearing in at least three places (near the top, middle and bottom of the specimen). A practical recommendation which is thought to result in a more accurate determination of the diameter, would be to place the volume controllers on a scale which can log any changes in mass such that an accurate volume measurement throughout the test can be established. Moreover, for these dry samples it is of paramount importance that care is taken such that these are air-dried evenly to prevent any stress and strain inhomogeneities.
    - The SSCC approach is not recommended to be used in combination with DSS tests. This due to a combination of both the pins being unable to penetrate highly unsaturated samples as well as insufficient restraint created by the membrane and the stack of rings due to shrinkage of the samples. This results that the tests are invalid given the imposed boundary conditions and the known corresponding assumptions which are required for interpretation of this relatively complex laboratory test. Based on this thesis, it would be recommended to only use this approach on conventional triaxial tests.

3. Strain compatibility

    - Design guidelines in the Netherlands recommend that the geotechnical strength parameters should be determined at 25% axial strain in triaxial test and at 40% shear strain in DSS tests. Similar to research by Gori (2020), it would be suggested to use the concept of strain

compatibility for large dike reinforcement projects where relatively stiff and heavy clay (18-19 kN/m^3) is found and excessive softening is observed in geotechnical laboratory tests. With strain compatibility, only few additional laboratory tests are required, and if found to be applicable, conservatism in the design parameters can be reduced. An important implication of this would be that if strength parameters can be determined at a lower strain percentage, the resulting strength parameters are generally slightly higher. This results in a higher design strength meaning that a dike reinforcement could be smaller which can potentially save both costs and emissions.

4. Slip in DSS tests

   - In DSS tests the slip phenomenon was extensively observed. Several suggestions were made to cope with this effect, but it would be recommended to model a DSS test using Discrete Element Modelling to discover the physical reasons as to why this phenomenon occurs and to investigate if this is caused due to the diagonal failure plane imposing an internal moment in the sample or whether this is unrelated but occurs approximately simultaneously. This could also verify the suggested approach in this thesis as well as come up with recommendations for the interpretation of a DSS test which exhibits these phenomena. Thus, this could verify whether the traditional approach or the AG approach should be used. With DEM the rotation of principal axis throughout the test is known as opposed to a laboratory test.
   - Practically, in the meanwhile, it would be suggested to watch for signs of slip during the test. It would be unwise to automatically determine the geotechnical strength parameters at the suggested 40% shear strain when signs of slip are present. To aid the engineer or the laboratory technician in detecting this, ideally a time-lapse would be available. At a minimum, before removing the sample from the apparatus, a picture should be taken of the stack of rings, as well as pictures of the top, bottom and of the cross-section of the sample.

7.2 The modelling of unsaturated soil behavior for a macro-stability analysis

1. Hydraulic conductivity

   - In this thesis the hydraulic conductivity of the different soil layers was assumed to be temporally and spatially constant. However, this is not the case in practice as due to suction, the local (unsaturated) hydraulic conductivity can be significantly different. Due to cracks the hydraulic conductivity may increase especially in the top layer. Moreover, the influence of trees was neglected in this thesis. Their root zone can cause significant local drawdown resulting in locally higher suction gradients as well as near the roots penetrating soil layers. Currently, it is highly time intensive both in the determination of properties in the laboratory and in modelling to take any of these effects into account. It would be recommended to execute a probabilistic study in which the spatial variability can be analysed or in which the hydraulic conductivity is given a probability distribution (from literature or from laboratory experiments) to investigate these effects as well as to establish a straightforward modelling approach.

2. Distribution of suction in a dike

   - In 2021 a high water event passed the suction sensors installed in the dikes, however this year has been irregularly wet for the Netherlands as a whole, resulting in little to no suction being measured at the time of the event. It therefore remains of interest to see how quickly suction (and therefore the additional strength) dissipates during a high water event. Although this can be modelled, it would be beneficial to verify these numerical calculations by means of sensors in the field. Currently these sensors are only installed in two locations, but in the view of the author it would be beneficial if more were to be installed in the Netherlands such that a more complete picture would be created.
   - Moreover, it would be recommended to execute an extensive numerical study which investigates the extent of the unsaturated zones and the magnitude of suction during such an event. Preferably, this would be done using a probabilistic approach as there are an infinite number

of combinations possible in which the precipitation, the evaporation, the groundwater level, the river water level, and the duration of (one or multiple successive) high water events may influence the temporal- and spatial distribution of suction in a dike. Before any additional strength may be attributed to a dike, both the influence and the magnitude of these effects should be investigated such that the dike remains safe even if a high water event occurs in a relatively wet year where little additional strength due to suction could have been created.

3. Constitutive modelling

   - An attempt was made to investigate which constitutive model provides the best match with laboratory tests, while using easily determinable parameters to model initially unsaturated soil in daily engineering practice. Although the SSCC concept is based on the Mohr-Coulomb concept, this does not mean that the observed soil behaviour matches the predicted behaviour by the Mohr-Coulomb (or any other) constitutive model well. It would be recommended to perform further research that the soil behaviour can be accurately modelled in a FEM program such as Plaxis, such that the time-dependent aspect of the geotechnical parameters can be modelled effectively.

8. References

Aas, G., Lacasse, S., Lunne, T., & Hoeg, K. (1986). Use of in situ tests for foundation design on clay. *Use of In Situ Tests in Geotechnical Engineering*, 1–30.

Abelev, A. V., & Lade, P. V. (2004). Characterization of failure in cross-anisotropic soils. *Journal of Engineering Mechanics*, *130*(5), 599–606.

Airey, D. W., & Wood, D. (1987). An evaluation of direct simple shear tests on clay. *Géotechnique*, *37*(1), 25–35.

Alonso, E. E., Gens, A., & Josa, A. (1990). A constitutive model for partially saturated soils. *Géotechnique*, *40*(3), 405–430.

Arthur, J. R. F., Rodriguez del C, J. I., Dunstan, T., & Chua, K. S. (1980). Principal stress rotation: A missing parameter. *Journal of the Geotechnical Engineering Division*, *106*(4), 419–433.

Atkinson, J. et al. (1993). *An introduction to the mechanics of soils and foundations: Through critical state soil mechanics.* McGraw-Hill Book Company (UK) Ltd.

Bakker, J., van den Akker, J., & Cornelissen, P. (1995). *Oorzaak en preventie van schade aan wegen door vochtonttrekking door bomen.* DLO-Staring Centrum.

Bao, C., Gong, B.-w., & Zhan, L.-t. (1998). Properties of unsaturated soils and slope stability of expansive soils. *Proceedings of the Second International Conference on Unsaturated Soils–UNSAT98, Beijing, China*, 71–98.

Bareither, C. A., Benson, C. H., & Edil, T. B. (2008). Reproducibility of direct shear tests conducted on granular backfill materials. *Geotechnical Testing Journal*, *31*(1), 84–94.

Bear, J. (1979). Hydraulics of groundwater new york. *Mc GrawHill Inc.*

Bjerrum, L. et al. (1974). Problems of soil mechanics and construction on soft clays.

Bjerrum, L., & Landva, A. (1966). Direct simple-shear tests on a norwegian quick clay. *Geotechnique*, *16*(1), 1–20.

Borden, R. H., & Putrich, S. F. (1986). *Drained-strength parameters from direct shear tests for slope stability analyses in overconsolidated fissured residual soils.*

Borin, D. L. (1973). *The behaviour of saturated kaolin in the simple shear apparatus* (Doctoral dissertation). University of Cambridge.

Bronswijk, J. J. B. (1988). Modeling of water balance, cracking and subsidence of clay soils. *Journal of Hydrology*, *97*(3-4), 199–212.

Budhu, M. (1984). Nonuniformities imposed by simple shear apparatus. *Canadian Geotechnical Journal*, *21*(1), 125–137.

Buiten, H. W. (2020). The influence of suction on the shear strength of a clay dike. (MSc Thesis TU Delft).

Calabresi, G., Colleselli, F., Danese, D., Giani, G., Mancuso, C., Montrasio, L., Nocilla, A., Pagano, L., Reali, E., & Sciotti, A. (2013). Research study of the hydraulic behaviour of the po river embankments. *Canadian Geotechnical Journal*, *50*(9), 947–960.

Chatzis, K. (2018). Advances in modelling the deviatoric response of peat. (MSc Thesis TU Delft).

Chotkan, S. (2021). Predicting drought-induced cracks in dikes with artificial intelligence. (MSc Thesis TU Delft).

Croney, D., & Coleman, J. (1954). Soil structure in relation to soil suction (pf). *Journal of soil science*, *5*(1), 75–84.

Dabeet, A. (2014). *Discrete element modeling of direct simple shear response of granular soils and model validation using laboratory tests* (Doctoral dissertation). University of British Columbia.

DeGroot, D. J., & Lutenegger, A. J. (2005). Characterization by sampling and in situ testing–connecticut valley varved clay. *Studia Geotechnica et Mechanica*, *27*.

de Josselin de Jong, G. (1971). Discussion on stress-strain behavior of soils. *Proc. Roscoe Memorial Symposium, Parry R.H.G. (Editor)*, 258–261.

Deng, J., Gu, D. S., & Li, X. B. (2004). Parameters and quantile estimation for fatigue life distribution using probability weighted moments. *Chin. J. Comput. Mech*, *21*(5), 609–613.

Ding, D., & Loehr, J. E. (2019). Variability and bias in undrained shear strength from different sampling and testing methods. *Journal of Geotechnical and Geoenvironmental Engineering*, *145*(10), 04019082.

Doherty, J., & Fahey, M. (2011). A three-dimensional finite element study of the direct simple shear test. *Proceedings. 2nd Int. Symp. on Frontiers in Offshore Geotechnics, ISFOG2, Perth, Western Australia*, *1*, 341–346.

Dyvik, R., Berre, T., Lacasse, S., & Raadim, B. (1987). Comparison of truly undrained and constant volume direct simple shear tests. *Geotechnique*, *37*(1), 3–10.

Ehrgott, J. Q. (1971). *Calculation of stress and strain from triaxial test data on undrained soil specimens.* Waterways Experiment Station.

Escario, V., & Saez, J. (1986). The shear strength of partly saturated soils. *Geotechnique*, *36*(3), 453–456.

Farrell, E., Jonker, S., Knibbeler, A., & Brinkgreve, R. (1999). The use of direct simple shear test for the design of a motorway on peat. *Twelfth European Conference on Soil Mechanics and Geotechnical Engineering (Proceedings) The Netherlands Society of Soil Mechanics and Geotechnical Engineering; Ministry of Transport, Public Works and Water Management; AP van den Berg Machinefabriek; Fugro NV; GeoDelft; Holland Railconsult*, (Volume 2).

Finn, W. L., Pickering, D. J., & Bransby, P. L. (1971). Sand liquefaction in triaxial and simple shear tests. *Journal of the soil mechanics and foundations division*, *97*(4), 639–659.

Fissel, L., & Breitmeyer, R. J. (2016). Evaluation of uncertainty for soil water characteristic curve measurements and the implications for predicting the hydro-mechanical behavior of unsaturated soils. *Geotechnical frontiers 2017* (pp. 579–588).

Franke, E., Kiekbusch, M., & Schuppener, B. (1979). A new direct simple shear device. *Geotechnical testing journal*, *2*(4), 190–199.

Fredlund, D. G., Rahardjo, H., & Fredlund, M. D. (2012). Unsaturated soil mechanics in engineering practice. john wiley & sons. *Inc., Hoboken, New Jersey, USA*.

Fredlund, D. G., & Morgenstern, N. R. (1977). Stress state variables for unsaturated soils. *Journal of the geotechnical engineering division*, *103*(5), 447–466.

Fredlund, D. G., & Rahardjo, H. (1987). Soil mechanics principles for highway engineering in arid regions. *Transportation research record*, *1137*, 1–11.

Fredlund, D. G., & Rahardjo, H. (1993). *Soil mechanics for unsaturated soils.* John Wiley & Sons.

Fredlund, D. G., & Xing, A. (1994). Equations for the soil-water characteristic curve. *Canadian geotechnical journal*, *31*(4), 521–532.

Gallage, C. P. K., & Uchimura, T. (2010). Effects of dry density and grain size distribution on soil-water characteristic curves of sandy soils. *Soils and foundations*, *50*(1), 161–172.

Gallipoli, D., Gens, A., Sharma, R., & Vaunat, J. (2003). An elasto-plastic model for unsaturated soil incorporating the effects of suction and degree of saturation on mechanical behaviour. *Géotechnique*, *53*(1), 123–135.

Gan, J., Fredlund, D., & Rahardjo, H. (1988). Determination of the shear strength parameters of an unsaturated soil using the direct shear test. *Canadian Geotechnical Journal*, *25*(3), 500–510.

Gens, A. (1982). Stress-strain and strength characteristics of a low plasticity clay.

Goh, S. G., Rahardjo, H., & Leong, E. C. (2014). Shear strength of unsaturated soils under multiple drying-wetting cycles. *Journal of Geotechnical and Geoenvironmental Engineering*, *140*(2), 06013001.

Goh, S. G. (2012). Hysteresis effects on mechanical behaviour of unsaturated soils. (PhD thesis Nanyang Technological University).

Goh, S. G., Rahardjo, H., & Choon, L. E. (2010). Shear strength equations for unsaturated soil under drying and wetting. *Journal of Geotechnical and Geoenvironmental Engineering*, *136*(4), 594–606.

Google, (2021). Google maps.

Gori, A. (2020). The unexpected softening of the undrained shear strength of organic and silty clays in rhine delta: A conceptual study. (MSc Thesis TU Delft).

Greeuw, G., Essen, H. M., van, & Van Duinen, T. A. (2016). Protocol laboratoriumproeven voor grondonderzoek aan waterkeringen. (Deltares report 1230090-0190GEO-0002).

Greeuw, G., Adel, H. d., Schapers, A. L., & Haan, E. J. d. (2001). Reduction of axial resistance due to membrane and side drains in the triaxial test. *Soft ground technology* (pp. 30–42).

Grimstad, G., Andresen, L., & Jostad, H. P. (2012). Ngi-adp: Anisotropic shear strength model for clay. *International journal for numerical and analytical methods in geomechanics*, *36*(4), 483–497.

Grognet, M. F. (2011). The boundary conditions in direct simple shear tests: Developments for peat testing at low normal stress. (MSc Thesis TU Delft).

Heinen, M., Bakker, G., & Wösten, J. (2020). *Waterretentie-en doorlatendheidskarakteristieken van boven-en ondergronden in nederland: De staringreeks: Update 2018* (tech. rep.). Wageningen Environmental Research.

Hillel, D., & Mottes, J. (1966). Effect of plate impedance, wetting method, and aging on soil moisture retention. *Soil Science*, *102*(2), 135–139.

Hillel, D. (1971). *Soil and water: Physical and processes*. Academic Press.

Hoogewerf, S., & Leemkuil, M. (2019). Voorkeursalternatief meanderende maas.

Houston, W., Dye, H., Zapata, C., Perera, Y., & Harraz, A. (2006). Determination of swcc using one point suction measurement and standard curves. *Unsaturated soils 2006* (pp. 1482–1493).

Jafarzadeh, F., Ahmadinezhad, A., & Sadeghi, H. (2020). Coupled effects of suction and degree of saturation on large strain shear modulus of unsaturated sands. *Unsaturated soils: Research & applications* (pp. 1559–1564). CRC Press.

Jefferies, M., & Been, K. (2019). *Soil liquefaction: A critical state approach*. CRC press.

Joer, H., Erbrich, C., & Sharma, S. (2010). A new interpretation of the simple shear test. *Proc. 2nd*.

Joer, H., Lanier, J., & Fahey, M. (1998). Deformation of granular materials due to rotation of principal axes. *Géotechnique*, *48*(5), 605–619.

Jommi, C., & Della Vecchia, G. (2013). Geomechanical analysis of river embankments. *Mechanics of Unsaturated Geomaterials*, 353–374.

Kanwar, N. S., & Deng, J. (2019). A comparison of probabilistic distributions of undrained shear strength of soils in nipigon river, canada. *IOP Conference Series: Earth and Environmental Science*, *351*(1), 012024.

Karlsrud, K., Lunne, T., Kort, D., & Strandvik, S. (2005). Cptu correlations for clays. *Proceedings of the 16th international conference on soil mechanics and geotechnical engineering*, 693–702.

Khalili, N., & Zargarbashi, S. (2010). Influence of hydraulic hysteresis on effective stress in unsaturated soils. *Géotechnique*, *60*(9), 729–734.

Khalili, N., & Khabbaz, M. (1998). A unique relationship for χ for the determination of the shear strength of unsaturated soils. *Geotechnique*, *48*(5), 681–687.

Kjellman, W. (1951). Testing the shear strength of clay in sweden. *Géotechnique*, *2*(3), 225–232.

Klar, A., Roed, M., Rocchi, I., & Paegle, I. (2019). Evaluation of horizontal stresses in soil during direct simple shear by high-resolution distributed fiber optic sensing. *Sensors*, *19*(17), 3684.

Konstadinou, M., & Zwanenburg, C. (2019). A critical review of membrane and filter paper correction formulas for the triaxial testing of soft soils. *Geotechnical Testing Journal*, *43*(1), 1–19.

Koutsoftas, D. C., & Ladd, C. C. (1985). Design strengths for an offshore clay. *Journal of Geotechnical Engineering*, *111*(3), 337–355.

Ladd, C. C. (1991). Stability evaluation during staged construction. *Journal of geotechnical engineering*, *117*(4), 540–615.

Ladd, C. C., & Foott, R. (1974). New design procedure for stability of soft clays. *Journal of the Geotechnical Engineering Division*, *100*(7), 763–786.

Ladd, C. C., & DeGroot, D. J. (2004). *Recommended practice for soft ground site characterization: Arthur casagrande lecture*. Massachusetts Institute of Technology.

Le Meil, G., Hendry, M., & Martin, D. (2016). Direct simple shear (dss) testing of a very stiff glaciolacustrine clay.

Lee, I.-M., Sung, S.-G., & Cho, G.-C. (2005). Effect of stress state on the unsaturated shear strength of a weathered granite. *Canadian Geotechnical Journal*, *42*(2), 624–631.

Lu, N. (2008). Is matric suction a stress variable? *Journal of Geotechnical and Geoenvironmental Engineering*, *134*(7), 899–905.

Lu, N., & Godt, J. W. (2013). *Hillslope hydrology and stability*. Cambridge University Press.

Lu, N., Godt, J. W., & Wu, D. T. (2010). A closed-form equation for effective stress in unsaturated soil. *Water Resources Research*, *46*(5).

Lu, N., & Likos, W. J. (2006). Suction stress characteristic curve for unsaturated soil. *Journal of geotechnical and geoenvironmental engineering*, *132*(2), 131–142.

Lupini, J., Skinner, A., & Vaughan, P. (1982). Discussion: The drained residual strength of cohesive soils. *Géotechnique*, *32*(1), 76–76.

Mayne, P. W. (1985). A review of undrained strength in direct simple shear. *Soils and foundations*, *25*(3), 64–72.

Ministerie van Infrastructuur en Waterstaat, (2019). Schematiseringshandleiding macrostabiliteit - wbi 2017 v3.0.

Molenaar, F. (2020). Numerical analysis of the influence of desiccation cracks on the stability of dutch river dykes. (MSc Thesis TU Delft).
Mun, W., Teixeira, T., Balci, M., Svoboda, J., & McCartney, J. S. (2016). Rate effects on the undrained shear strength of compacted clay. *Soils and Foundations*, *56*(4), 719–731.
Muraro, S. (2019). The deviatoric behaviour of peat: A route between past empiricism and future perspectives.
Nam, S., Gutierrez, M., Diplas, P., Petrie, J., Wayllace, A., Lu, N., & Muñoz, J. J. (2010). Comparison of testing techniques and models for establishing the swcc of riverbank soils. *Engineering Geology*, *110*(1-2), 1–10.
Nelder, J. A., & Mead, R. (1965). A simplex method for function minimization. *The computer journal*, *7*(4), 308–313.
NEN. (2014). Nen-en-iso 17892-2:2014 geotechnical investigation and testing – laboratory testing of soil – part 2: Determination of bulk density.
NEN. (2018). Nen-en-iso 17892-9:2018 geotechnical investigation and testing – laboratory testing of soil – part 9: Consolidated triaxial compression tests on water-saturated soils.
NEN. (2019a). Nen-en-iso 14688-1:2019 geotechnisch onderzoek en beproeving - identificatie en classificatie van grond - deel 1: Identificatie en beschrijving.
NEN. (2019b). Nen-en-iso 14688-2:2019 geotechnisch onderzoek en beproeving - identificatie en classificatie van grond - deel 2: Grondslagen voor een classificatie.
NEN. (2019c). Nen-en-iso 17892-10:2019 geotechnical investigation and testing – laboratory testing of soil – part 10: Direct shear test.
Ng, C. W., & Pang, Y. (2000). Influence of stress state on soil-water characteristics and slope stability. *Journal of geotechnical and geoenvironmental engineering*, *126*(2), 157–166.
Ochiai, H. (1981). A method for calculating the undrained strength ratio, cu/p, of normally consolidated clay measured in the simple shear test. *Soils and Foundations*, *21*(1), 109–115.
Oda, M. (1975). On the relation τ/σn= $\kappa \cdot$ tanψ in the simple shear test. *Soils and Foundations*, *15*(4), 35–41.
Oda, M., & Konishi, J. (1974). Rotation of principal stresses in granular material during simple shear. *Soils and Foundations*, *14*(4), 39–53.
O'Neill, D. A. (1987). *Undrained strength anisotropy of an overconsolidated thixotropic clay* (Doctoral dissertation). Massachusetts Institute of Technology.
Patil, U. D., Hoyos, L. R., Puppala, A. J., & Congress, S. S. C. (2020). Suction stress characteristic curves of cohesive-frictional soils from multiple suction-controlled testing methods. *International Journal of Geomechanics*, *20*(7), 04020077.
Perera, Y. Y., Zapata, C. E., Houston, W. N., & Houston, S. L. (2005). Prediction of the soil-water characteristic curve based on grain-size-distribution and index properties. *Advances in pavement engineering* (pp. 1–12).
Pham, H., & Fredlund, D. (2003). Dynamic programming method in slope stability computations. *Proceedings of the 12th Asian Regional Conference on Soil Mechanics and Geotechnical Engineering.*
Ponzoni, E., Nocilla, A., & Coop, M. (2017). The behaviour of a gap graded sand with mixed mineralogy. *Soils and foundations*, *57*(6), 1030–1044.
Ponzoni, E., Nocilla, A., Coop, M., & Colleselli, F. (2014). Identification and quantification of transitional modes of behaviour in sediments of venice lagoon. *Géotechnique*, *64*(9), 694–708.
Prakash, A., Hazra, B., & Sreedeep, S. (2021). Probabilistic analysis of soil-water characteristic curve using limited data. *Applied Mathematical Modelling*, *89*, 752–770.
Prevost, J.-H., & Høeg, K. (1976). Reanalysis of simple shear soil testing. *Canadian Geotechnical Journal*, *13*(4), 418–429.
Rahardjo, H., & Fredlund, D. G. (2003). K o-volume change characteristics of an unsaturated soil with respect to various loading paths. *Geotechnical Testing Journal*, *26*(1), 79–91.
Rahardjo, H., Heng, O. B., & Choon, L. E. (2004). Shear strength of a compacted residual soil from consolidated drained and constant water content triaxial tests. *Canadian Geotechnical Journal*, *41*(3), 421–436.
Rasool, A. M., & Aziz, M. (2020). Advanced triaxial tests on partially saturated soils under unconfined conditions. *International Journal of Civil Engineering*, *18*, 1139–1156.
Rassam, D. W., & Williams, D. J. (1999). A relationship describing the shear strength of unsaturated soils. *Canadian Geotechnical Journal*, *36*(2), 363–368.
Ren, J. (2019). *Interpretation of the frozen soils behavior extending the mechanics of unsaturated soils* (Doctoral dissertation). Université d'Ottawa/University of Ottawa.

Roscoe, K. H. (1953). An apparatus for the application of simple shear to soil samples. *Proc. 3rd ICSMFE*, *1*, 186–191.

Sayem, H. M., & Kong, L.-W. (2016). Effects of drying-wetting cycles on soil-water characteristic curve. *DEStech Transactions on Environment, Energy and Earth Sciences*.

Schmertmann, J. H. (2006). Estimating slope stability reduction due to rain infiltration mounding. *Journal of geotechnical and geoenvironmental engineering*, *132*(9), 1219–1228.

Schofield, A. N., & Wroth, P. (1968). *Critical state soil mechanics* (Vol. 310). McGraw-hill London.

Sharma, S. S., Ramsey, N., Lee, F., & Bhattarai, B. N. (2017). Challenges in assessing the shear strength of offshore sediments using simple shear tests. *Geotechnical frontiers 2017* (pp. 327–336).

Sheahan, T. C., Ladd, C. C., & Germaine, J. T. (1996). Rate-dependent undrained shear behavior of saturated clay. *Journal of Geotechnical Engineering*, *122*(2), 99–108.

Stowa. (2001). Bomen op en nabij waterkeringen - achtergrondrapport.

Sun, D., You, G., Annan, Z., & Daichao, S. (2016). Soil–water retention curves and microstructures of undisturbed and compacted guilin lateritic clay. *Bulletin of Engineering Geology and the Environment*, *75*(2), 781–791.

TAW. (2001). Technisch rapport waterkerende grondconstructies; geotechnische aspecten van dijken, dammen en boezemkaden. *TR19-prepared by GeoDelft*.

Taylor, D. W. (1948). *Fundamentals of soil mechanics* (Vol. 66). LWW.

Terzaghi, K., Peck, R. B., & Mesri, G. (1996). *Soil mechanics in engineering practice*. John Wiley & Sons.

Thu, T. M., Rahardjo, H., & Leong, E.-C. (2007). Soil-water characteristic curve and consolidation behavior for a compacted silt. *Canadian Geotechnical Journal*, *44*(3), 266–275.

Tripathy, S., Elgabu, H., & Thomas, H. R. (2012). Matric suction measurement of unsaturated soils with null-type axis-translation technique. *Geotechnical Testing Journal*, *35*(1), 91–102.

Tse, E., & Ng, C. W. W. (2008). Effects of drying and wetting cycles on unsaturated shear strength. *Proceedings of the 1st European conference on unsaturated soils, E-UNSAT*, 481–486.

van den Akker, J., Hendriks, R., Frissel, J., Oostindie, K., & Wesseling, J. (2014). *Gedrag van verdroogde kades : Fase b, c, d: Onstaan en gevaar van krimpscheuren in klei- en veenkades*. Alterra.

Van Duinen, T. A. (2020). Shear strength for initially unsaturated soil – intermediate results measurements oijen and westervoort. (Deltares report 11204453-002-GEO-0001).

Vanapalli, S. K., Fredlund, D. G., Pufahl, D. E., & Clifton, A. W. (1996). Model for the prediction of shear strength with respect to soil suction. *Canadian geotechnical journal*, *33*(3), 379–392.

Vanapalli, S. K., Fredlund, D. G., & Pufahl, D. E. (1999). The influence of soil structure and stress history on the soil–water characteristics of a compacted till. *Geotechnique*, *49*(2), 143–159.

Wang, L., Cao, Z.-J., Li, D.-Q., Phoon, K.-K., & Au, S.-K. (2018). Determination of site-specific soil-water characteristic curve from a limited number of test data–a bayesian perspective. *Geoscience Frontiers*, *9*(6), 1665–1677.

Wheeler, S. J., Näätänen, A., Karstunen, M., & Lojander, M. (2003). An anisotropic elastoplastic model for soft clays. *Canadian Geotechnical Journal*, *40*(2), 403–418.

Witteveen+Bos. (2021). Project meanderende maas: Geotechnisch interpretatie rapport.

Wood, D. M. (1990). *Soil behaviour and critical state soil mechanics*. Cambridge university press.

Wood, D. M. (2017). *Geotechnical modelling*. CRC press.

Wroth, C. (1984). The interpretation of in situ soil tests. *Geotechnique*, *34*(4), 449–489.

Xing, X., Li, T., & Fu, Y. (2016). Determination of the related strength parameters of unsaturated loess with conventional triaxial test. *Environmental Earth Sciences*, *75*(1), 82.

Yang, H., Rahardjo, H., Leong, E.-C., & Fredlund, D. G. (2004). Factors affecting drying and wetting soil-water characteristic curves of sandy soils. *Canadian Geotechnical Journal*, *41*(5), 908–920.

Zapata, C. E., Houston, W. N., Houston, S. L., & Walsh, K. D. (2000). Soil–water characteristic curve variability. *Advances in unsaturated geotechnics* (pp. 84–124).

Zein, A. K. M. (2017). Estimation of undrained shear strength of fine grained soils from cone penetration resistance. *International Journal of Geo-Engineering*, *8*(1), 1–13.

Zhang, C., & Lu, N. (2020). Unified effective stress equation for soil. *Journal of Engineering Mechanics*, *146*(2), 04019135.

Zhang, L., & Yan, W. (2015). Stability analysis of unsaturated soil slope considering the variability of soil-water characteristic curve. *Geotechnical safety and risk V*, 281–286.

Zwanenburg, C., de Lange, D., & Teunissen, J. (2019). Lateral stress measurement in dss testing.

Part V: Appendix

A. Triaxial test results

A.1 $\theta_{vol} = 51.50\%$

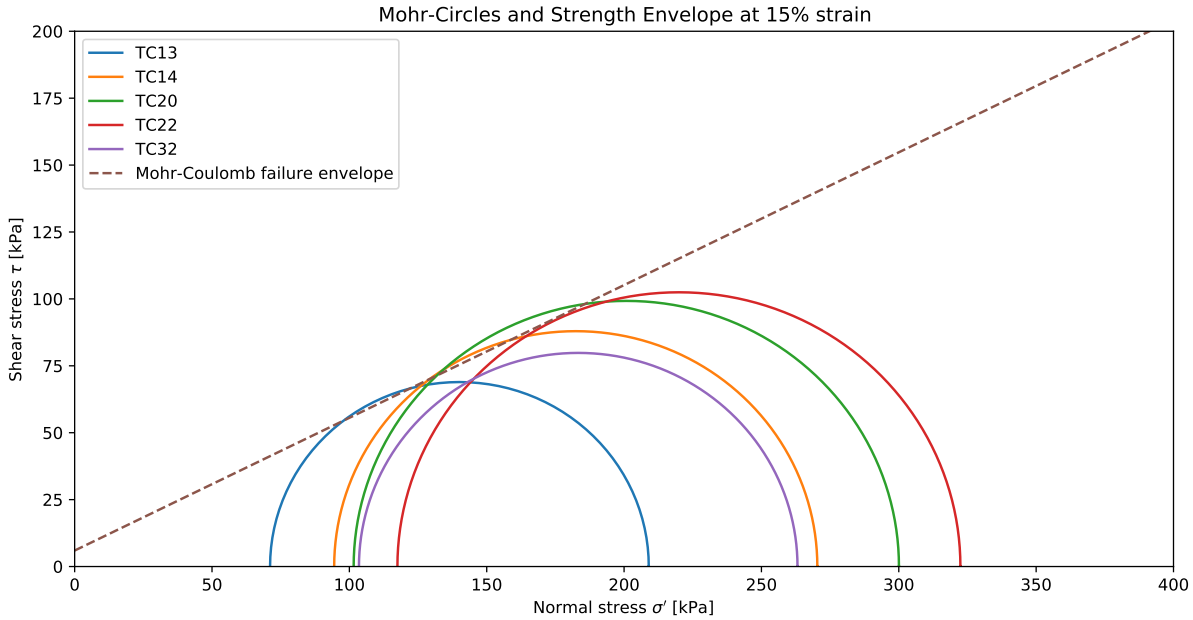

Figure A.1: Mohr-circles and strength envelope at 10% axial strain

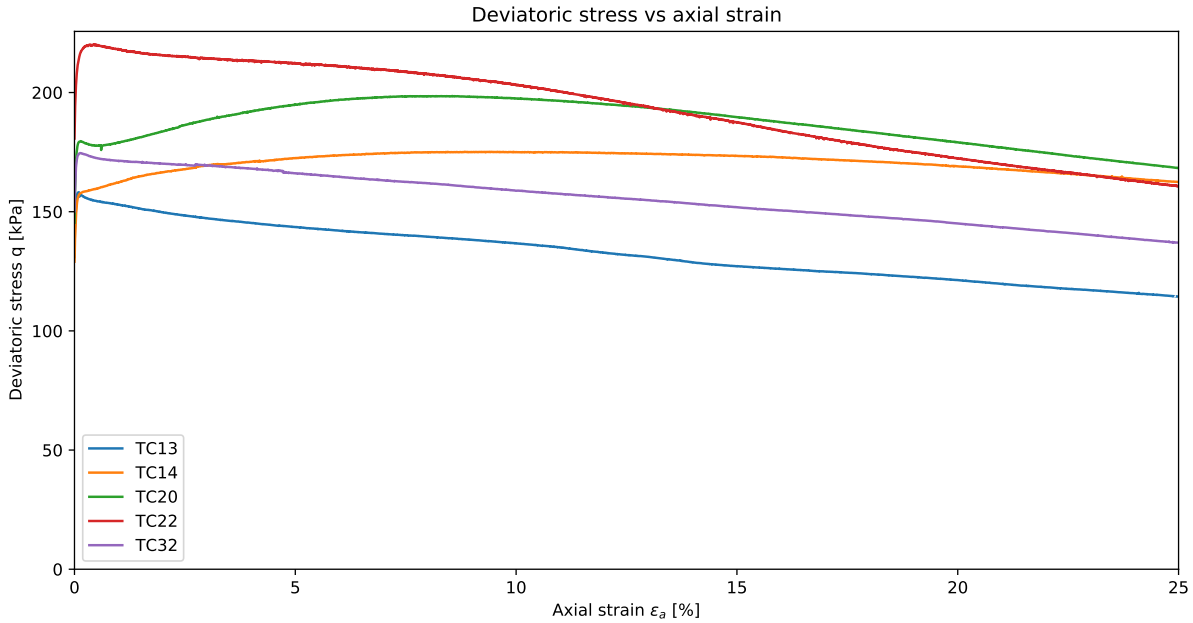

Figure A.2: q vs ϵ_a

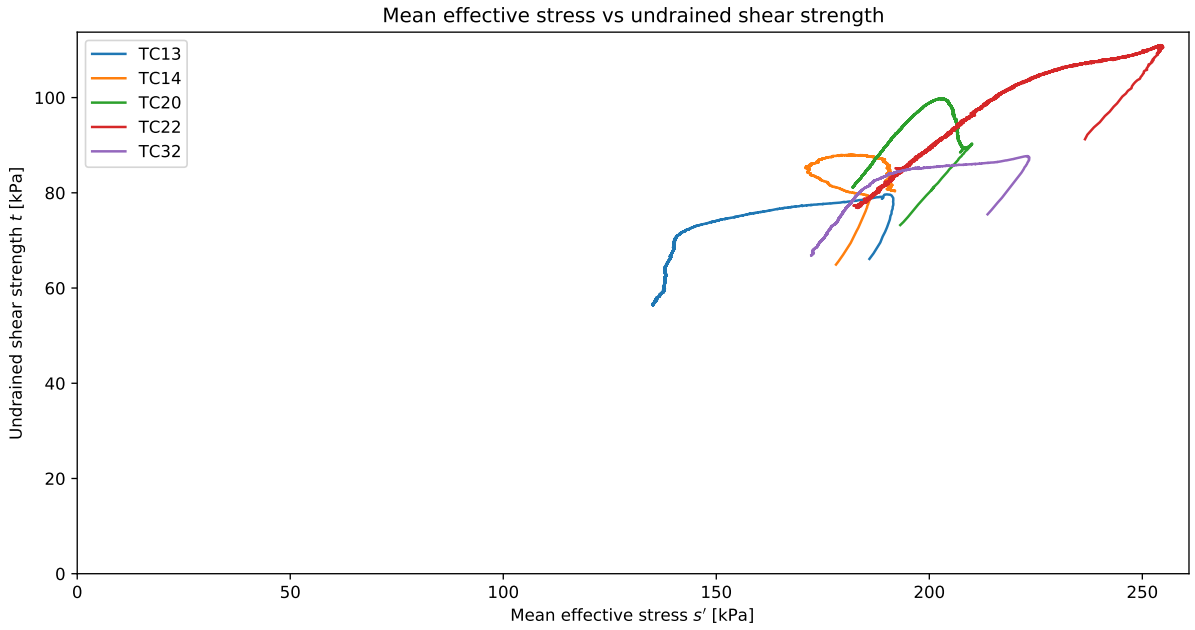

Figure A.3: s', t diagram

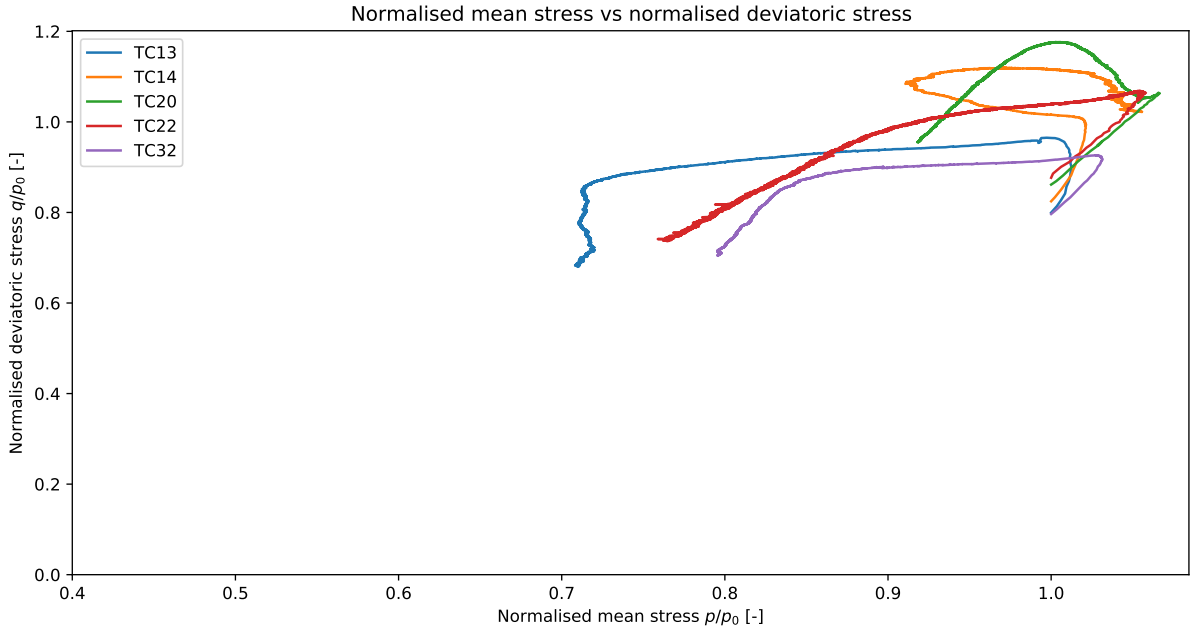

Figure A.4: q/p_0 vs p/p_0

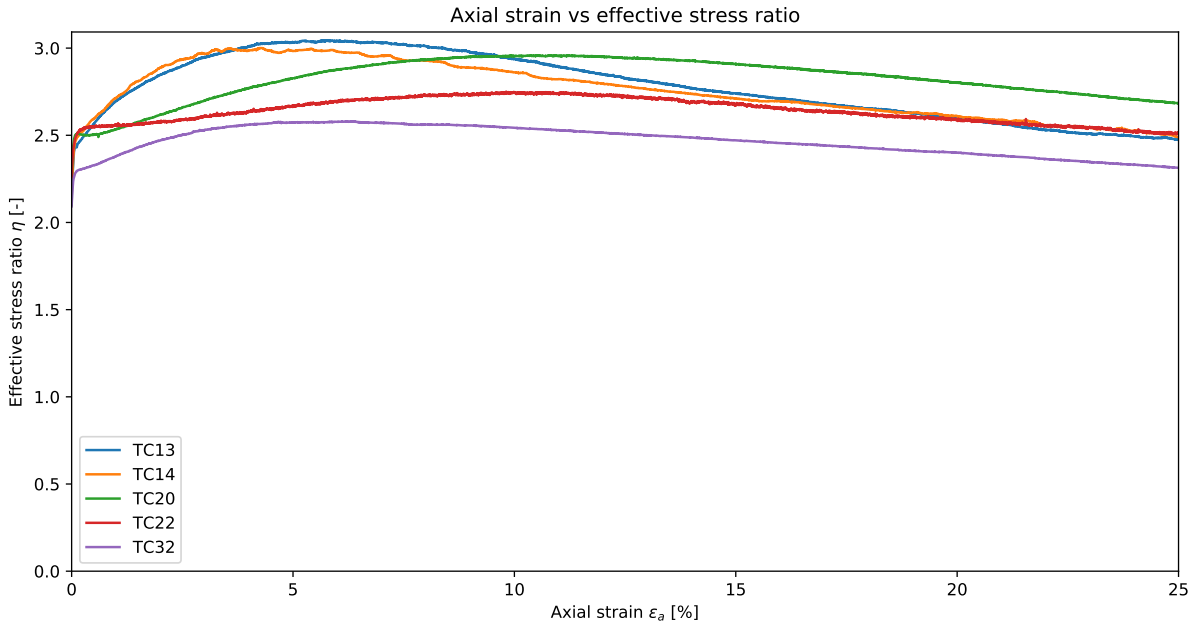

Figure A.5: ϵ_a vs η

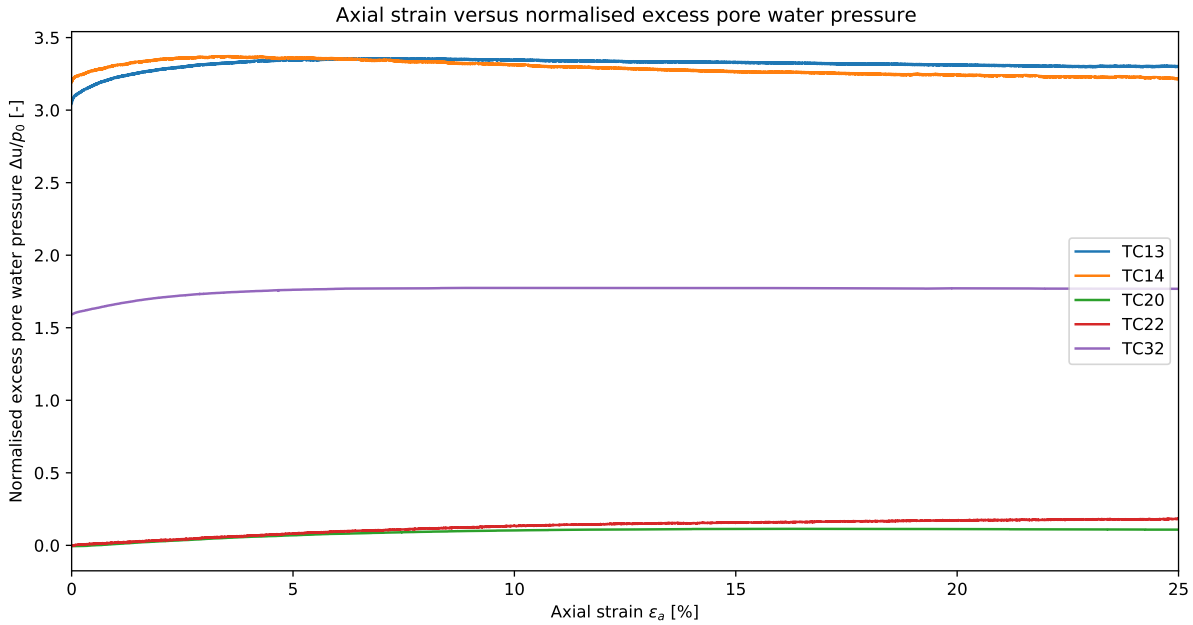

Figure A.6: ϵ_a vs Δ_u/p_o

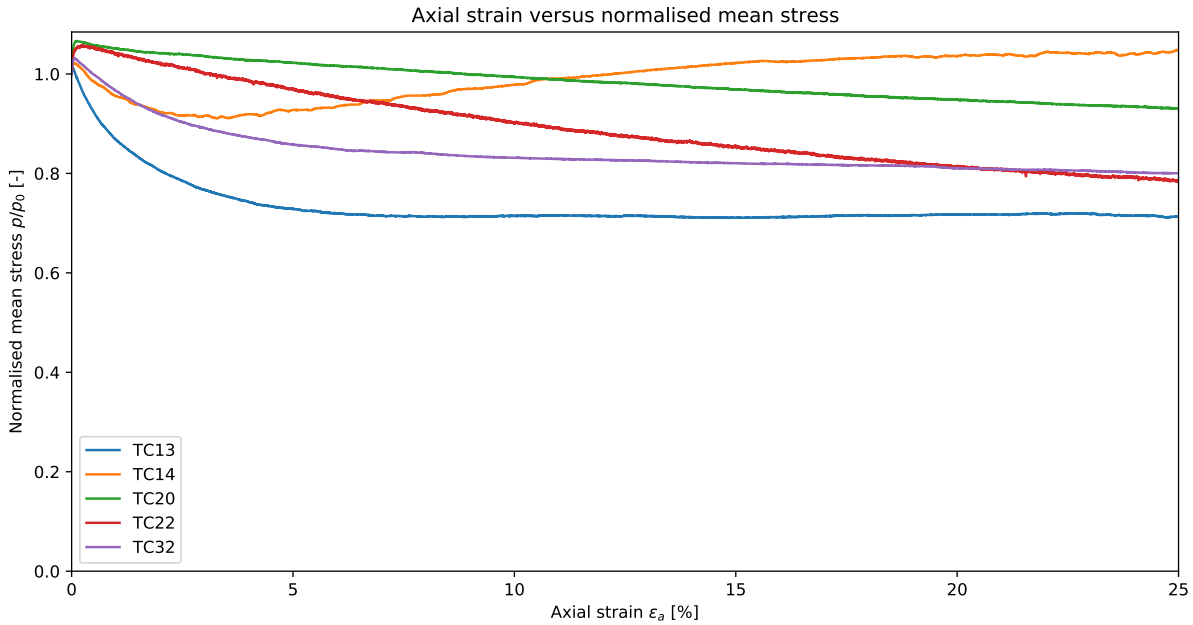

Figure A.7: ϵ_a vs p/p_0

A.2 $\theta_{vol} = 42.05\%$

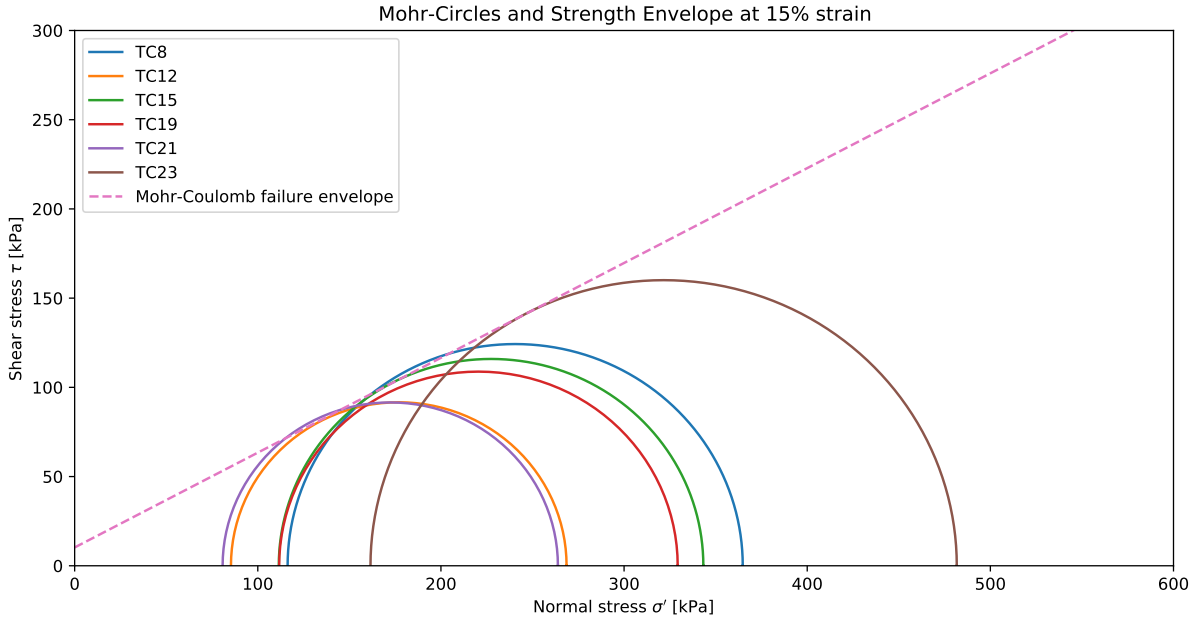

Figure A.8: Mohr-circles and strength envelope at 10% axial strain

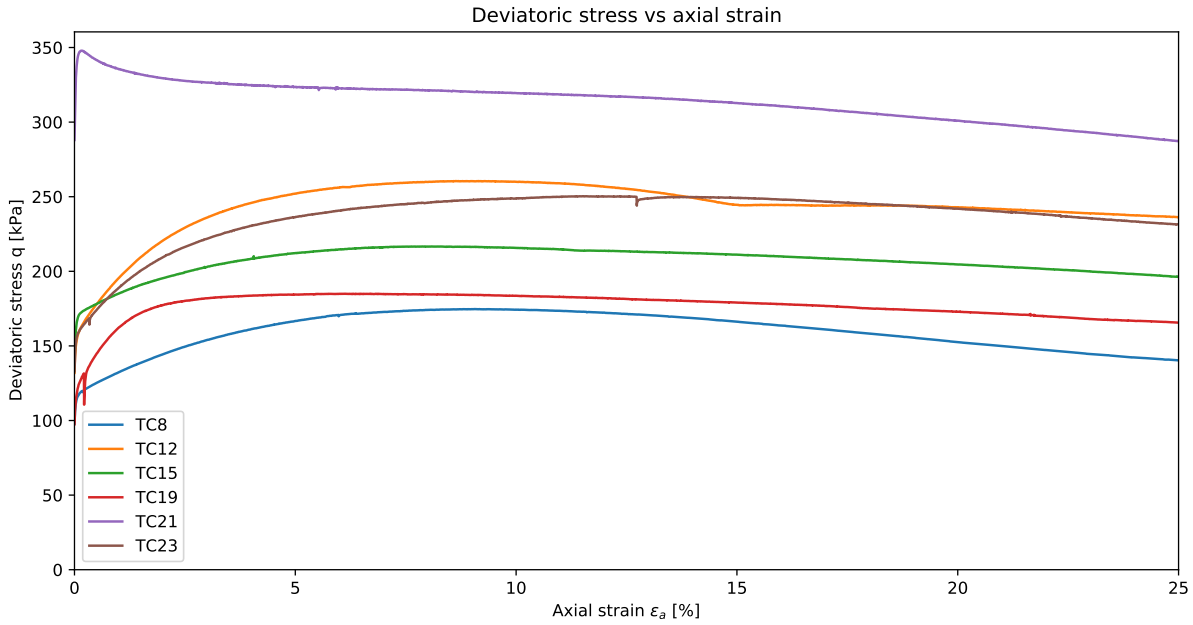

Figure A.9: q vs ϵ_a

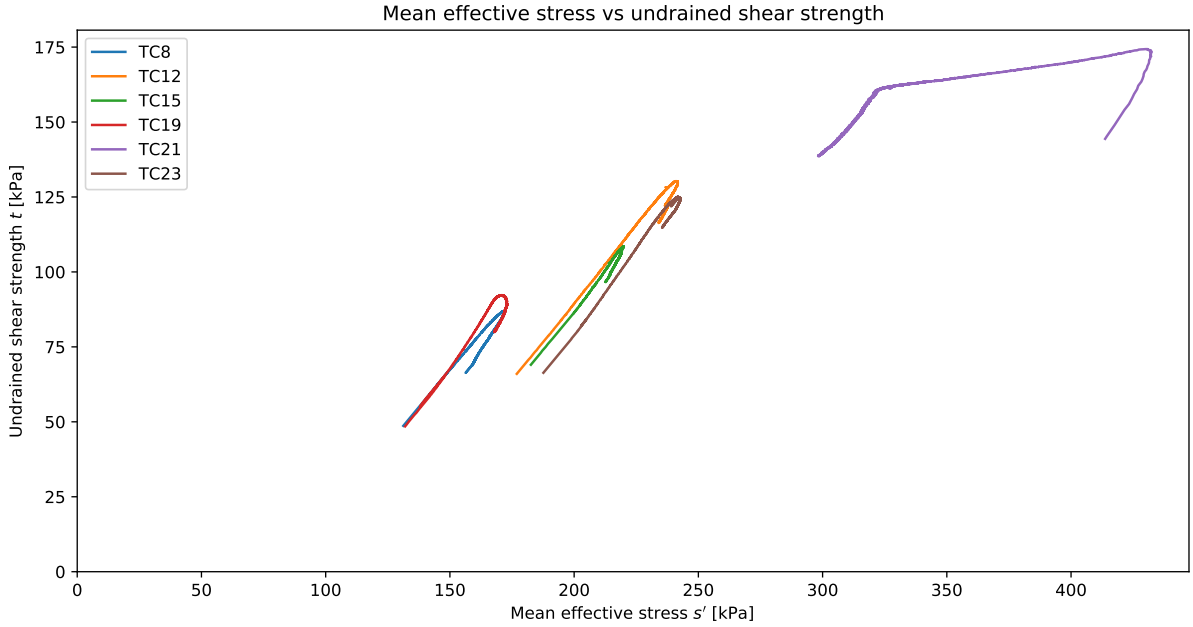

Figure A.10: s', t diagram

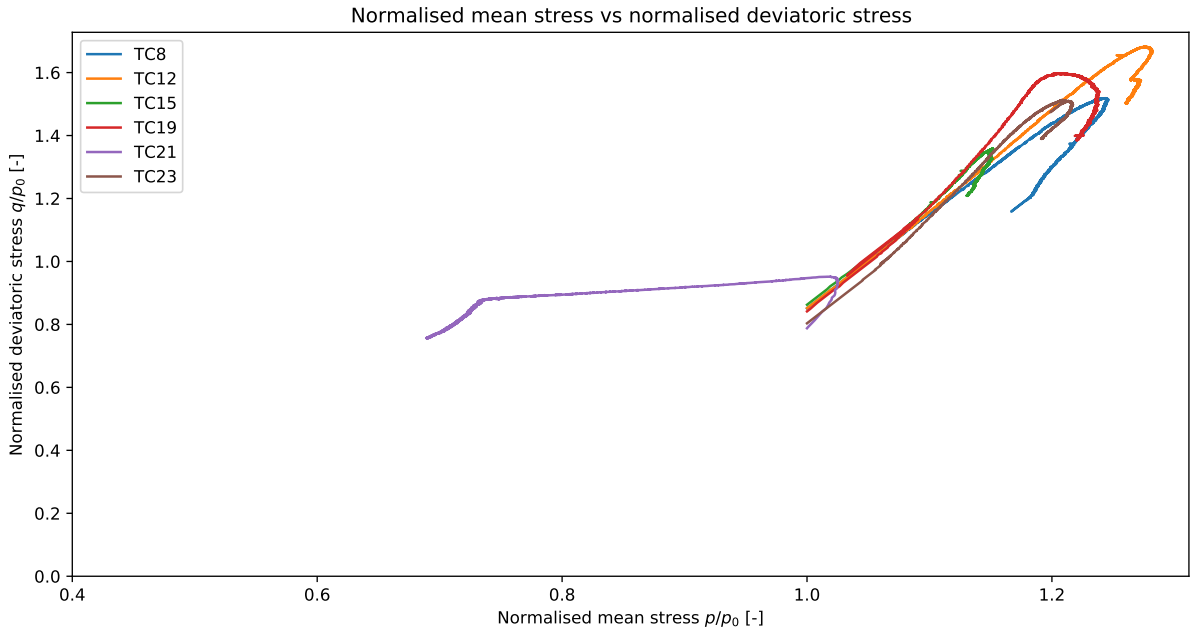

Figure A.11: q/p_0 vs p/p_0

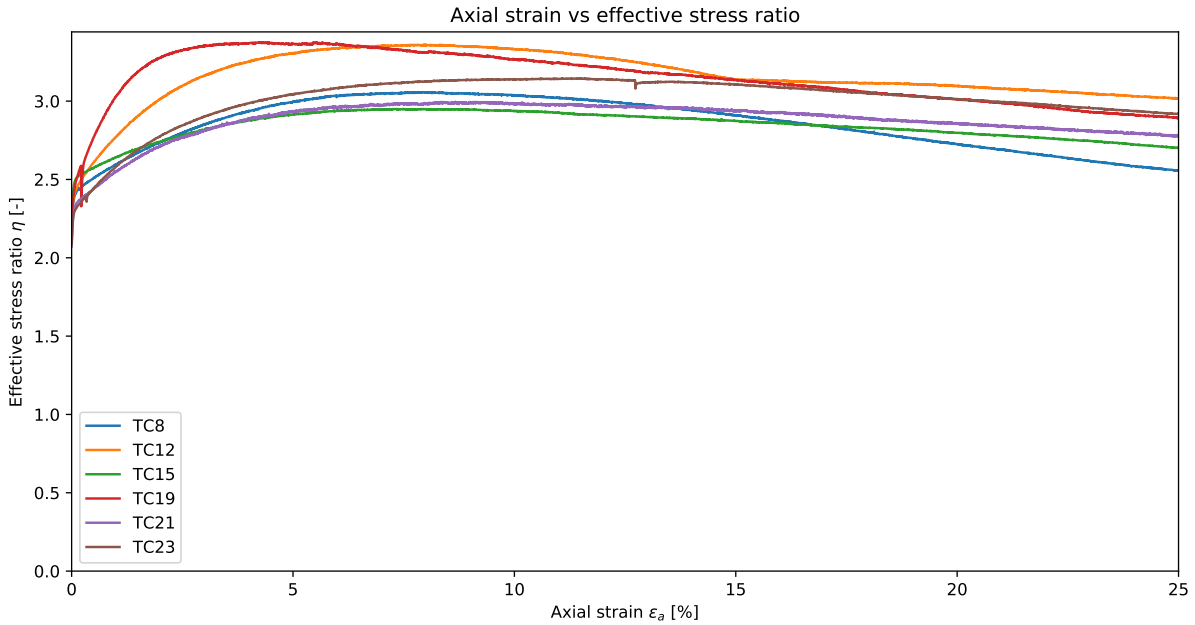

Figure A.12: ϵ_a vs η

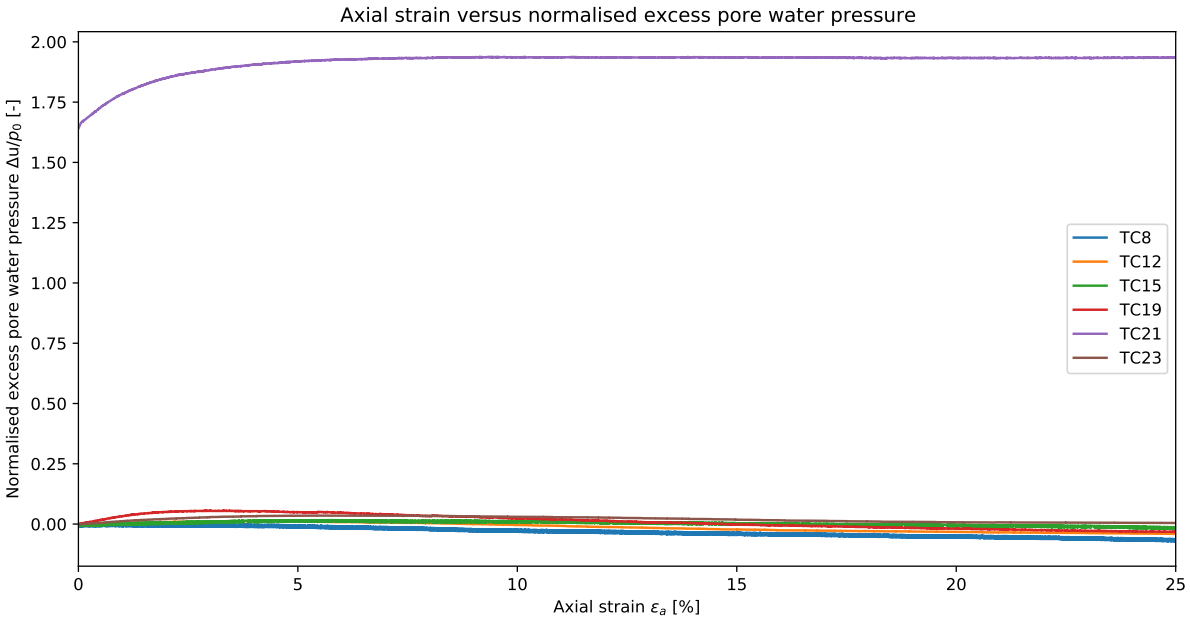

Figure A.13: ϵ_a vs Δ_u/p_o

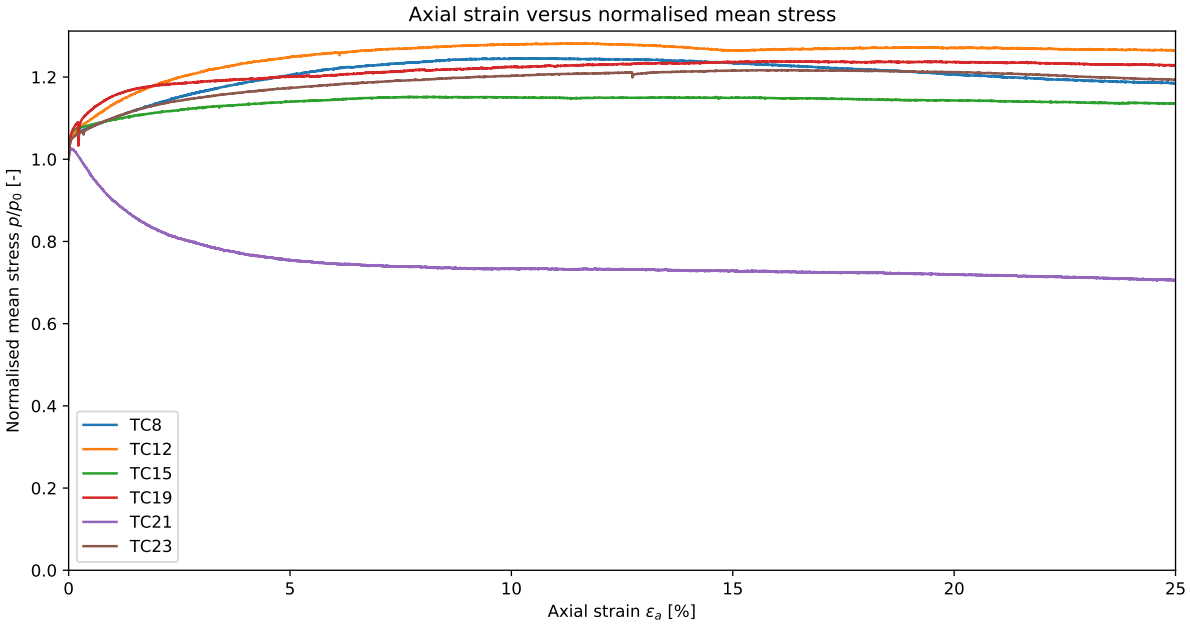

Figure A.14: ϵ_a vs p/p_0

A.3 $\theta_{vol} = 35.87\%$

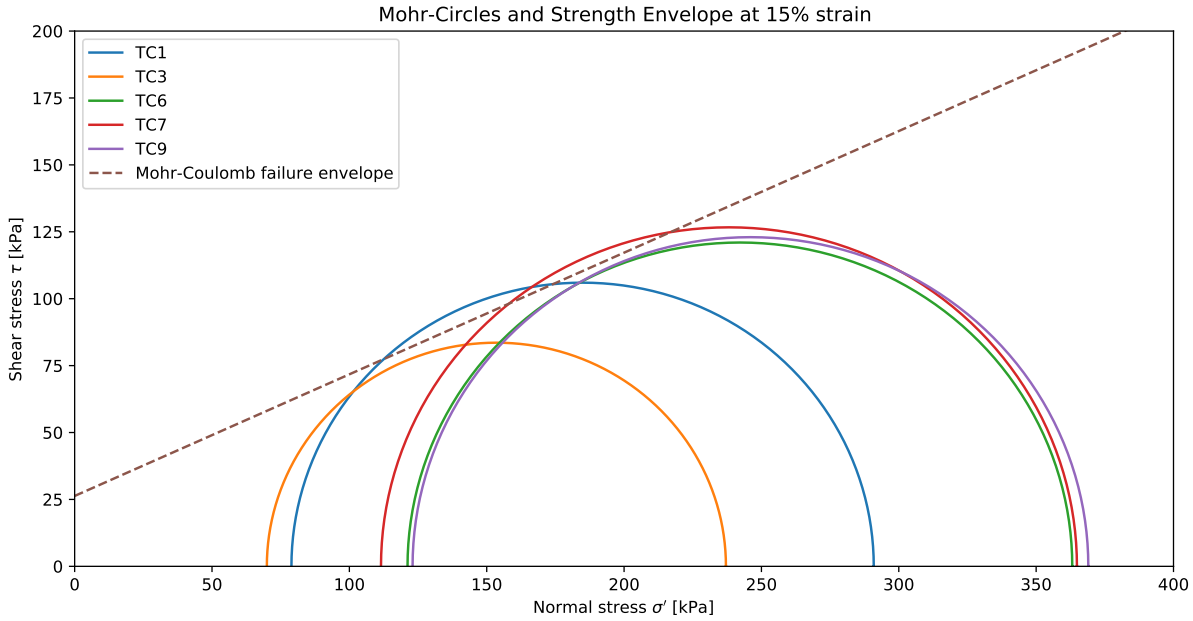

Figure A.15: Mohr-circles and strength envelope at 10% axial strain

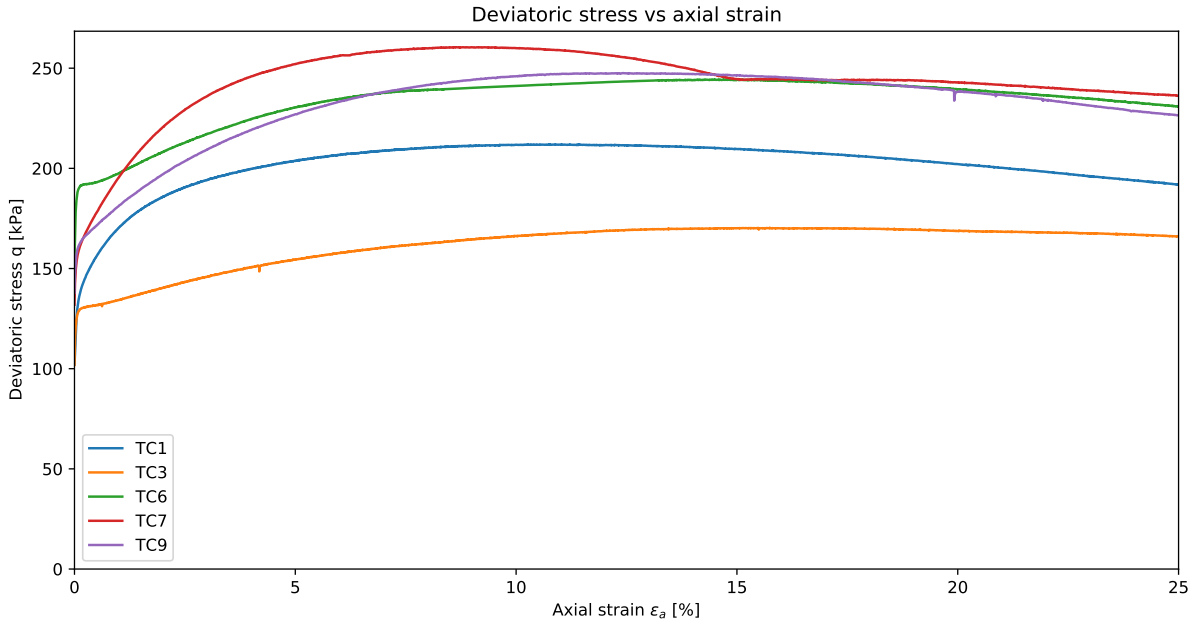

Figure A.16: q vs ϵ_a

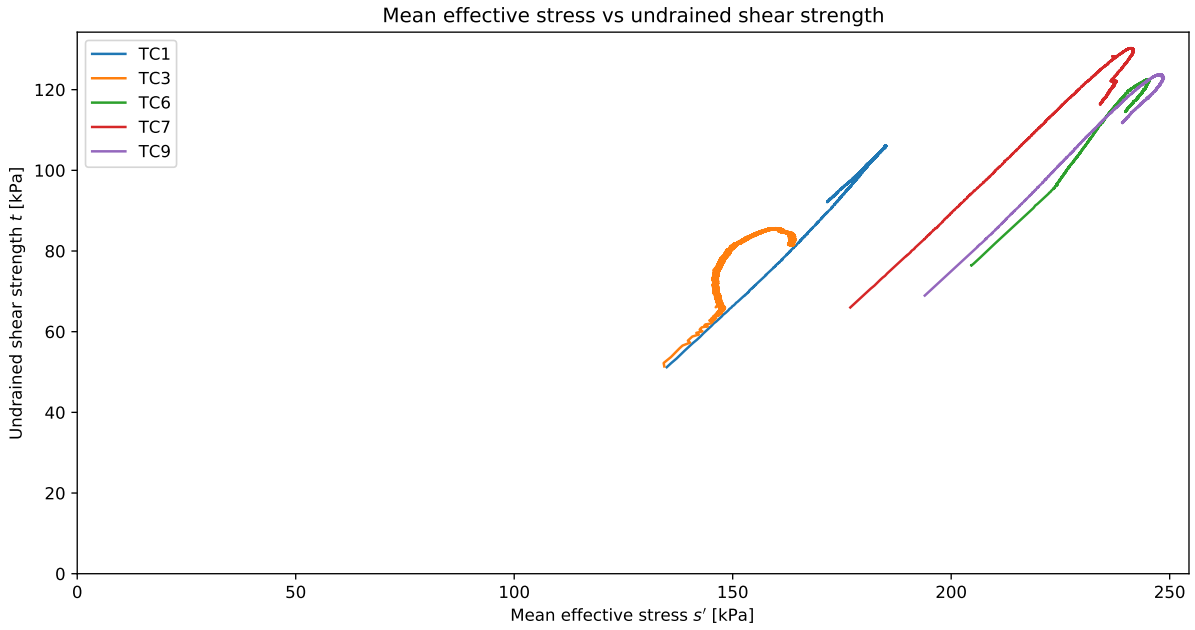

Figure A.17: s', t diagram

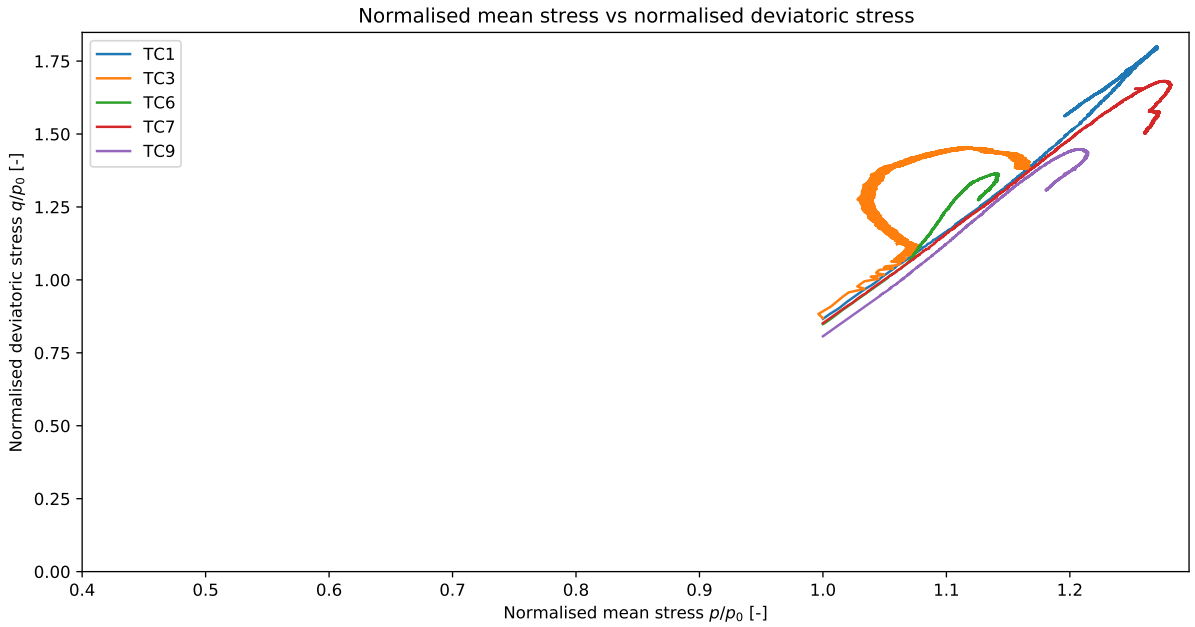

Figure A.18: q/p_0 vs p/p_0

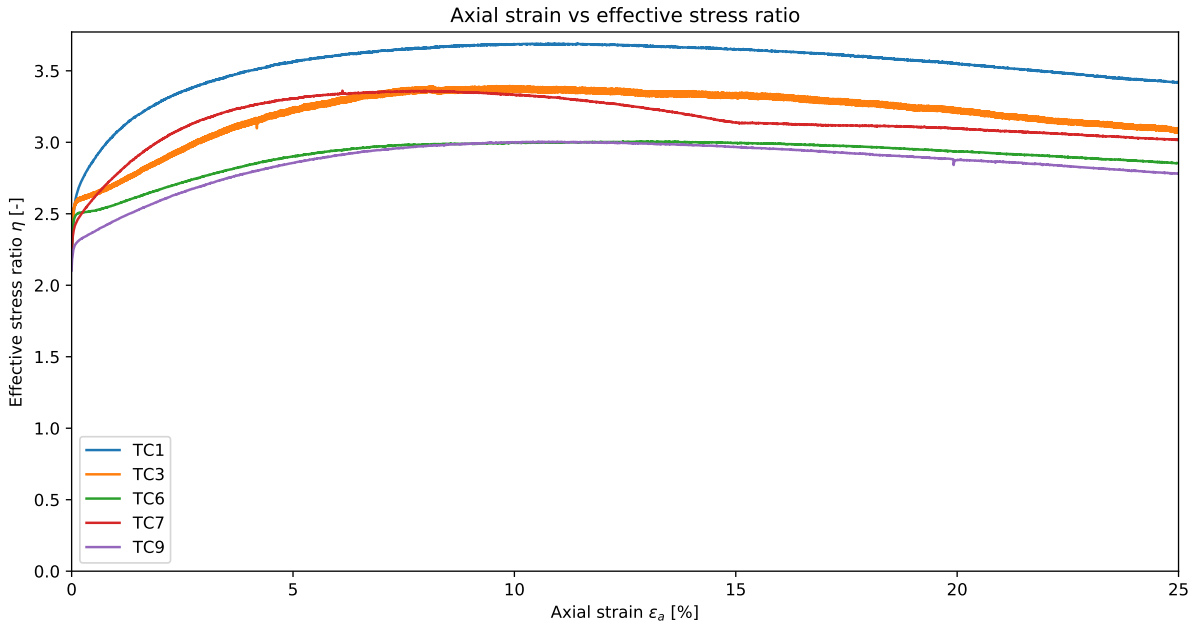

Figure A.19: ϵ_a vs η

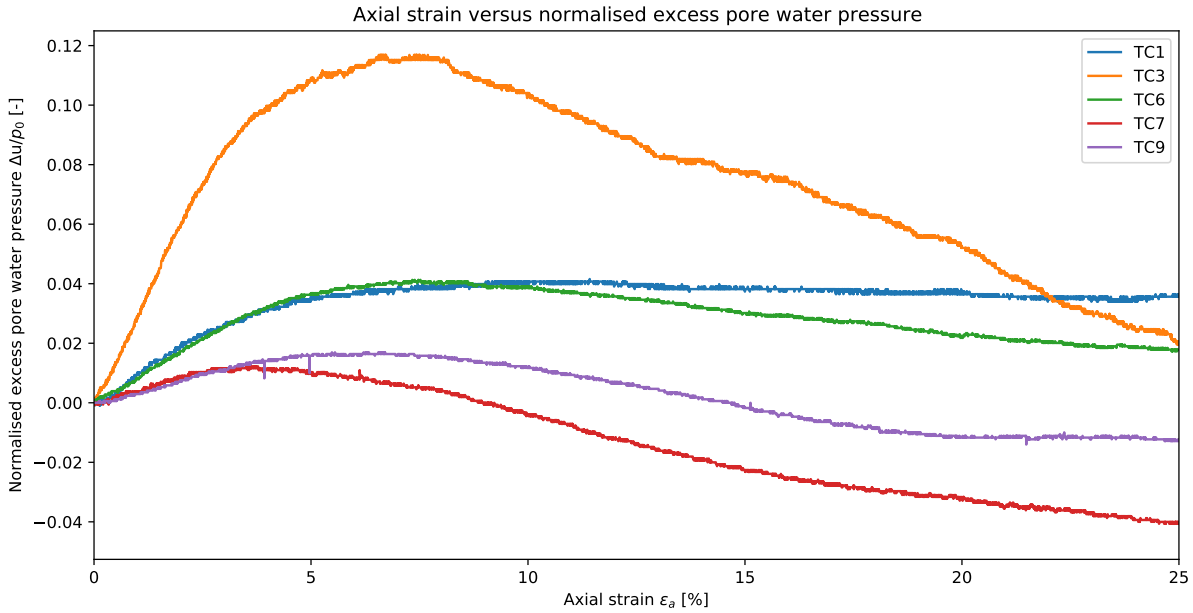

Figure A.20: ϵ_a vs Δ_u/p_o

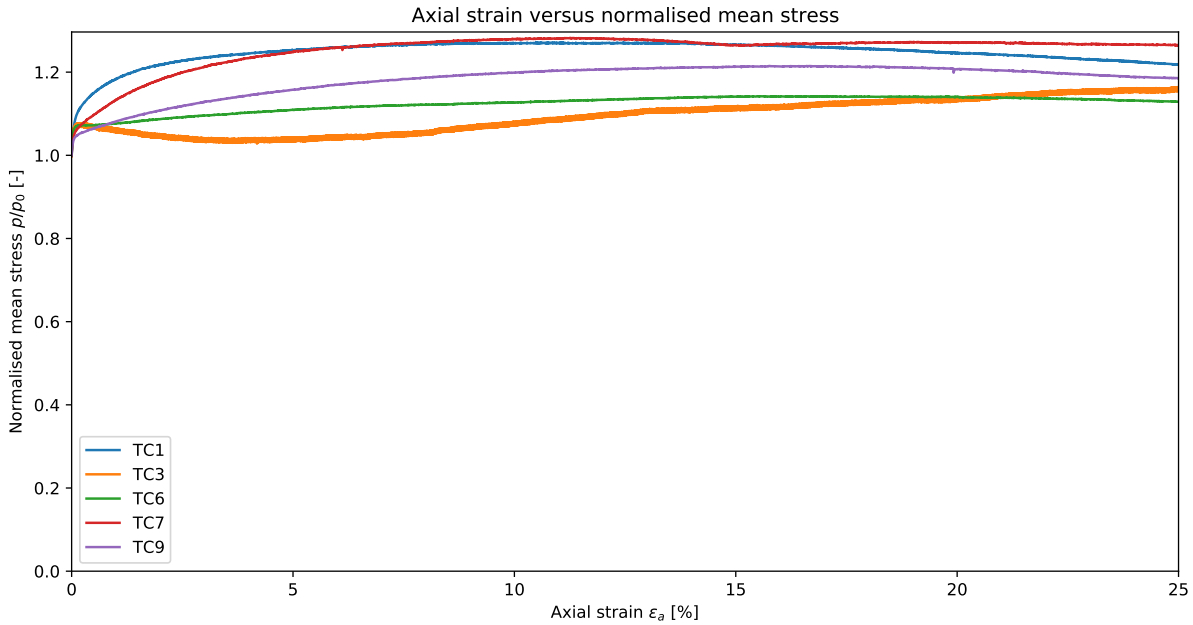

Figure A.21: ϵ_a vs p/p_0

A.4 $\theta_{vol} = 33.50\%$

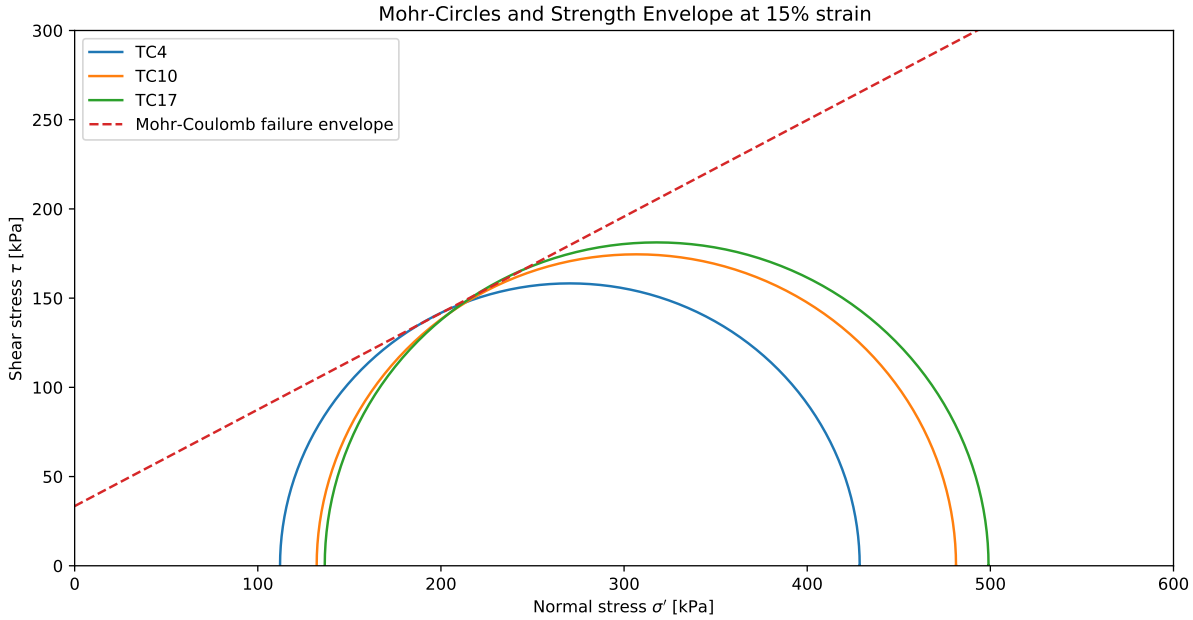

Figure A.22: Mohr-circles and strength envelope at 10% axial strain

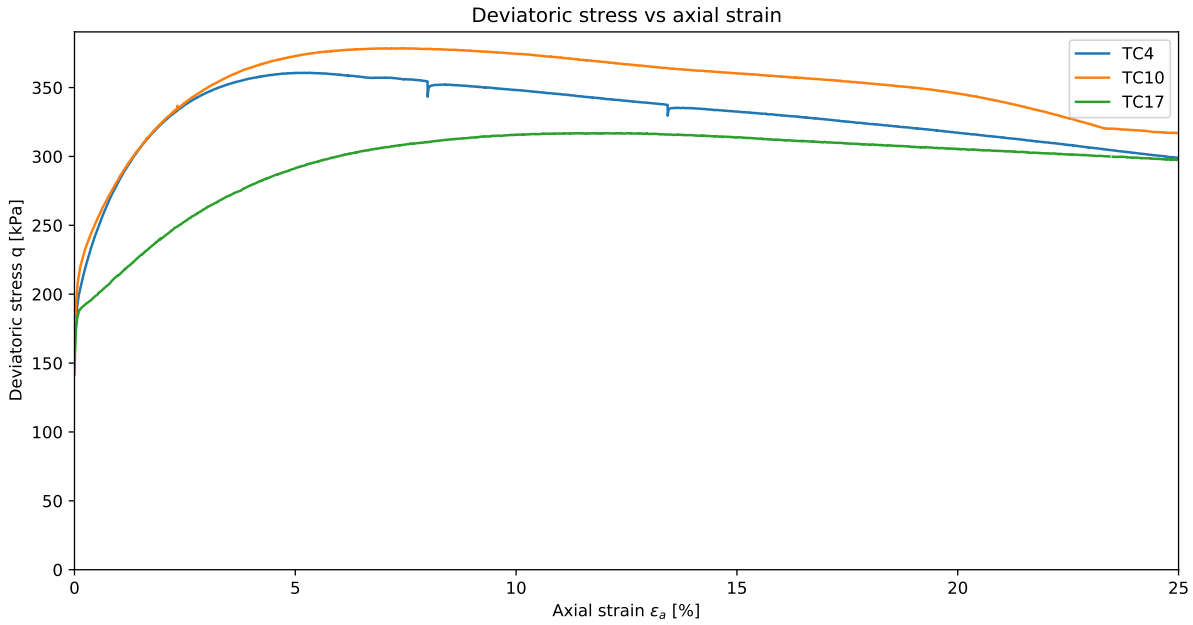

Figure A.23: q vs ϵ_a

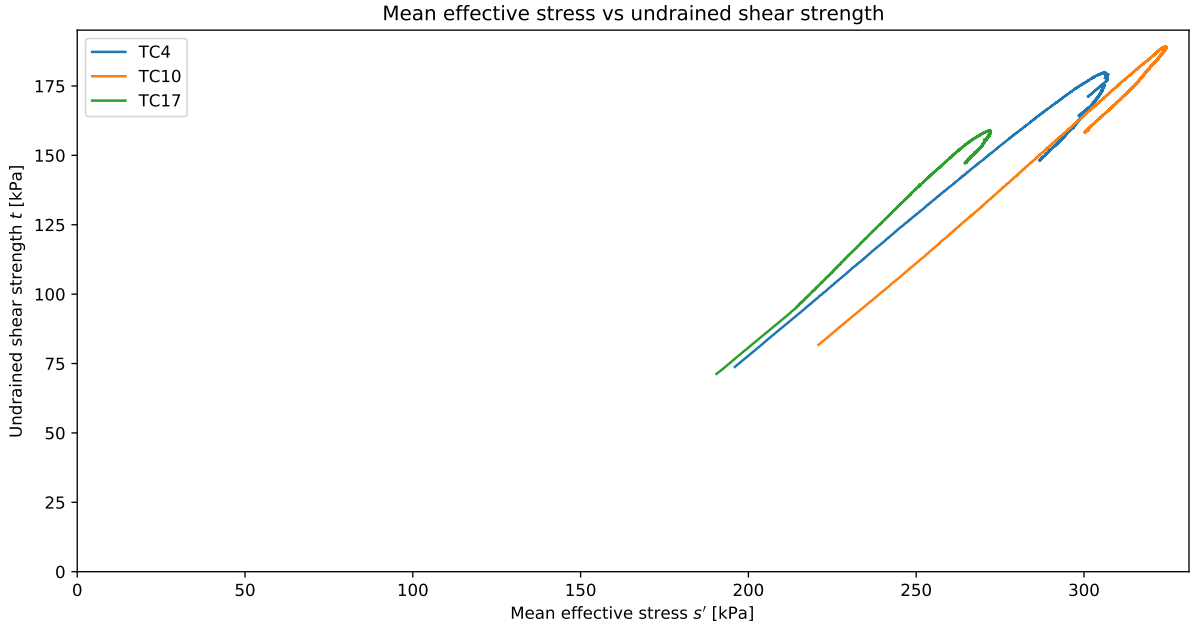

Figure A.24: s',t diagram

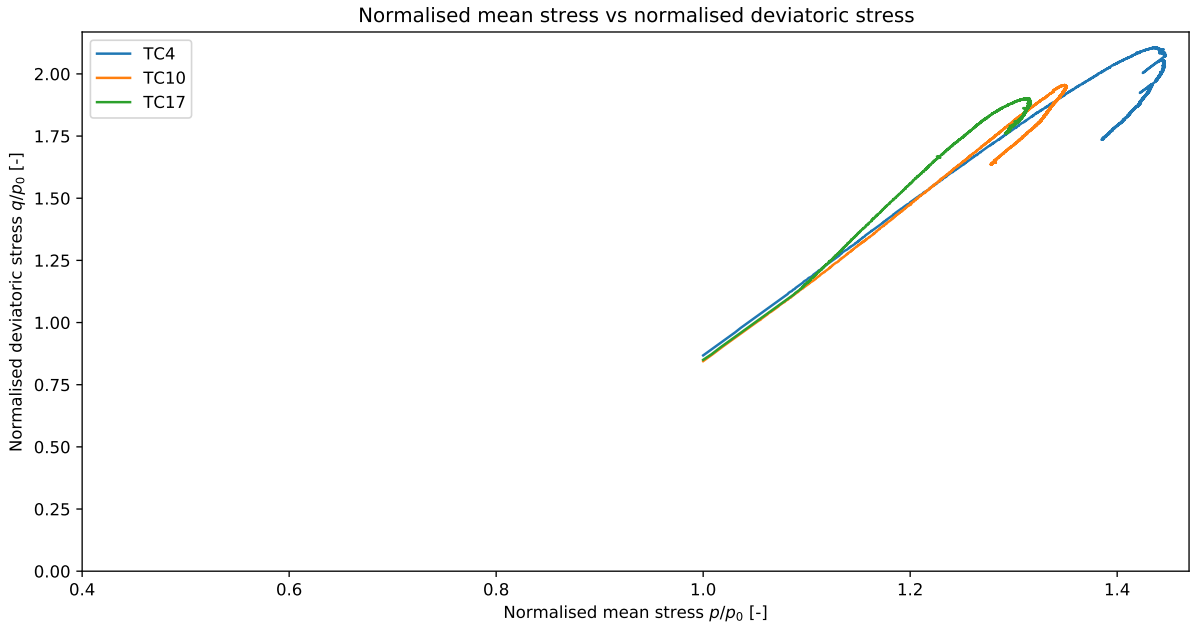

Figure A.25: q/p_0 vs p/p_0

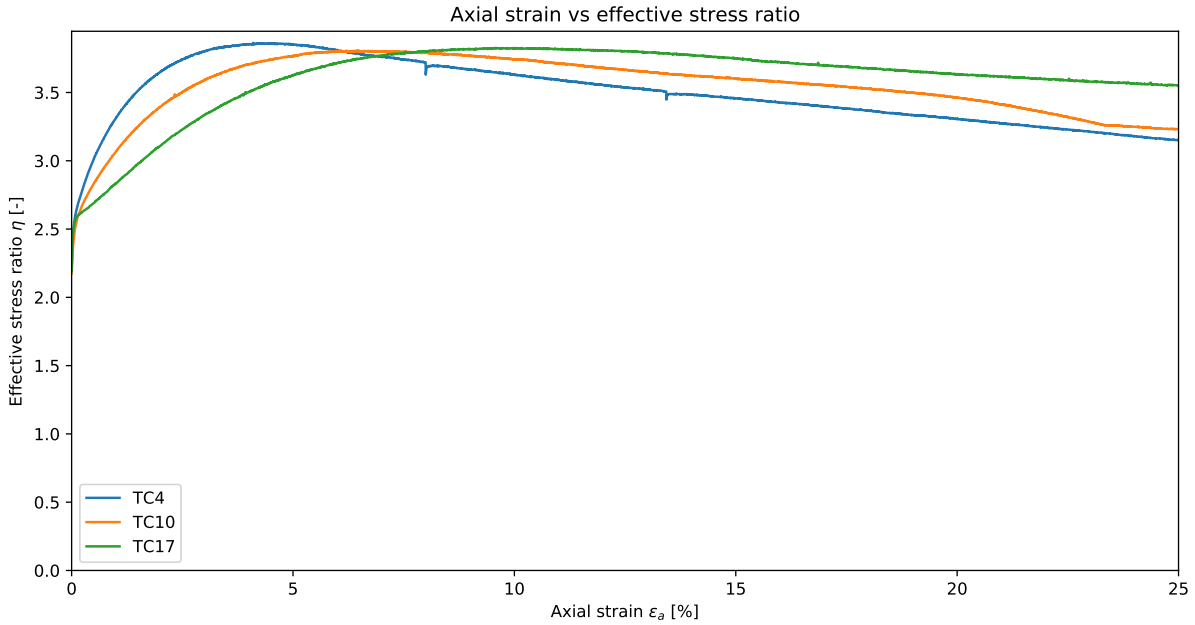

Figure A.26: ϵ_a vs η

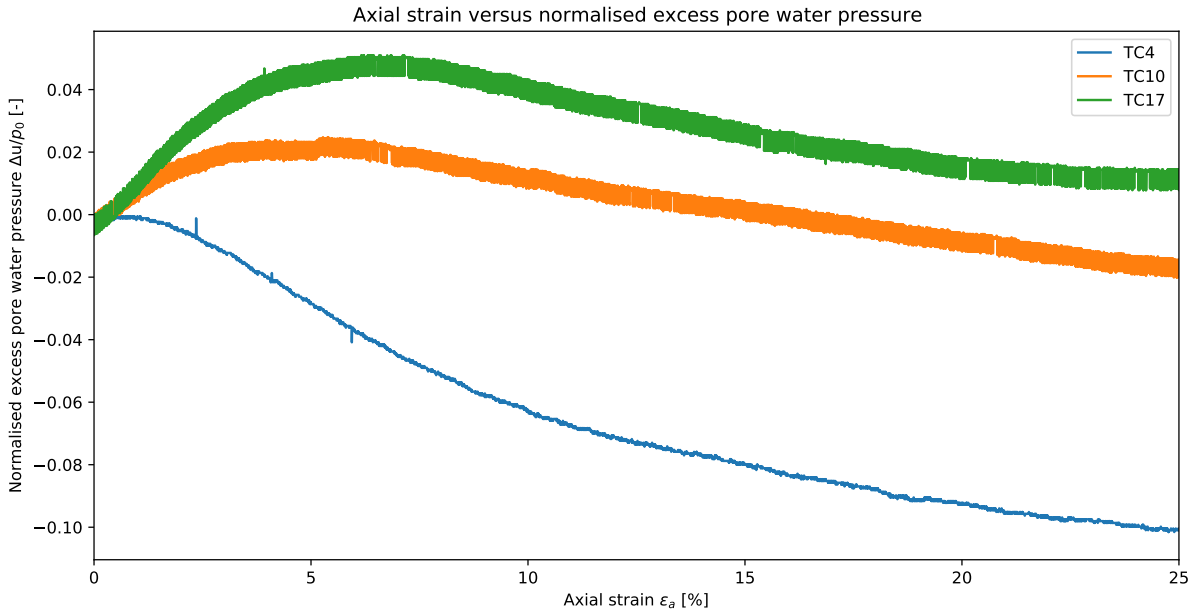

Figure A.27: ϵ_a vs Δ_u/p_o

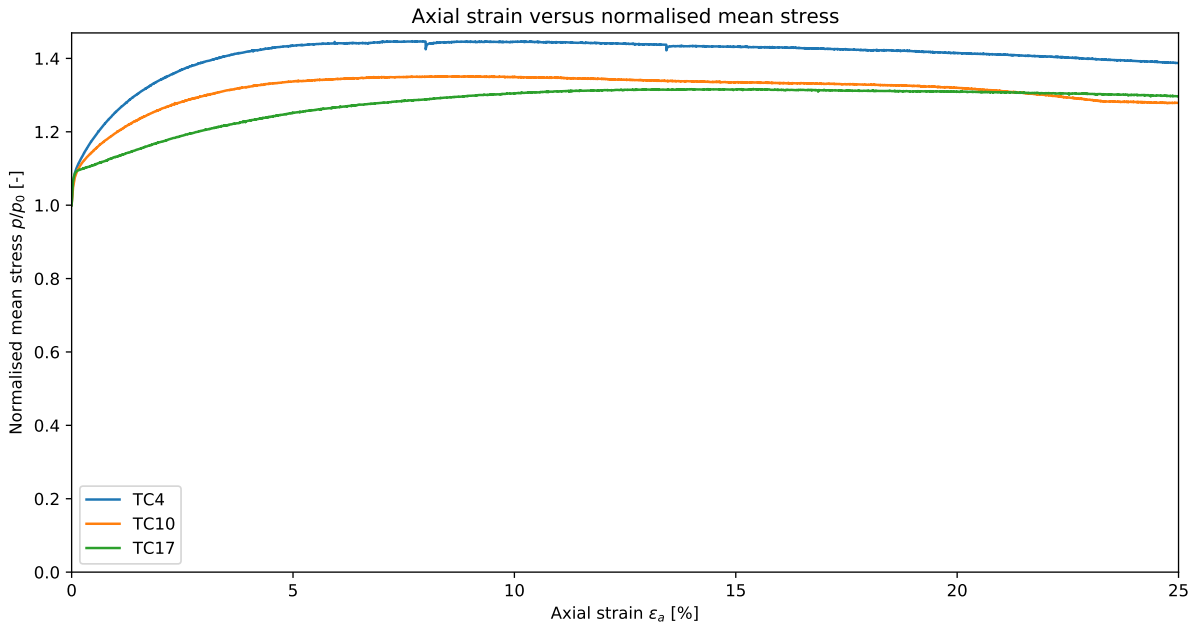

Figure A.28: ϵ_a vs p/p_0

A.5 $\theta_{vol} = 26.53\%$

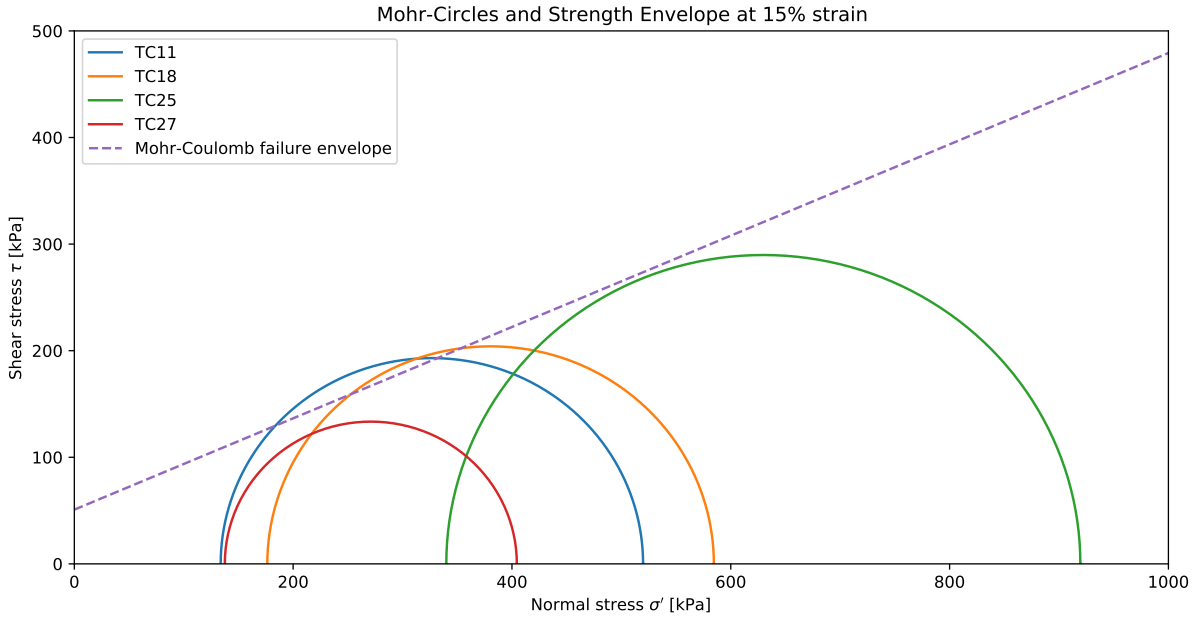

Figure A.29: Mohr-circles and strength envelope at 10% axial strain

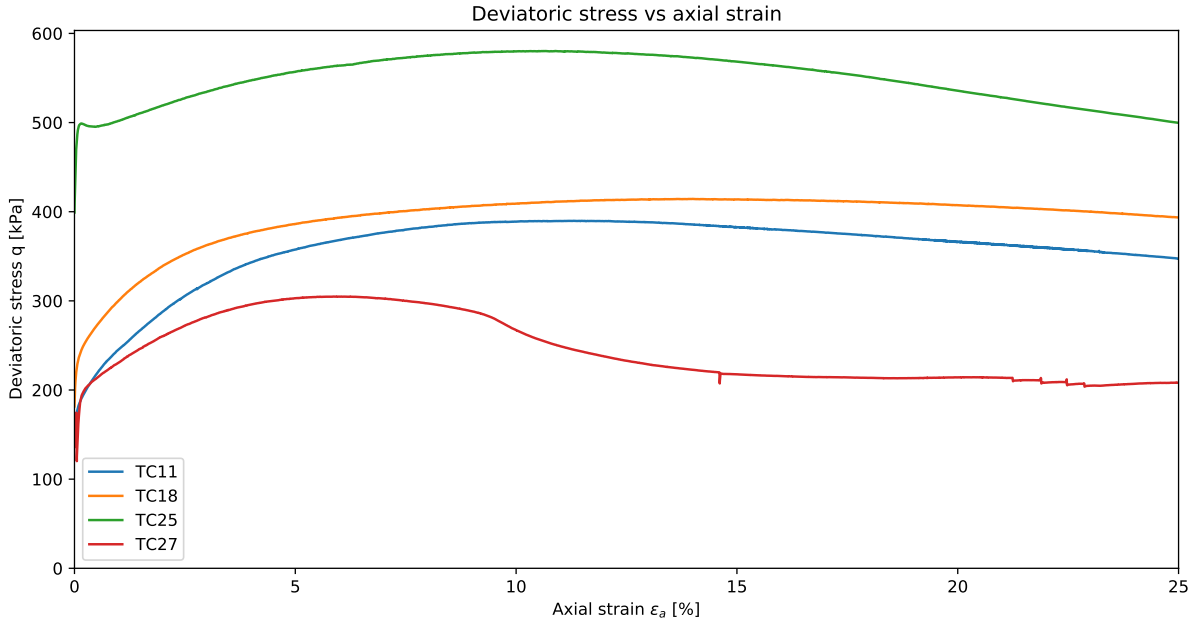

Figure A.30: q vs ϵ_a

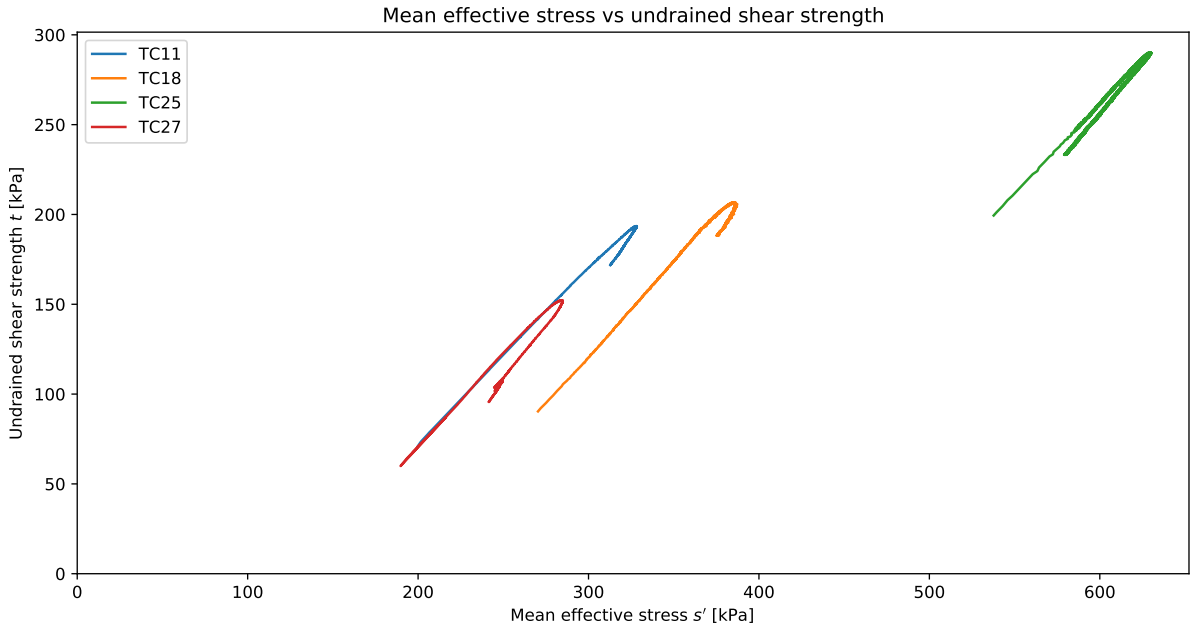

Figure A.31: s', t diagram

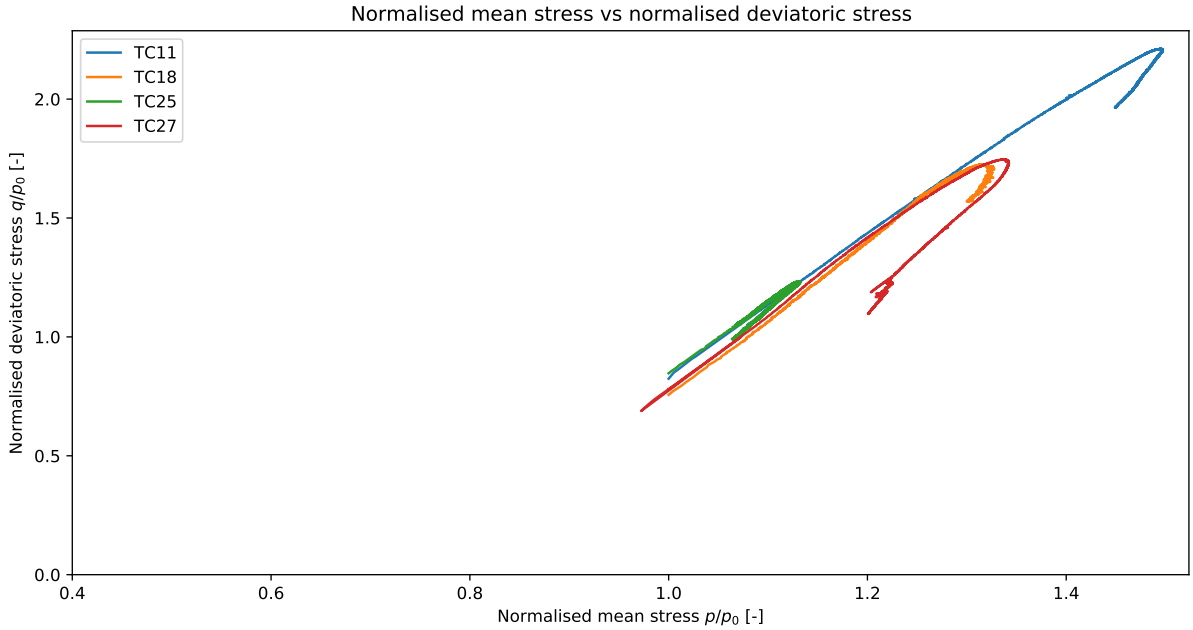

Figure A.32: q/p_0 vs p/p_0

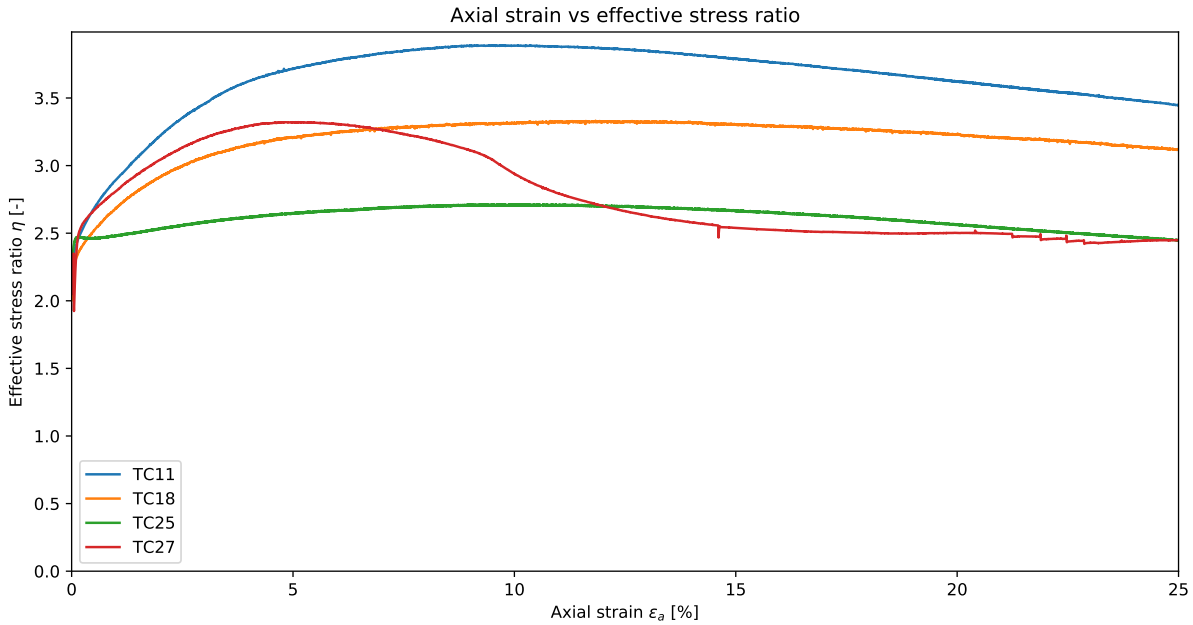

Figure A.33: ϵ_a vs η

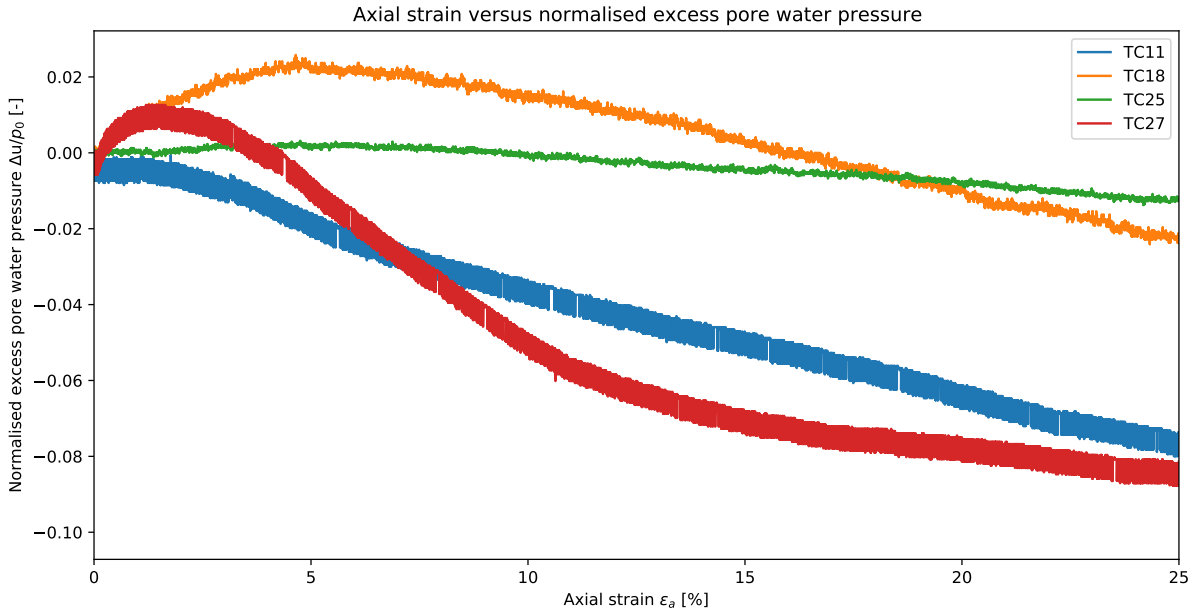

Figure A.34: ϵ_a vs Δ_u/p_o

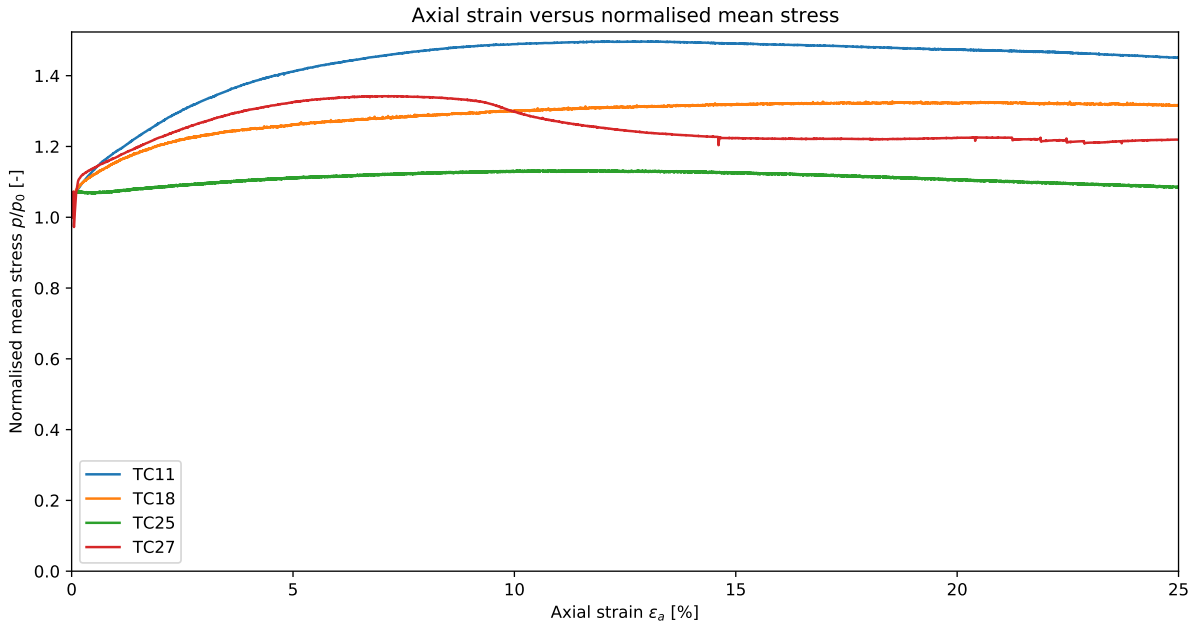

Figure A.35: ϵ_a vs p/p_0

A.6 $\theta_{vol} = 16.09\%$

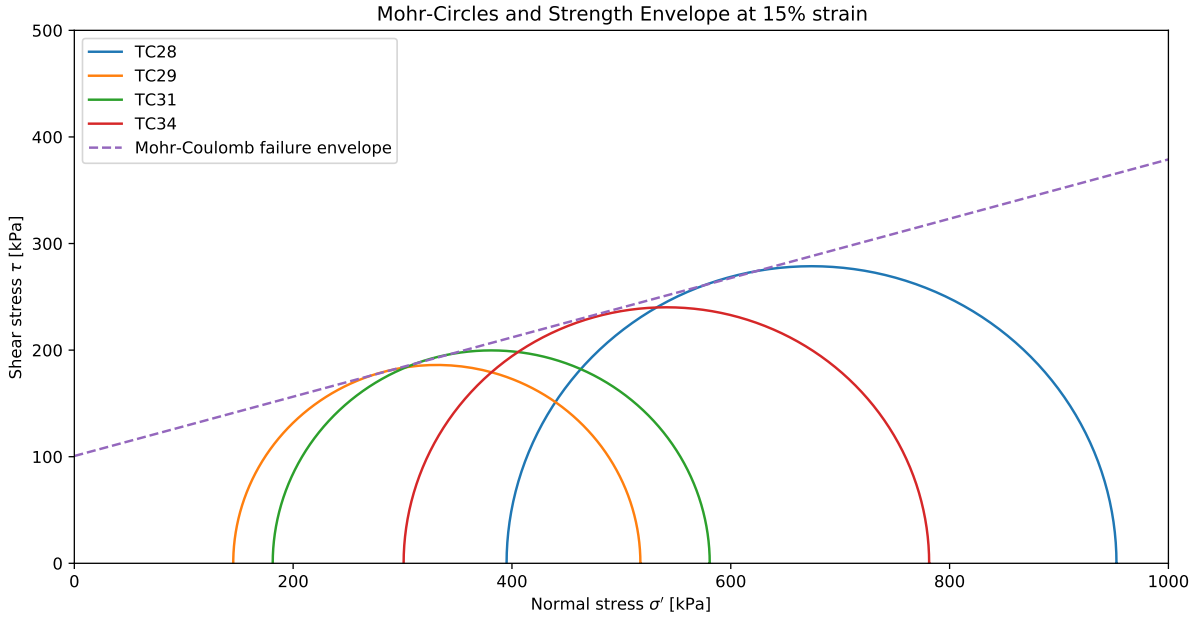

Figure A.36: Mohr-circles and strength envelope at 10% axial strain

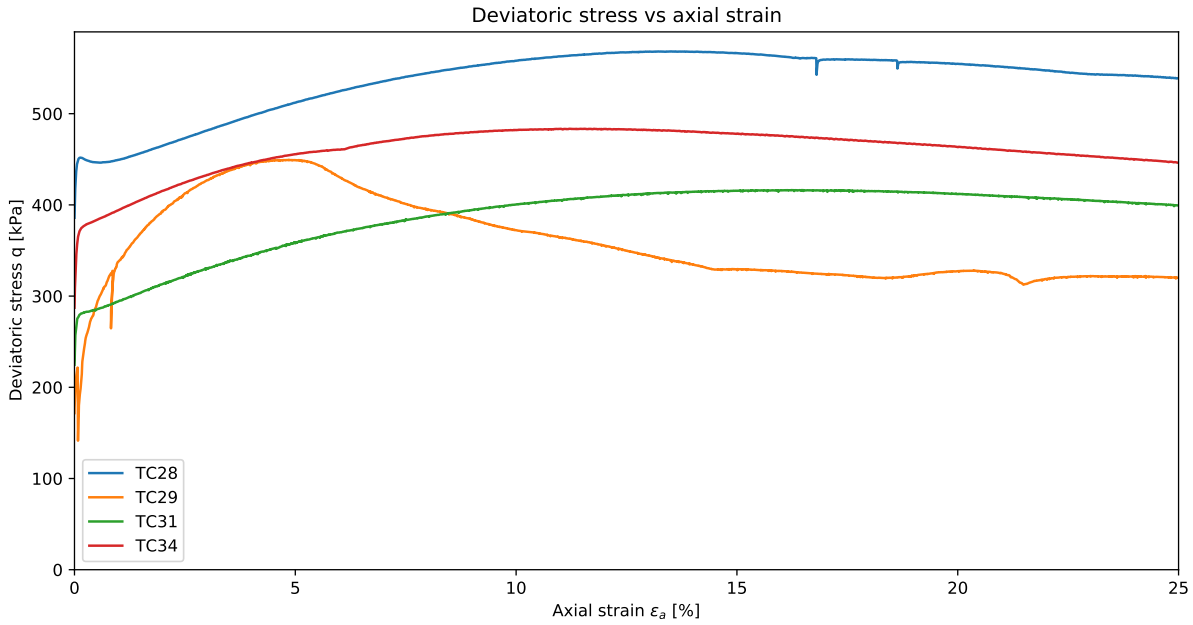

Figure A.37: q vs ϵ_a

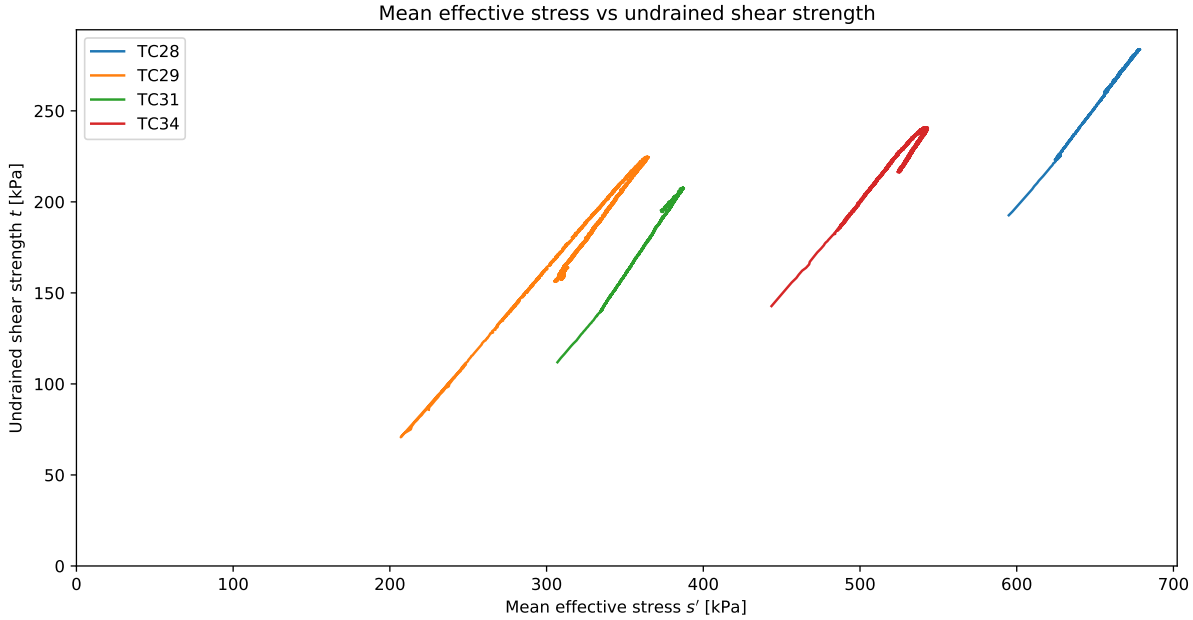

Figure A.38: s', t diagram

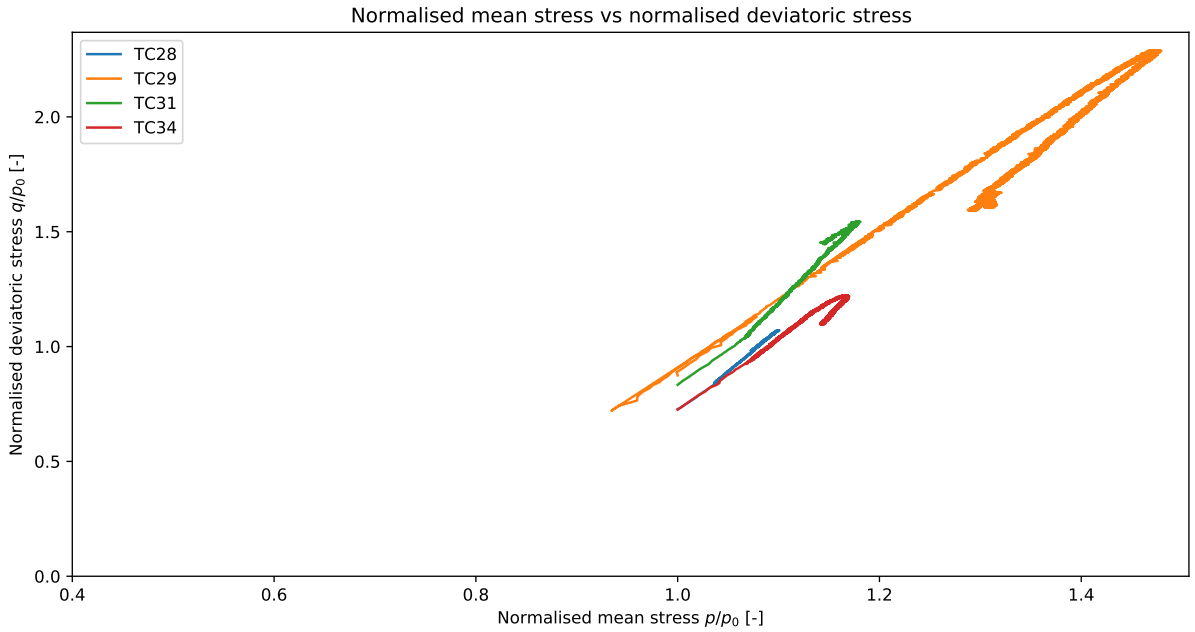

Figure A.39: q/p_0 vs p/p_0

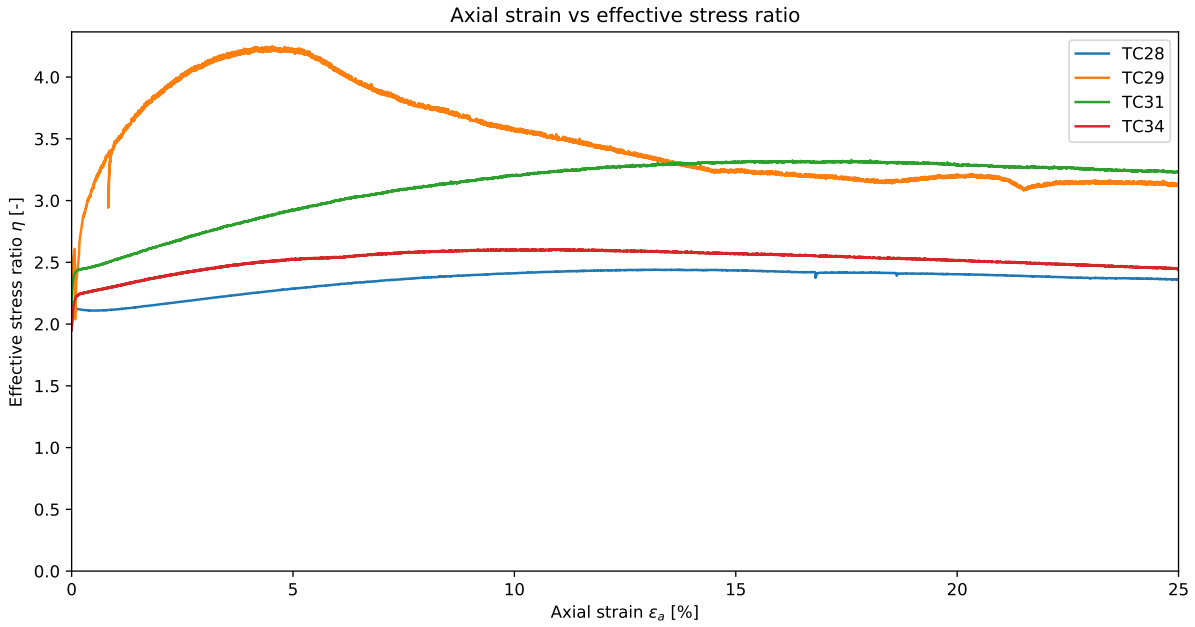

Figure A.40: ϵ_a vs η

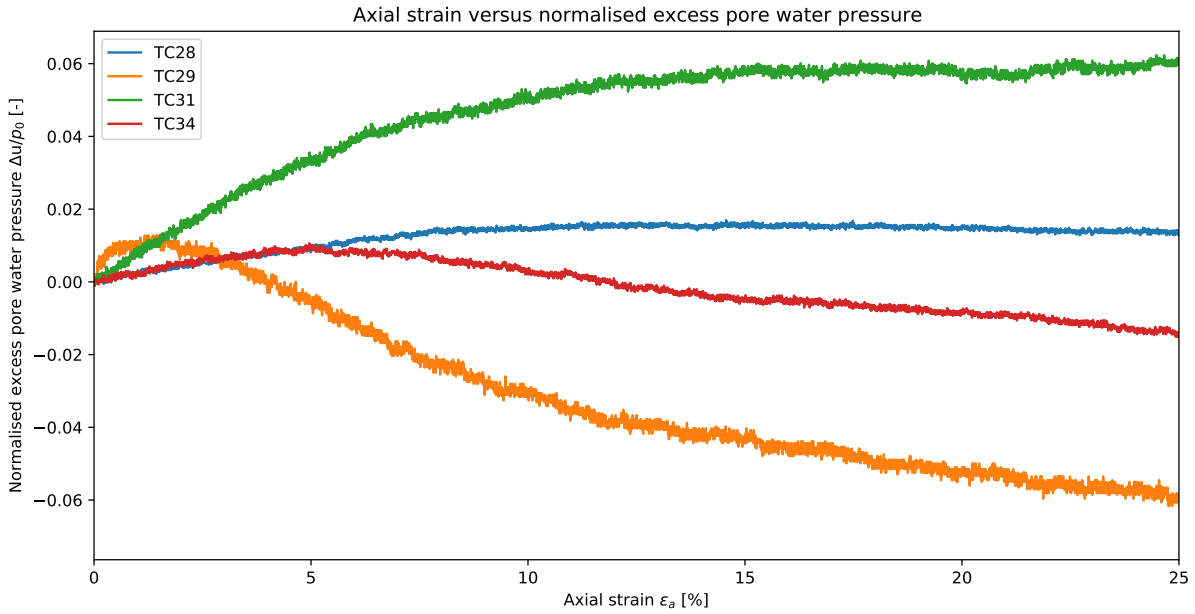

Figure A.41: ϵ_a vs Δ_u/p_o

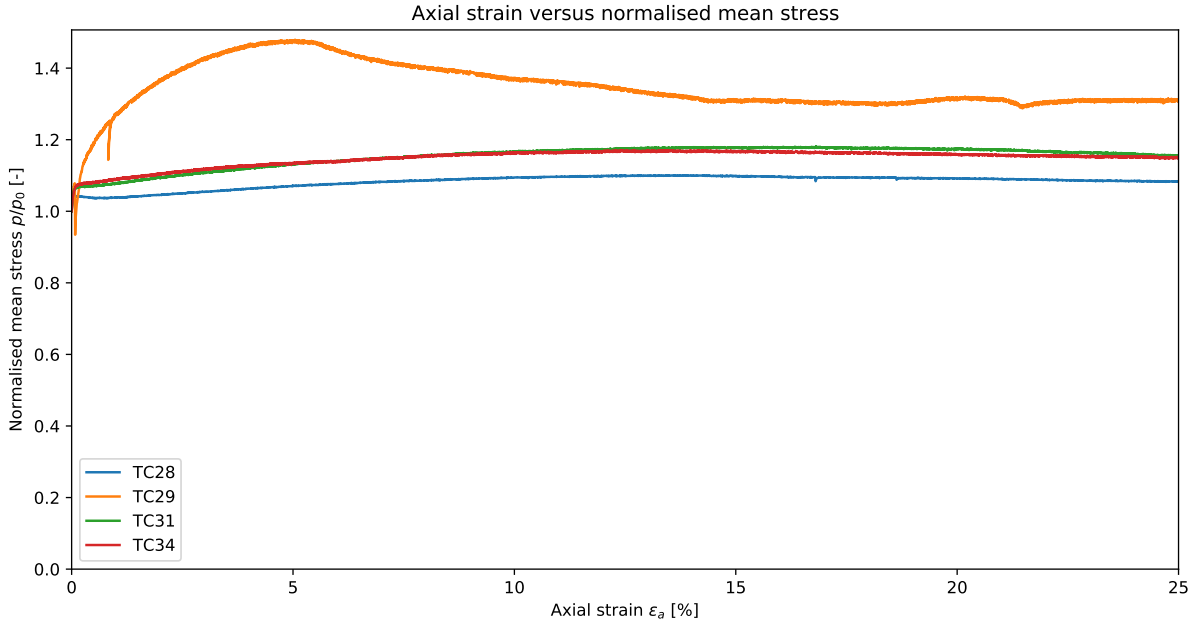

Figure A.42: ϵ_a vs p/p_0

B. Guide to performing an unsaturated K0-CAU triaxial test

This section aims to provide a comprehensive overview of how a K0-CAU triaxial test should be performed while adhering to the SSCC approach based on this thesis. Each triaxial test should in principle be performed according to NEN-EN-ISO 17892-9 (2018) as well as the test protocol by Greeuw et al. (2016) combined with the deviations mentioned below.

B.1 Required information before designing a triaxial test program

- All tests should be performed on an approximately homogeneous cohesive soil. This can be checked by performing index tests for which the determination of the particle sieve curves and the determination of the Atterberg limits would be recommended in addition to a visual description of the soil.
- For each approximately homogeneous soil layer a unique SWCC should be determined. Measurements must at least be taken in the 1 to 1500 kPa range as these values are expected to occur in practice. Samples are advised to be air-dried and stored such that the moisture content within the sample can be homogeneously distributed internally. This process typically takes 1-2 weeks.
- The yield stress should be available. This can be determined using either oedometer or (K0-) CRS tests. Depending on the type of test chosen expect to need 1-4 weeks.
- Determine whether the concept of strain compatibility is applicable to the soil of interest and determine the parameters. For this several conventional (so without the SSCC approach) K0-CAU and DSS tests are recommended, and the required time is approximately 2-4 weeks. It must be noted that this inherently implies that sufficient test capacity is available, otherwise this process might take even longer.

B.2 Preparation of samples

- Determine at which volumetric water content each sample should be tested. Preferably, a minimum of three tests are performed for each volumetric water content with varying stress levels. These stress levels can be determined with the aid of the yield stress in case of NC triaxial tests and by the in-situ vertical stress for OC triaxial tests. It is recommended to perform these tests for at least three different volumetric water contents for which the corresponding value of matric suction in the SWCC is available, and which is to be expected in practice. Based on the available field measurements a volumetric water content corresponding to a matric suction of 0 kPa, 100 and 200 kPa. *Note: 0 kPa means, that the sample can be tested with a saturation stage as normally is done. If more tests can be done, it would be advised to perform more test per datapoint such that the accuracy of each point is improved before samples at intermediate volumetric water content are tested.*
- Trim the triaxial samples in accordance with normal procedures and tolerances such that sample disturbance is limited. Please note that the sample should immediately be wrapped in plastic foil and stored in a temperature-controlled storage location. This is required as the moisture content of each specific triaxial sample is unknown before trimming, and hence, can be determined by drying the trimmings in the oven.
- After 24 hours in the oven at 105 degrees, the gravimetric moisture content can be determined, as well as the specific weight by means of a pycnometer such that the target mass of the sample can be determined.

- Each sample can then be air-dried to its target mass. Depending on the target mass this process may take several hours to several days. The sample should be supervised regularly to ensure that it dries evenly. Depending on both the sample and the laboratory climate characteristics, the sample should be wrapped in plastic foil after a few hours of air-drying such that the formation of shrinkage cracks is prevented. By wrapping the sample in foil followed by storage in a temperature-controlled room, the water content inside the sample is allowed to become approximately homogeneous again. *Note: if the sample at in-situ water content is dryer than its target, it is advised to adjust the volumetric water content at which tests are performed. Samples at in-situ water content can only be fully saturated in a triaxial cell and not to an intermediate water content if a conventional triaxial set-up is used due to large uncertainties in the determination of the pore water volume.*
- Once the sample has reached it target mass, the sample should be wrapped in plastic foil and stored for at least 24 hours in a temperature-controlled room such that internal homogenization of water content is allowed.

B.3 Execution of a K0-CAU triaxial test

- The sample can then be installed in a triaxial cell and set-up as normally would be done.
- Normally, in a K0-CAU, the sample would first encounter a saturation stage, but using the SSCC approach, this stage must be skipped.
- Thus, this means that first the sample is isotropically consolidated and a consolidation check must be performed. This process typically takes 24-48 hours.
- Next, the sample can be anisotropically consolidated and afterwards again a consolidation check must be performed. The time required for completion of this stage is dependent on the required anisotropic stresses. This stage typically takes 48 hours for low stress levels (up to 150 kPa) and up to a week for high stress levels.
- The sample can then be sheared to failure. The loading rate is determined by the rate of consolidation and therefore this stage typically takes 24-48 hours.
- Remove the sample after the test has been completed and make pictures of i) the intact sample and ii) the sample cut in half to get a good visualization of possible inhomogeneity in the sample. It is further advised to determine the sample volume after the test using wet weighing according to NEN-EN-ISO 17892-2 (2014). If any discrepancies between the calculated volume from the raw test data and the measured volume are found, these can then subsequently be corrected.

All in all, expect to need approximately 2-3 weeks to perform K0-CAU triaxial tests in accordance with the SSCC concept if all information is available. If this is not available, or funds are insufficient in an early design phase, it would be recommended to solely investigate the SWCC parameters for each unique soil layer and then apply Lu et al. (2010) closed form of the SSCC.